

SECURITY CLASSIFICATION OF THIS PAGE

REPORT DOCUMENTATION PAGE				Form Approved OMB No. 0704-0188	
1a. REPORT SECURITY CLASSIFICATION UNCLASSIFIED			1b. RESTRICTIVE MARKINGS NONE		
2a. SECURITY CLASSIFICATION AUTHORITY			3. DISTRIBUTION / AVAILABILITY OF REPORT APPROVED FOR PUBLIC RELEASE; DISTRIBUTION UNLIMITED.		
AD-A217 952			5. MONITORING ORGANIZATION REPORT NUMBER(S) AFIT/CI/CIA-89-024		
6a. NAME OF PERFORMING ORGANIZATION AFIT STUDENT AT UNIV OF OK		6b. OFFICE SYMBOL (if applicable)	7a. NAME OF MONITORING ORGANIZATION AFIT/CIA		
6c. ADDRESS (City, State, and ZIP Code)			7b. ADDRESS (City, State, and ZIP Code) Wright-Patterson AFB OH 45433-6583		
8a. NAME OF FUNDING / SPONSORING ORGANIZATION		8b. OFFICE SYMBOL (if applicable)	9. PROCUREMENT INSTRUMENT IDENTIFICATION NUMBER		
8c. ADDRESS (City, State, and ZIP Code)			10. SOURCE OF FUNDING NUMBERS		
			PROGRAM ELEMENT NO.	PROJECT NO.	TASK NO.
					WORK UNIT ACCESSION NO.
11. TITLE (Include Security Classification) (UNCLASSIFIED) Derivation of Kinematic Fields Using Wind Profiler Data From The 1985 Pre-storm Experiment					
12. PERSONAL AUTHOR(S) JEFFREY DOUGLAS POWELL					
13a. TYPE OF REPORT THESIS/DISSERTATION		13b. TIME COVERED FROM _____ TO _____		14. DATE OF REPORT (Year, Month, Day) 1989	
				15. PAGE COUNT 138	
16. SUPPLEMENTARY NOTATION APPROVED FOR PUBLIC RELEASE IAW AFR 190-1 ERNEST A. HAYGOOD, 1st Lt, USAF Executive Officer, Civilian Institution Programs					
17. COSATI CODES			18. SUBJECT TERMS (Continue on reverse if necessary and identify by block number)		
FIELD	GROUP	SUB-GROUP			
19. ABSTRACT (Continue on reverse if necessary and identify by block number)					
<div style="text-align: center;"> <b>DTIC</b>  <b>ELECTE</b>  <b>S FEB 13 1990 D</b>  <i>cc</i> </div>					
90 02 12 004					
20. DISTRIBUTION / AVAILABILITY OF ABSTRACT <input checked="" type="checkbox"/> UNCLASSIFIED/UNLIMITED <input type="checkbox"/> SAME AS RPT. <input type="checkbox"/> DTIC USERS			21. ABSTRACT SECURITY CLASSIFICATION UNCLASSIFIED		
22a. NAME OF RESPONSIBLE INDIVIDUAL ERNEST A. HAYGOOD, 1st Lt, USAF			22b. TELEPHONE (Include Area Code) (513) 255-2259		22c. OFFICE SYMBOL AFIT/CI

GRADUATE COLLEGE

A THESIS

in partial fulfillment of the requirements for the

degree of

MASTER OF SCIENCE IN METEOROLOGY

JEFFREY DOUGLAS POWELL

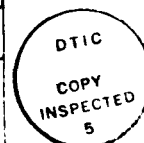
Norman, Oklahoma

1989

90-000000000

DERIVATION OF KINEMATIC FIELDS USING WIND PROFILER  
 DATA FROM THE 1985 PRE-STORM EXPERIMENT  
 A THESIS  
 APPROVED FOR THE SCHOOL OF METEOROLOGY

Accession for	
NTIS (GPO)	<input checked="" type="checkbox"/>
DTIC TAB	<input type="checkbox"/>
Unannounced	<input type="checkbox"/>
Justification	
By	
Excluded from	
Distribution	
DTIC	
A-1	



By Frederick H. Carr  
Charles A. Roswell III  
Howard B. B. Luntz

#### ACKNOWLEDGEMENTS

I sincerely thank Dr. Frederick Carr, my committee chairman, for sharing his time, expertise, and innate ability to let one "see the forest through the trees" during my graduate studies. Dr. Charles Doswell III, a committee member, provided vital analysis input for this study while supplying his interesting and applicable mixture of useful advice and philosophy. Many thanks also go to Dr. Howard Bluestein for his suggestions and ideas.

My appreciation is extended to John Augustine and Jose Meitin from NOAA/ERL for providing PRE-STORM rawinsonde data and satellite imagery. I am also grateful to Laurie Hermes from NSSL for supplying the PRE-STORM profiler data and some initial processing hints. Brian Curran, also at NSSL, deserves great credit for providing PRE-STORM mesonetwork surface data. Day to day assistance from Wes Roberts, Dwight Moore, and Bill Standefer at GCN actually made the necessary VAX time enjoyable. I will fondly remember the many people I've recently met that I now count as friends. They made my graduate school experience much more than bearable.

Finally, I thank the United States Air Force for providing me the opportunity to serve my beloved country through the pursuit of higher academic knowledge.

## TABLE OF CONTENTS

	Page
ACKNOWLEDGEMENTS.....	iii
LIST OF TABLES.....	vi
LIST OF FIGURES.....	vii
ABSTRACT.....	xii
 Chapter	
I. INTRODUCTION.....	1
1.1 Background.....	1
1.2 PRE-STORM and profiler review....	4
1.3 Overview.....	10
II DATA SETS AND WEATHER SUMMARIES.....	12
2.1 General comments.....	12
2.2 3-4 June.....	14
2.3 12-13 May.....	23
2.4 26-27 June.....	32
2.5 Sources of error in the data sets.....	40
III QUALITY CONTROL.....	42
3.1 General comments.....	42
3.2 Median check.....	43
3.3 Vertical consistency check.....	48
IV OBJECTIVE ANALYSIS AND KINEMATIC FIELD CALCULATIONS.....	68
4.1 A Barnes objective analysis review.....	68
4.2 Time to space conversion.....	72
4.3 Final parameter decisions.....	77
4.4 Kinematic fields calculations....	95
V KINEMATIC FIELD RESULTS AND DISCUSSION.....	101
5.1 3-4 June.....	101
5.2 12-13 May.....	109
5.3 26-27 June.....	116
5.4 Sensitivity studies.....	120

Chapter	Page
VI CONCLUSIONS AND FUTURE WORK.....	127
BIBLIOGRAPHY.....	133
APPENDIX.....	136

## LIST OF TABLES

TABLE	PAGE
1.1. Operation specifications for the three PRE-STORM profilers (Augustine and Zipser, 1987).....	6
2.1. Times for simultaneous PRE-STORM profiler operation. Chosen data sets are highlighted by lines of asterisks.....	13
4.1. Values of average station separation, $\Delta n_c$ .....	79
4.2. Values of "random" station separation, $\Delta n_r$ .....	79
4.3. RMS vector differences between analyzed and quality controlled wind fields for 3-4 June.....	96
4.4. Same as 4.3. but for 12-13 May.....	96
4.5. Same as 4.3. but for 26-27 June.....	97
4.6. Same as 4.3. but for $\Delta n = 600$ meters.....	97

## LIST OF FIGURES

FIGURE	PAGE
1.1. Overview of the various PRE-STORM measurement networks (Meitin and Cuning, 1985).....	5
1.2. Simple schematic of a three beam Doppler radar wind profiler (Hogg et al., 1983).....	8
2.1 "Raw" McPherson profiler data for 3-4 June. Time, in hours, increases from right to left. Height is in units of kilometers. Scale vector length is shown in lower right corner.....	15
2.2. Same as 2.1. but for 3-4 June Norman.....	16
2.3. Same as 2.1. but for 3-4 June Liberal.....	17
2.4. NMC surface analysis for 1200 GMT, 3 June.....	19
2.5. NMC 850 mb analysis for 0000 GMT, 4 June.....	19
2.6. GOES visible imagery at 1930 GMT, 3 June.....	20
2.7. GOES infrared imagery at 0000 GMT, 4 June.....	20
2.8. Same as 2.7. but at 0600 GMT, 4 June.....	22
2.9. Same as 2.7. but at 0900 GMT, 4 June.....	22
2.10. "Raw" McPherson profiler data for 12-13 May.....	24
2.11. Same as 2.10. but for 12-13 May Norman.....	25
2.12. Same as 2.10. but for 12-13 May Liberal.....	26
2.13. NMC 500 mb analysis for 1200 GMT, 12 May.....	28
2.14. GOES infrared imagery at 2100 GMT, 12 May.....	29

2.15.	Same as 2.14. but for 0000 GMT, 13 May.....	29
2.16.	Same as 2.14. but for 0400 GMT, 13 May.....	31
2.17.	Same as 2.14. but for 0830 GMT, 13 May.....	31
2.18.	"Raw" McPherson profiler data for 26-27 June.....	33
2.19.	Same as 2.18. but for 26-27 June Norman.....	34
2.20.	Same as 2.18. but for 26-27 June Liberal.....	35
2.21.	NMC surface analysis for 2100 GMT, 26 June.....	36
2.22.	NMC 850 mb analysis for 0000 GMT, 27 June.....	36
2.23.	Same as 2.22 but for 500 mb.....	38
2.24.	GOES infrared imagery at 2200 GMT, 26 June.....	38
2.25.	Same as 2.24. but for 0100 GMT, 27 June.....	39
2.26.	Same as 2.24 but for 0900 GMT, 27 June.....	39
3.1.	"Centered" template for the median quality control check.....	44
3.2.	The median quality control check threshold envelope.....	44
3.3.	"Non-centered" template for real-time median quality control check.....	44
3.4.	Rejected wind data from the 3-4 June McPherson profiler data after application of the quality control technique.....	50
3.5.	Quality controlled 3-4 June McPherson profiler data.....	51
3.6.	Same as 3.4. but for 3-4 June Norman.....	52
3.7.	Same as 3.5. but for 3-4 June Norman.....	53
3.8.	Same as 3.4. but for 3-4 June Liberal.....	54
3.9.	Same as 3.5. but for 3-4 June Liberal.....	55
3.10.	Same as 3.4. but for 12-13 May McPherson.....	56
3.11.	Same as 3.5. but for 12-13 May McPherson.....	57

3.12.	Same as 3.4. but for 12-13 May Norman.....	58
3.13.	Same as 3.5. but for 12-13 May Norman.....	59
3.14.	Same as 3.4. but for 12-13 May Liberal.....	60
3.15.	Same as 3.5. but for 12-13 May Liberal.....	61
3.16.	Same as 3.4. but for 26-27 June McPherson.....	62
3.17.	Same as 3.5. but for 26-27 June McPherson.....	63
3.18.	Same as 3.4. but for 26-27 June Norman.....	64
3.19.	Same as 3.5. but for 26-27 June Norman.....	65
3.20.	Same as 3.4. but for 26-27 June Liberal.....	66
3.21.	Same as 3.5. but for 26-27 June Liberal.....	67
4.1.	U-component correlations ( $\times 100$ ) for the Fleming CO profiler during June 1987 as a function of height and vertical separation. Differences are from a 24-hour running mean. Contours are in tenths (Brewster and Schlatter, 1988).....	74
4.2.	Same as 4.1. but as a function of height and time separation (Brewster and Schlatter, 1988).....	74
4.3.	Graphs of the various calculated time to space conversion factors as functions of height.....	75
4.4.	Barnes first pass weight function using $\Delta n = 600$ meters.....	81
4.5.	Barnes second pass weight function using $\Delta n = 600$ meters and $\gamma = 0.2$ .....	82
4.6.	Same as 4.4. but for $\Delta n = 1200$ meters.....	83
4.7.	Same as 4.5. but for $\Delta n = 1200$ meters.....	84
4.8.	Barnes first and second pass response functions.....	85
4.9.	Analyzed wind field for the 3-4 June McPherson profiler data. height interval is 200 meters.....	86

4.10.	Same as 4.9. but for 3-4 June Norman.....	87
4.11.	Same as 4.9. but for 3-4 June Liberal.....	88
4.12.	Same as 4.9 but for 12-13 May McPherson.....	89
4.13.	Same as 4.9. but for 12-13 May Norman.....	90
4.14.	Same as 4.9. but for 12-13 May Liberal.....	91
4.15.	Same as 4.9 but for 26-27 June McPherson.....	92
4.16.	Same as 4.9 but for 26-27 June Norman.....	93
4.17.	Same as 4.9. but for 26-27 June Liberal.....	94
5.1.	Kinematically derived omega field for 3-4 June. Values are in units of $10^2 \mu\text{bs}^{-1}$ .....	102
5.2.	GOES visible imagery at 1900 GMT, 3 June.....	103
5.3.	Same as 5.2. but at 2230 GMT.....	103
5.4.	NMC radar summary for 1935 GMT, 3 June.....	104
5.5.	Same as 5.4 but for 2235 GMT.....	104
5.6.	GOES infrared imagery at 0300 GMT, 4 June.....	106
5.7.	Same as 5.6. but at 0800 GMT.....	106
5.8.	NMC radar summary for 0335 GMT, 4 June.....	107
5.9.	Same as 5.8 but for 0835 GMT.....	107
5.10.	Kinematically derived omega field for 12-13 May. Values are in units of $10^2 \mu\text{bs}^{-1}$ .....	110
5.11.	GOES infrared imagery at 2200 GMT, 12 May.....	111
5.12.	Same as 5.11. but at 0030 GMT, 13 May.....	111
5.13.	Same as 5.11. but at 0800 GMT.....	113
5.14.	Same as 5.11. but at 0630 GMT.....	113
5.15.	Schematic diagram of a composite comma cloud on the 317 K isentropic surface (Carr and Millard, 1984).....	114
5.16.	NMC 850 mb analysis for 0000 GMT, 13 May.....	115

5.17.	Same as 5.16. but for 500 mb.....	115
5.18.	Kinematically derived omega field for 26-27 June. Values are in units of $10^1 \mu\text{bs}^{-1}$ .....	117
5.19.	GOES infrared imagery at 2100 GMT, 26 June.....	118
5.20.	Same as 5.19. but for 0300 GMT, 27 June.....	118
5.21.	Same as 5.20. but for 0500 GMT.....	119
5.22.	Same as 5.1. but for $\Delta n = 1200$ meters.....	122
5.23.	Same as 5.18. but for $\delta = 0.6$ .....	124
5.24.	Same as 5.23. but for $\omega = 0$ at 100 mb after divergence adjustment.....	125
A1.	Orientation of unit vectors for line integral calculations around a triangle.....	138

## ABSTRACT

During the May and June 1985 PRE-STORM experiment, three 50 MHz wind profilers were installed for the first time in the Great Plains to enhance the understanding of mesoscale system development and evolution. In order to utilize these profiler data for the computation of kinematic quantities, many instances of poor or missing data must be dealt with. Often, this requires the performance of separate screening, filling, interpolation, and filtering steps. This study proposes the accomplishment of the latter three steps at once through the adaption of a Barnes objective analysis technique. Using wind covariance statistics from a Colorado profiler, a weight function is designed which assigns equal weight to equally correlated data in time and in the vertical. Features within vertical motion fields derived after application of this technique correspond well with features seen in satellite imagery and contain detail unobtainable via analysis of rawinsonde data.

DERIVATION OF KINEMATIC FIELDS USING WIND PROFILER  
DATA FROM THE 1985 PRE-STORM EXPERIMENT

CHAPTER I

INTRODUCTION

1.1 Background

From the era of the first all-metal airplane until recently, weather forecasters have had to rely on wind data from twice-daily soundings taken from balloon-borne devices, called rawinsondes, for purposes of analysis and forecasting. While advances in rawinsonde technology over the years have ensured the high reliability of data from this source, the sampling interval prevents observation of fluctuations in the wind field with periods of less than 24 hours. When deriving kinematic fields (e.g. divergence and vertical motion fields) from the existing rawinsonde network, small-scale features in the divergence field can pass almost undetected (Zamora et al., 1987). Missed or inadequately sampled kinematic features denies meteorologists the opportunity to improve forecasting of such events as the development and movement of Mesoscale

Convective Systems (MCS), widespread airmass thunderstorm activity and inclement weather caused by shortwave troughs. After-the-fact analysis and understanding of the structure of these features is also hindered.

The development of clear air wind observation systems through advances in Doppler radar technology has provided the meteorologist with a new generation measuring device - the wind profiler. A thorough history of clear air radar technology is provided by Gage and Balsey (1978) and updated versions appear in Profiler Forum every few months.

Wind profilers can provide tropospheric wind "profiles" every few minutes at height intervals of 200 meters or less. It has long been known, via satellite imagery, that small-scale upper air features exist and could partially be responsible for poor forecasts. Soon after the completion of a five-profiler network in Colorado by mid-1983 (Strauch, 1984), it became apparent that these features behaved according to understood principles of meteorology (e.g. Shapiro et al., 1984; Strauch et al., 1984). While shortcomings of this new system (such as an inherent data gap between the ground and first profiler observation height and the lack of thermodynamic data) prevent profilers from becoming the total alternative to rawinsondes, the combination of profiler and rawinsonde networks can greatly enhance our ability to diagnose and forecast weather features on a subsynoptic scale.

The determination of wind field kinematic properties via

Doppler radar is a concept that has been around for some time. For example, Browning and Wexler (1968) proposed a method for the estimation of divergence and deformation from a single Doppler velocity-azimuth display (VAD) in situations of widespread precipitation. Among the first to derive kinematic fields from a network of wind profilers were Zamora and Shapiro (1984). They determined that believable horizontal divergence fields could be derived on a continuous temporal basis using a line integral technique developed by Schaefer and Doswell (1979).

Since 1984, kinematic fields have been successfully derived many times from different profiler data sets (e.g., Zamora et al., 1986; Smith and Schlatter, 1988). Calculations of horizontal divergence and vertical velocity fields using real or simulated profiler networks have been used as intermediate steps towards retrieval of thermodynamic properties (e.g. Kuo and Anthes, 1985; Kuo et al., 1987 and Hermes, 1988).

In all of these studies, separate steps are used for quality control, data filling, data interpolation onto grids and grid filtering. One of the sub-goals of this study is the successful accomplishment of the latter three steps at once using a Barnes objective analysis technique (see Koch et al., 1983) to be developed in Chapter IV.

## 1.2 PRE-STORM and Profiler Review

The Oklahoma-Kansas Preliminary Regional Experiment for STORM Central (PRE-STORM) was a 58 day cooperative field experiment conducted from 1 May to 27 June, 1985. Among the accomplishments of this program was the first introduction of Doppler radar wind profilers to the Great Plains. Although representing only one measurement system used in the PRE-STORM experiment, wind data obtained from the three PRE-STORM wind profilers were used as the primary data source for this study. Figure 1.1 presents an overview of the various instrument arrays installed for the 1985 experiment, including the wind profiler locations, surface meso-network and supplemental rawinsonde sites (Meitin and Cuning, 1985).

Although all three profilers operated near 50 MHz, the antenna configurations varied from profiler to profiler. A profiler with a three beam antenna configuration was installed near Liberal, Kansas by ERL's Aeronomy Laboratory. The Radian Corporation installed a three beam system at McPherson, Kansas while the Wave Propagation Laboratory installed a two beam profiler at Norman, Oklahoma. As Table 1.1 shows, even the two profilers with three beam systems were configured differently.

Wind profilers can "see" clear air movement by detecting reflected energy from refractive index fluctuations caused by mixing or turbulence. These fluctuations are assumed to

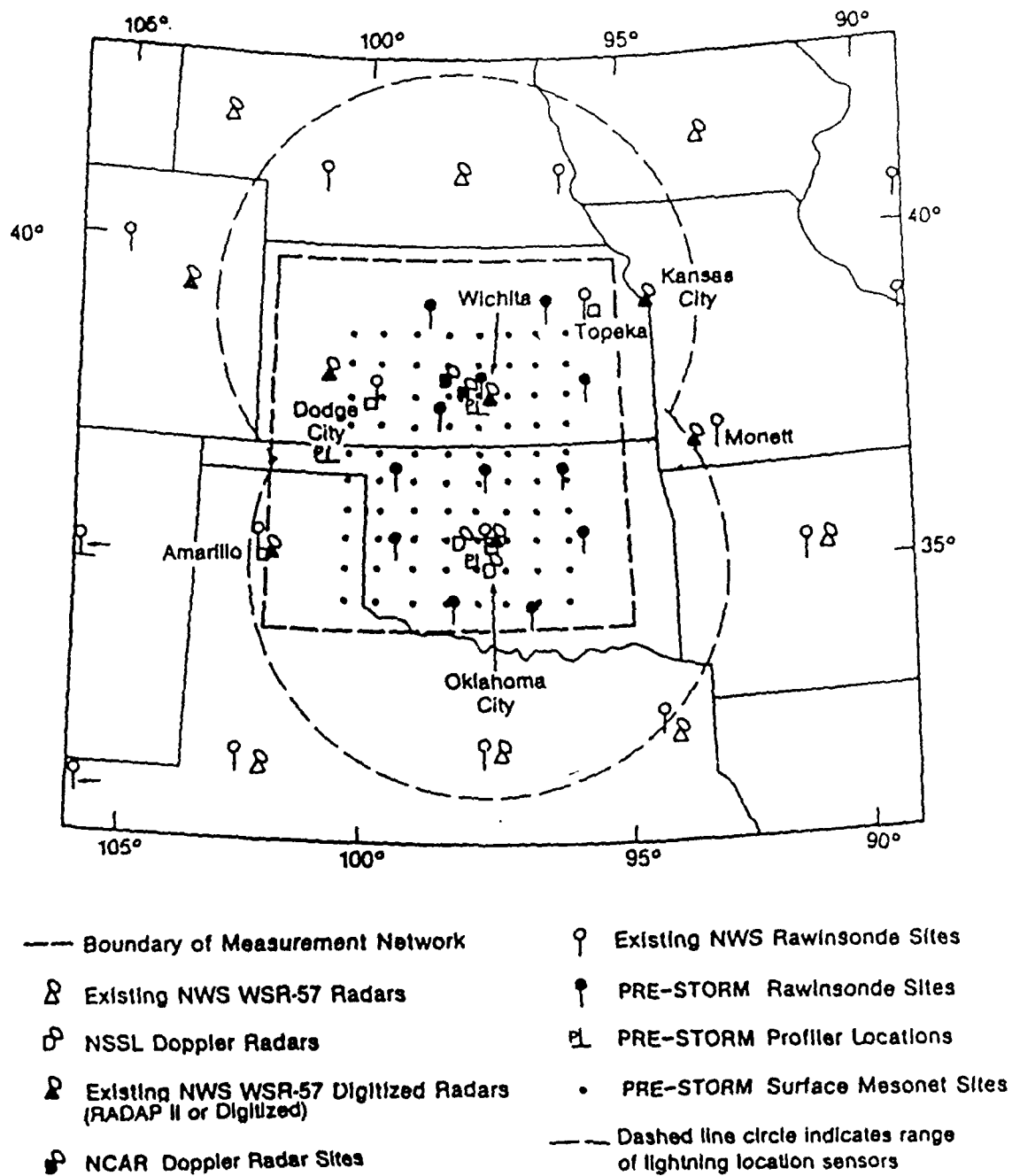


Fig. 1.1. Overview of the various PRE-STORM measurement networks (Meitin and Cuning, 1985).

	<u>McPherson</u>	<u>Liberal</u>	<u>Norman</u>
Frequency(MHz)	49.25	49.92	49.92
Number of Beams	3	3	2
Tilt angle of oblique beams off zenith(deg)	8	15	15
Peak Power (kW)	125	40	20
Average Power(W)	5000	200	400
Antenna Aperture(m)	49 X 49	100 X 100	50 X 50
Pulse Width (microsec)	1	4	3 (low altitude) 9 (high altitude)

Table 1.1. Operation specifications for the three PRE-STORM profilers (Augustine and Zipser, 1987).

be embedded in the mean wind flow and therefore can be used as tracers. Abundant water vapor in the atmosphere and mixing on the scale of several meters create the optimum operating conditions for 50 MHz wind profilers.

Wind measurement by profilers can be accomplished using either the two or three beam configuration. These beams are fixed in space, unlike scanning Doppler weather radar, and are arranged as in Fig. 1.2. The high elevation angle for the two oblique radar beams is chosen only after careful consideration of opposing influences of elevation angle on parameters such as effective aperture, power loss and measurement uncertainty (Hogg et al., 1983).

Approximately every five minutes, a profile is produced after many pulses have been transmitted along each antenna beam. The signal-to-noise ratio is boosted through integration of the returned signals at the desired height levels. Many consecutive five-minute profiles can then be averaged to further increase this ratio (Augustine and Zipser, 1987).

Assuming that the two oblique radar beams are pointed towards true north and east at an elevation angle  $Z$ , the radial velocities measured by the profiler are related to the total wind as follows:

$$V_1 = u \cos Z + w \sin Z \quad (1)$$

$$V_2 = v \cos Z + w \sin Z \quad (2)$$

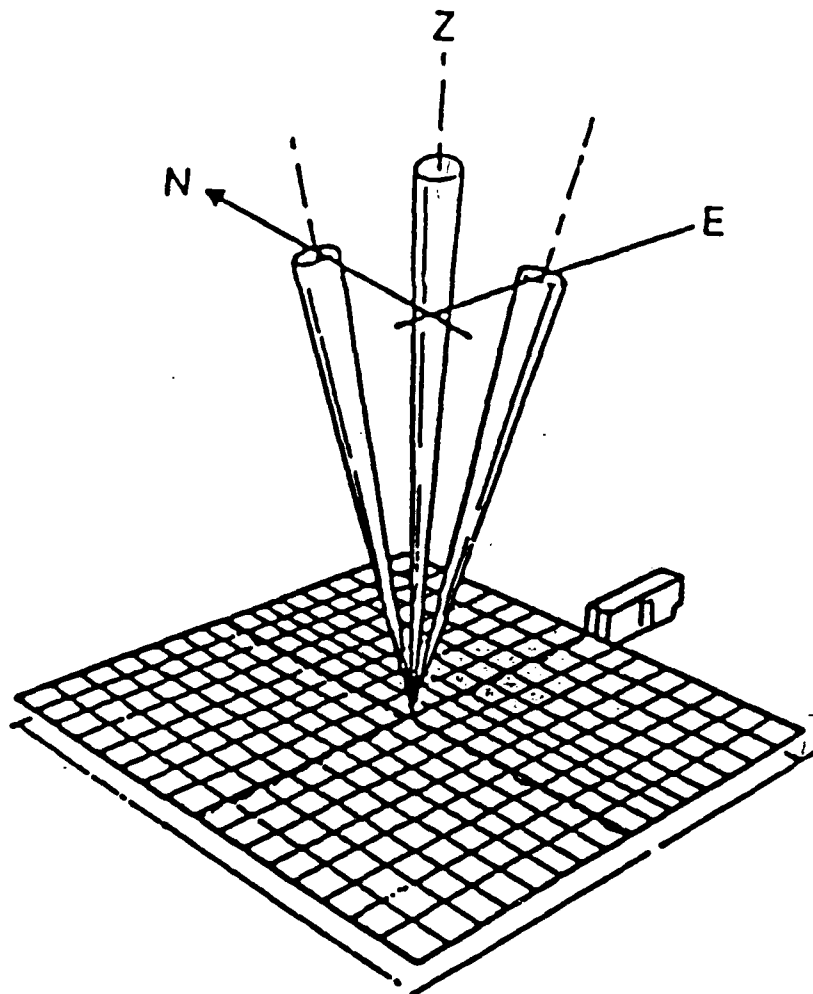


Fig. 1.2. Simple schematic of a three beam Doppler radar wind profiler (Hogg et al., 1983).

$$V_3 = w \quad (3)$$

where  $V_1, V_2$  and  $V_3$  are the radial velocities measured in the east, north and vertical directions, respectively. Winds are assumed to be uniform between the different beams at a given observation height. Solving the above equations for  $u$  and  $v$ , the eastward and northward total wind components, we find that:

$$u = V_1 \sec Z - w \tan Z \quad (4)$$

$$v = V_2 \sec Z - w \tan Z \quad (5)$$

Upon inspection of equations (4) and (5), it is easy to see that a large component of any vertical motion would be added to the estimates of  $u$  and  $v$  - especially since  $Z$  is usually chosen to be 75 degrees. To ensure accurate estimates of  $u$  and  $v$ , vertical velocity must either be measured directly by a third, vertically oriented beam or assumed to have an average value of zero through a sufficiently long time interval (typically one hour).

When horizontal uniformity is assumed across the space separating the profiler radar beams, errors proportional to the first spatial derivatives of the three total wind components are introduced (Strauch et al., 1984). Other sources of possible error are discussed in Chapter II.

### 1.3 Overview

The goal of this study is to derive believable kinematic vertical velocity fields through the depth of the troposphere using wind profiler data. Subsequent chapters will contain details of the process used to obtain this goal.

To balance the desire for upper tropospheric profiler data with the reality of highly unreliable or gappy data at these levels, a 13 kilometer ceiling was chosen as the top of the data domain for all three data sets after inspection of the PRE-STORM data archives.

Since divergence calculations are extremely sensitive to wind errors, a rigorous quality control scheme was adapted for use from the plethora of quality control tests developed for profiler data by Brewster and Schlatter (1986; 1988). While objective quality control was the goal here, several subjective quality control decisions were made in two of the three data sets to simulate the large number of passes of the quality control scheme that would have been necessary to eliminate all of the spurious data points from the Norman profiler time series in these data sets. A detailed discussion of the quality control techniques used in this study is contained in Chapter III.

The quality controlled data fields (vertical time sections) were then objectively analyzed onto 200 meter by half-hour grids (except for Norman fields, which contained

hourly data only). A two-pass Barnes objective analysis (OBAN) scheme discussed by Koch et al. (1983) was used after a time-to-space conversion was performed. Compatibility with the Barnes weight and response functions in two spatial dimensions was thus achieved. Further discussion of OBAN methods used for this study is contained in Chapter IV. The final data processing steps prior to kinematic analysis were the conversion of the half-hourly McPherson and Liberal profiles into hourly profiles and the interpolation of all time series onto pressure surfaces.

Using a line integral method, horizontal divergence and vorticity are calculated for the triangle at all points on the final p-t grids. After adjustment by a linear technique, upward integration is performed on these divergence fields to obtain kinematic vertical motion fields with the same grid resolution. A more detailed discussion of these calculations exists in Chapter IV.

## CHAPTER II

### DATA SETS AND WEATHER SUMMARIES

#### 2.1 General Comments

To test the methodology developed in this study, several wind profiler data sets containing minimal temporal gaps were sought. These data sets would have to be of sufficient length to verify features in the final kinematic vertical velocity fields with phenomena seen in satellite photos and on weather charts. Since the goal of this study was to derive kinematic fields from near ground level to tropopause height, potential data sets with a profiler time series exhibiting good temporal continuity but having no data above, say, eight kilometers were not used.

Owing to the numerous large temporal gaps in the McPherson wind profiler data archive, only a few data sets could be created of acceptable length ( $> 10$  hours). Table 2.1 provides a list of the available hours of simultaneous profiler operation during the PRE-STORM experiment with the three chosen data sets highlighted by lines of asterisks.

Because of the time necessary to switch a profiler

## POSSIBLE TRIANGLE COMPUTATION TIMES

THE FOLLOWING IS A LIST OF CONSECUTIVE OBSERVATION TIMES FOR  
SIMULTANEOUS PROFILER OPERATIONS DURING THE MAY AND JUNE 1985  
KANSAS-OKLAHOMA PRE-STORM EXPERIMENT.

<u>JULIAN</u> <u>DATE</u>	<u>CALENDAR</u> <u>DATE</u>	<u>HOURS (GMT)</u>	<u>CONSECUTIVE</u> <u>HOURS</u>	<u>COMMENTS</u>
130	10 MAY	1700	1	
		2000-2100	2	
132	12 MAY	0100-0500	5	
		2100	1*****	12 HOURS IF
		2300	1*****	2200 MCP AND
133	13 MAY	0000-0600	7*****	0700 MCP
		0800	1*****	FILLED
146	26 MAY	1900	1	
147	27 MAY	0000	1	
		0700-0900	3	
148	28 MAY	2300	1	
149	29 MAY	0300	1	
		0600-1100	6	
		1300-1500	3	
154	3 JUN	0000-0500	6	
		1900-2300	5*****	17 HOURS IF 0100
155	4 JUN	0000	1*****	NOR FILLED
		0200-1100	10*****	
165	14 JUN	1500-2100	7	
170	19 JUN	1500-1700	3	
172	21 JUN	1600-1800	3	
		2100	1	
176	25 JUN	1800-1900	2	
177	26 JUN	2200	1*****	12 HOURS IF 2300
178	27 JUN	0000-0400	5*****	MCP AND 0500-0700
		0800-0900	2*****	NOR FILLED
		1700	1	

NOR = NORMAN PROFILER  
MCP = MCPHERSON PROFILER  
LIB = LIBERAL PROFILER

Table 2.1. Times for simultaneous PRE-STORM profiler operation. Chosen data sets are highlighted by lines of asterisks.

antenna from transmit to receive mode, data are available only above, roughly, 1.5 kilometers above ground level (AGL). To obtain a crude approximation of the boundary layer, half hourly (or hourly for Norman) surface data from the closest PRE-STORM meso-network surface station to each profiler site were incorporated into the data sets. This presents a source of error in that a) the closest meso-network surface stations are five to twenty five kilometers from profiler sites, and b) profiler wind observations are derived from hourly or half-hourly consensus averages while surface meso-network wind observations are derived from two minute averages ending on the hour or half hour. No attempt was made in this study to correct for these differences. However, since the surface meso-network provided surface data continuously throughout the duration of the three chosen data sets, a decision was made to use data from this source.

## 2.2 3-4 JUNE

The longest of the three data sets is the 1900Z, 3 June to 1100Z, 4 June time series, representing 17 hours of almost continuous data. Only the 0100Z, 4 June profile from the Norman profiler is missing. Figures 2.1 through 2.3 show the raw horizontal winds obtained by the McPherson, Norman and Liberal profilers during this time span. Height

## RAW MCPHERSON DATA

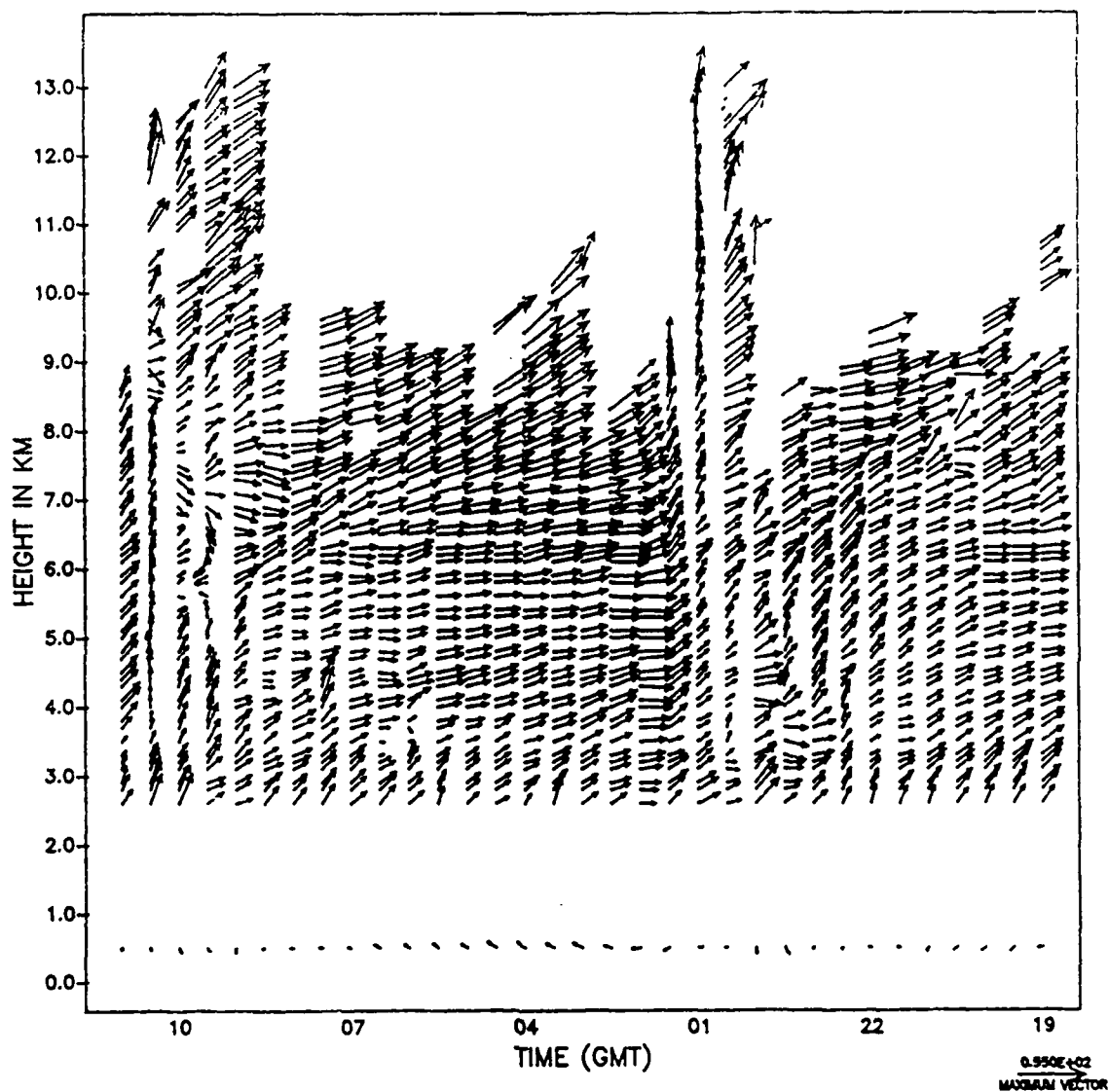


Fig. 2.1. "Raw" McPherson profiler data for 3-4 June. Time, in hours, increases from right to left. Height is in units of kilometers. Scale vector length is shown in lower right corner.

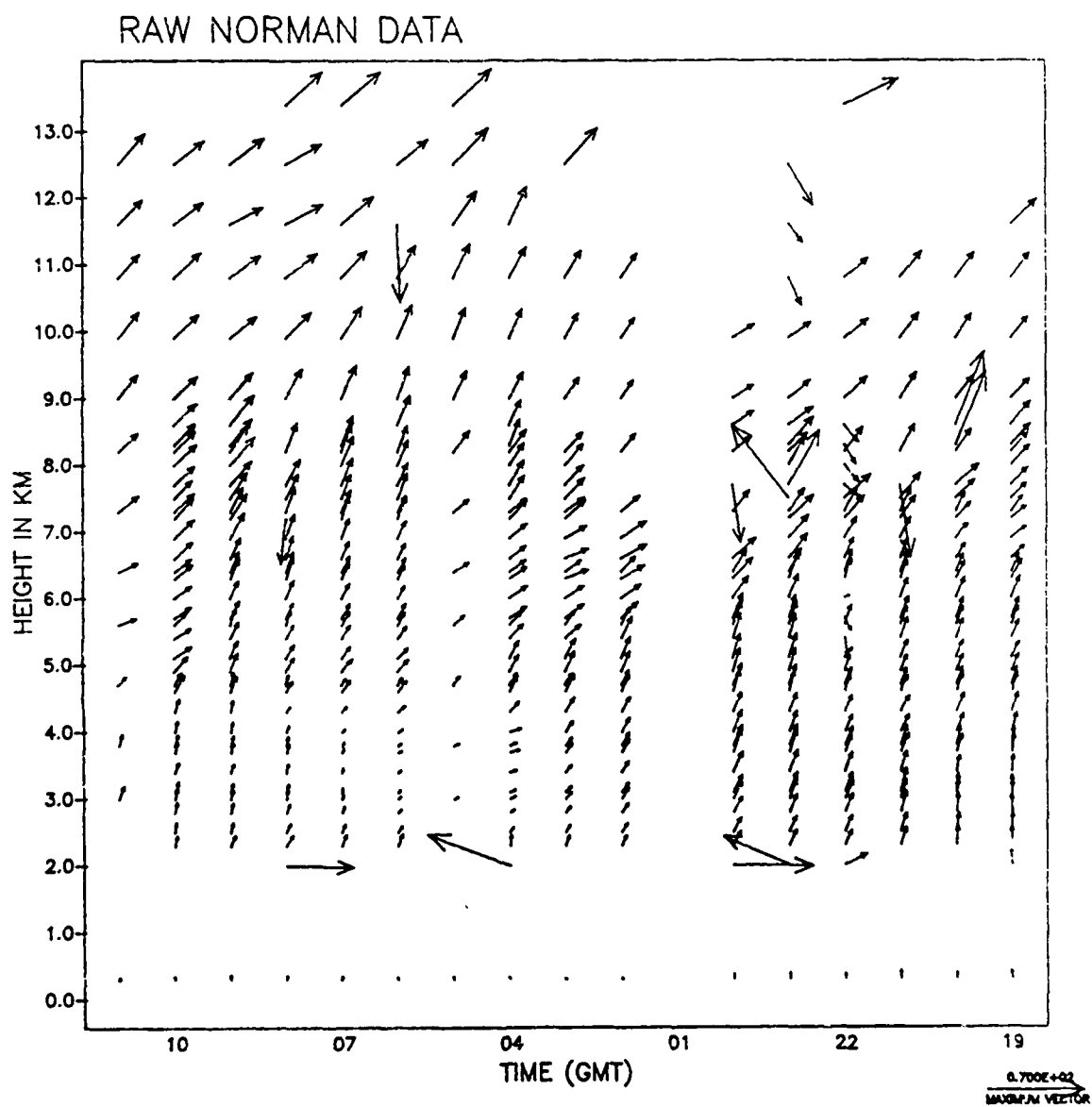


Fig. 2.2. Same as 2.1. but for 3-4 June Norman.

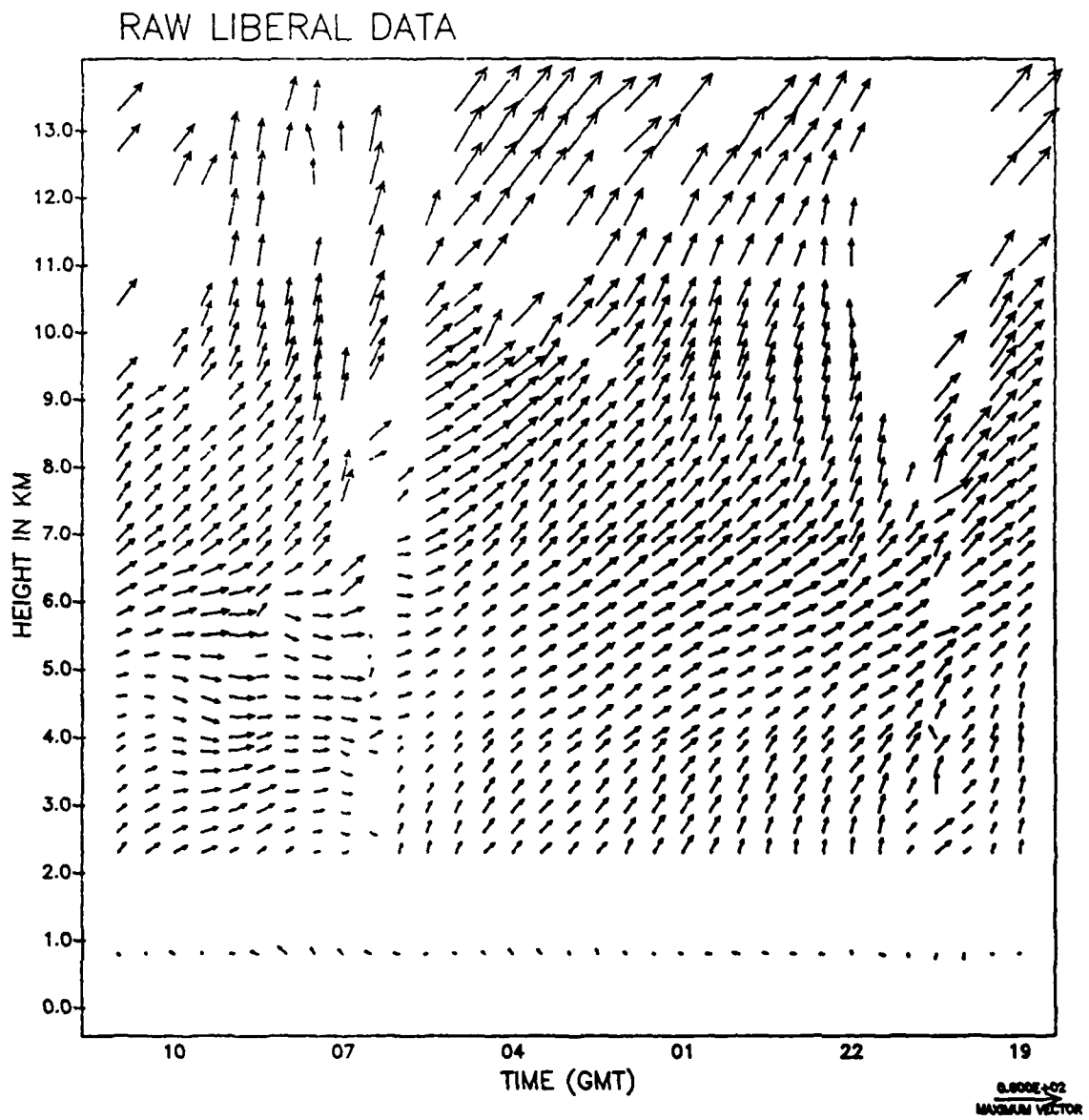


Fig. 2.3. Same as 2.1. but for 3-4 June Liberal.

is in kilometers above sea level (ASL) and time increases from right to left. The length of the reference vector in the lower right of each figure represents the wind speed scale.

On Monday morning, 3 June, a frontal system was stalled over Oklahoma with a surface low located in eastern New Mexico. Scattered showers were occurring along the front and patchy fog areas were indicated in western Oklahoma and southwest Kansas (Fig. 2.4). Moisture advection was already well established at the surface throughout Oklahoma and all but western Texas. Appreciable warm air advection was apparent at 850 mb throughout the Texas Panhandle and western sections of Oklahoma and Kansas. By evening, the 850 mb flow had backed enough in the southern plains to allow deep moisture advection into east Texas and Oklahoma (Fig. 2.5). A closed 500 mb low at the base of a trough existed in southern Arizona, placing the southern plains in a southwesterly flow pattern at mid and upper levels.

The first thunderstorms during this time period fired along the Kansas-Oklahoma border, just east of Liberal, around 1930 GMT as indicated by satellite imagery (Fig. 2.6). Liberal profiles around this time (see Fig. 2.3) indicated south-southwesterly winds from 2.3 to about 5.0 km. Veering to southwesterly directions with height is seen above 5.0 km.

The area of activity rapidly blossomed into an MCS which moved east-northeastward along the stalled front while

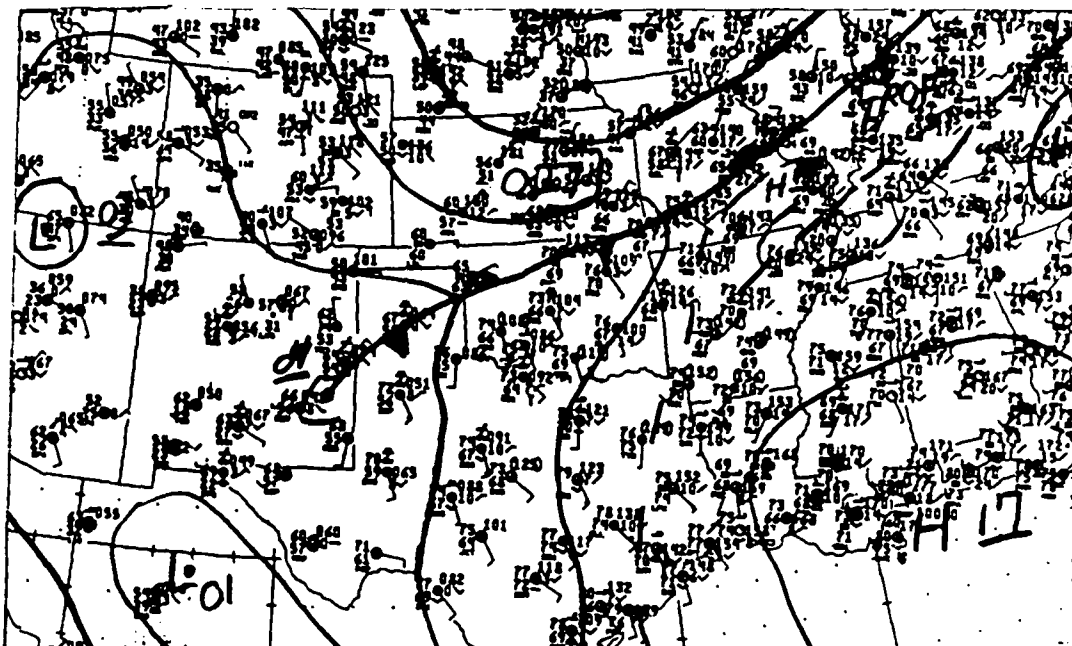


Fig. 2.4. NMC surface analysis for 1200 GMT, 3 June.

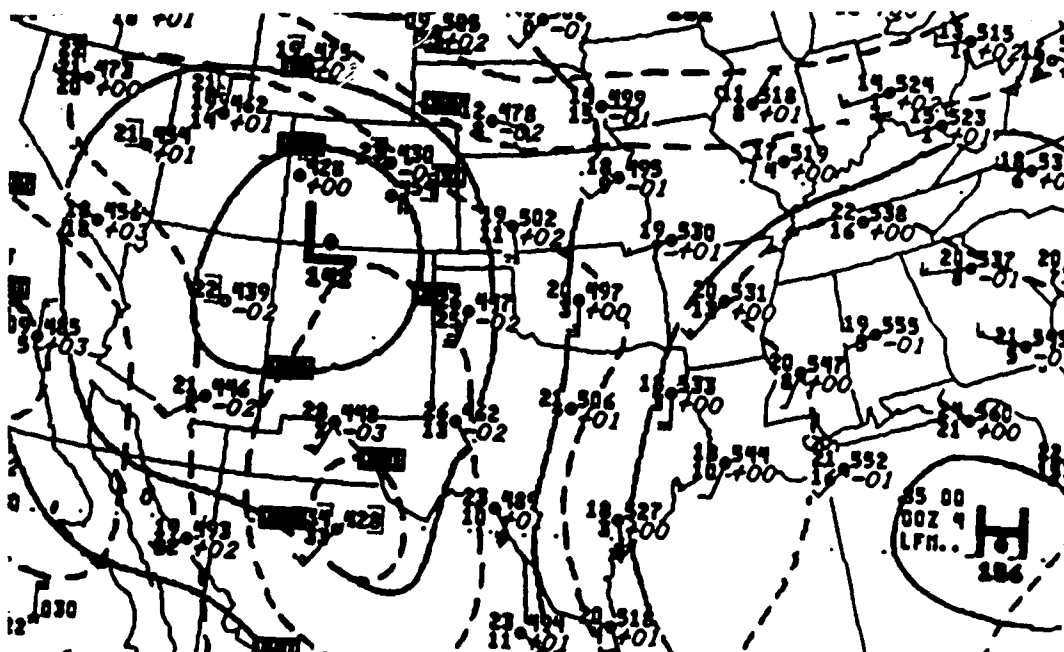


Fig. 2.5. NMC 850 mb analysis for 0000 GMT, 4 June.

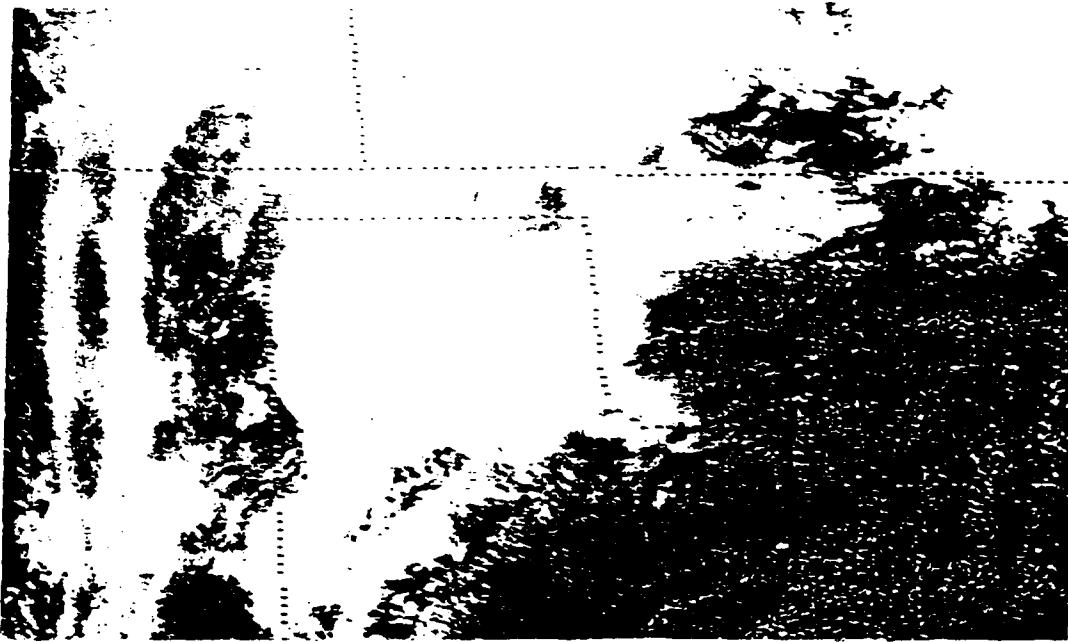


Fig. 2.6. GOES visible imagery at 1930 GMT, 3 June.

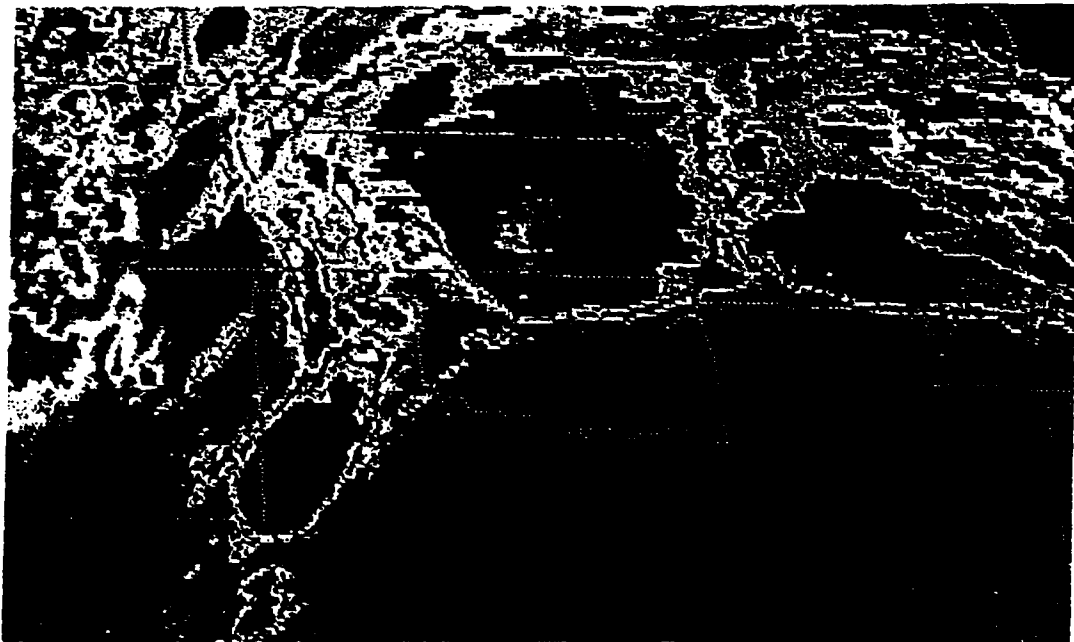


Fig. 2.7. GOES infrared imagery at 0000 GMT, 4 June.

spreading in areal extent into northern Oklahoma by 0000 GMT, 4 June (Fig. 2.7). This MCS eventually produced baseball-size hail at several locations throughout northern Oklahoma and, at 2310 GMT, produced an F1 tornado inside the city limits of Enid, Oklahoma.

As the first MCS was developing and moving through the PRE-STORM profiler triangle, a second area of thunderstorms was developing along the dryline in western Texas northwest of Odessa. It too developed into an MCS and by 0600 GMT (Fig. 2.8) was following a track similar (although slightly more southerly) to the first one into the profiler triangle. At Liberal, winds below 5.0 km veered from southwesterly to westerly with time between 0500 and 0700 GMT. Backing with height is evident above 6.0 km after 0530 GMT. By 0900 GMT (Fig. 2.9), the second MCS had cleared the profiler triangle leaving only scattered areas of unorganized convection within it.

Each profiler time series in this data set presented very different quality control and analysis problems. Of the three, only the time series from the Liberal profiler requires little or no quality control. In Chapter III it will be shown that, for all three data sets, the fewest observations eliminated in the quality control process were from the Liberal profiler time series.

The McPherson profiler time series contains no missing profiles but does contain significant gaps above, roughly, nine kilometers. Although suspect owing to possible

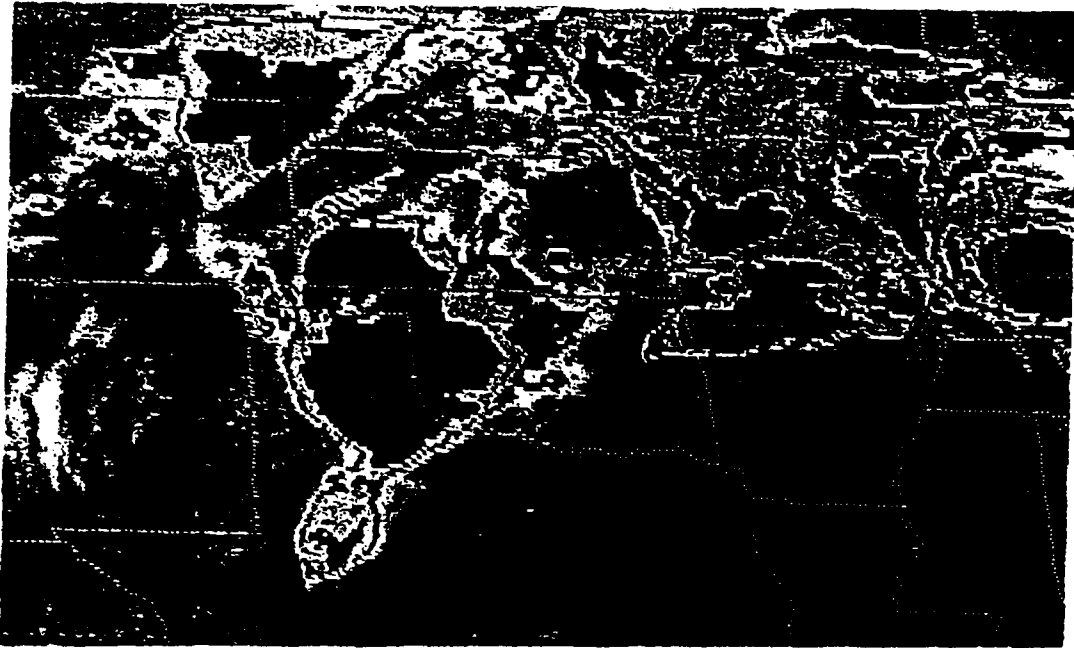


Fig. 2.8. Same as 2.7. but at 0600 GMT, 4 June.

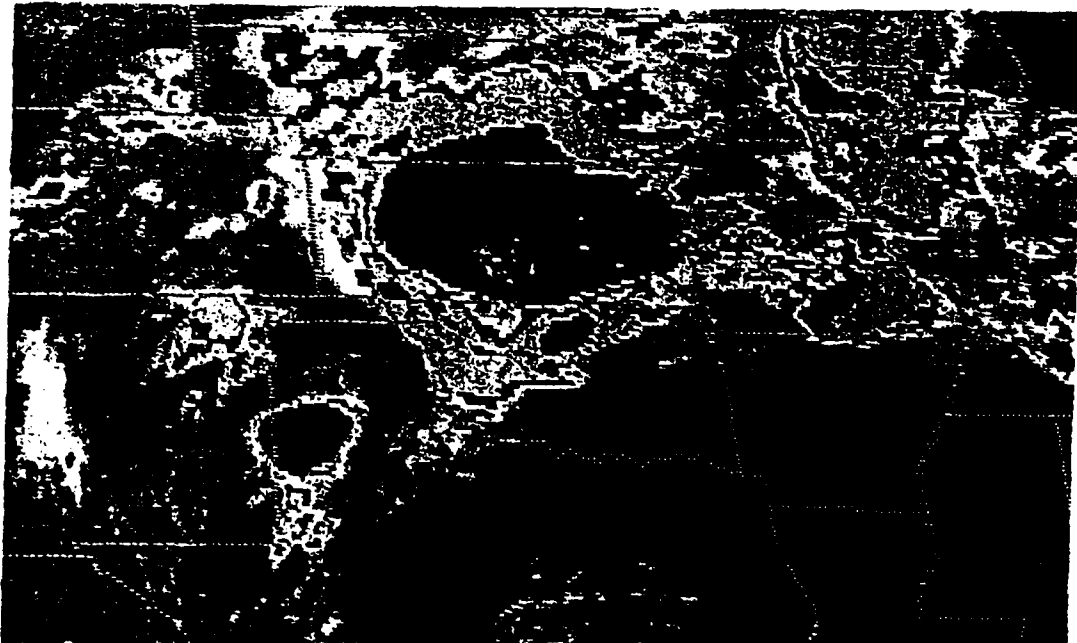


Fig. 2.9. Same as 2.7. but at 0900 GMT, 4 June.

precipitation contamination, it was by virtue of the 0030Z and 0100Z profiles that this entire data set wasn't rejected for use in this study. These two profiles, along with others near the end of this time series, provide enough data in the upper troposphere to attempt gap-filling through objective analysis.

The McPherson profiler provides the highest data density of the three time series in this data set. This characteristic provides an advantage and a disadvantage for purposes of quality control. The advantage is that more quality control tests can be performed within a profile with one quality control pass. The disadvantage is the greater possibility of correlated errors, which are more difficult to eliminate through an objective quality control process.

While the Norman profiler time series for this data set contains very few sizable data gaps, a moderate amount of spurious data points exists. These data points, however, clearly stand out against the remaining field, making an objective quality control procedure most appropriate for this time series.

### 2.3 12-13 May

This data set contains profiles from 2100Z, 12 May to 0800Z, 13 May 1985 (Figs. 2.10-2.12). The only missing data are the 0630Z and 0700Z profiles from the McPherson profiler

## MCPHERSON DATA (12-13 MAY)

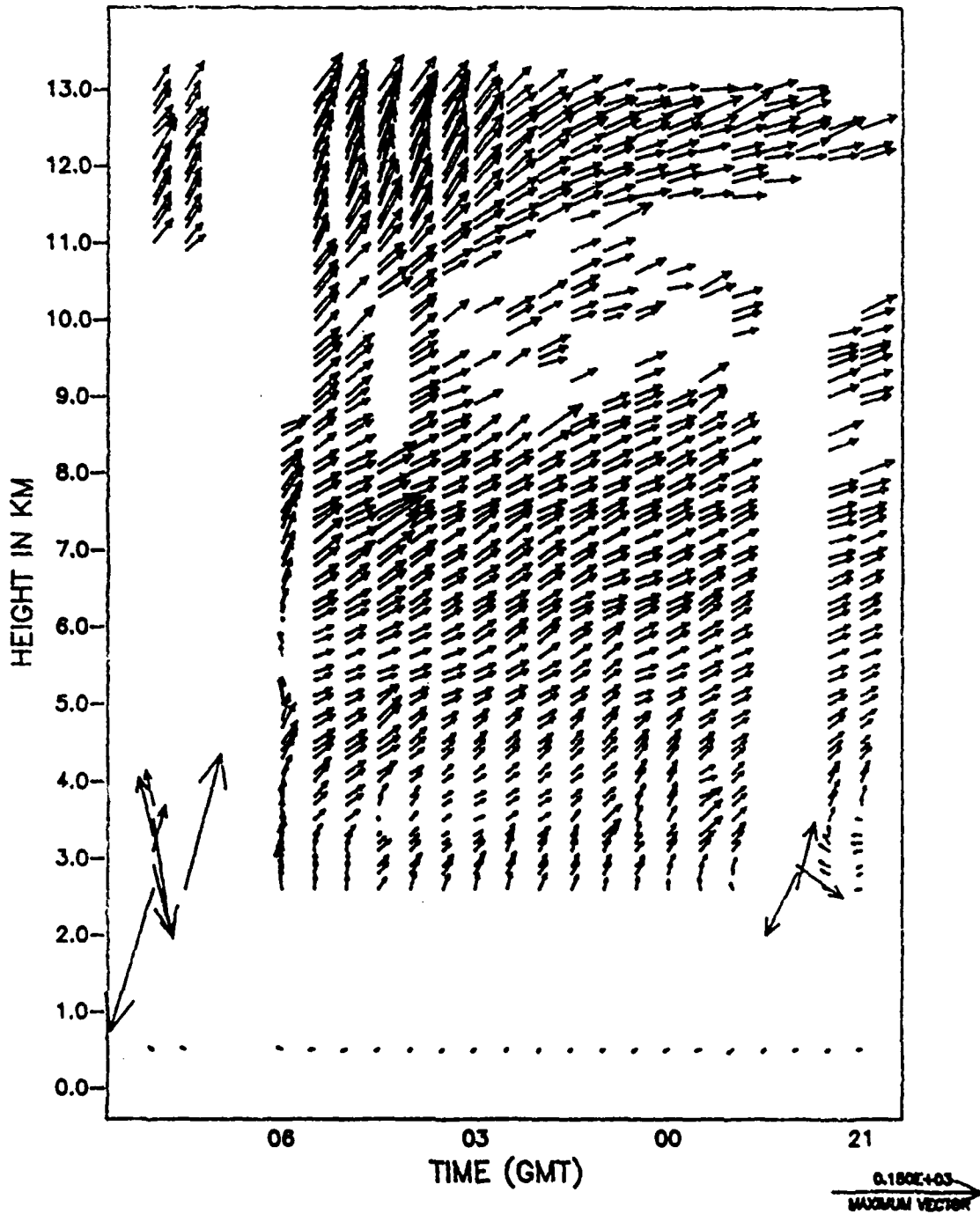


Fig. 2.10. "Raw" McPherson profiler data for 12-13 May.

## NORMAN DATA (12-13 MAY)

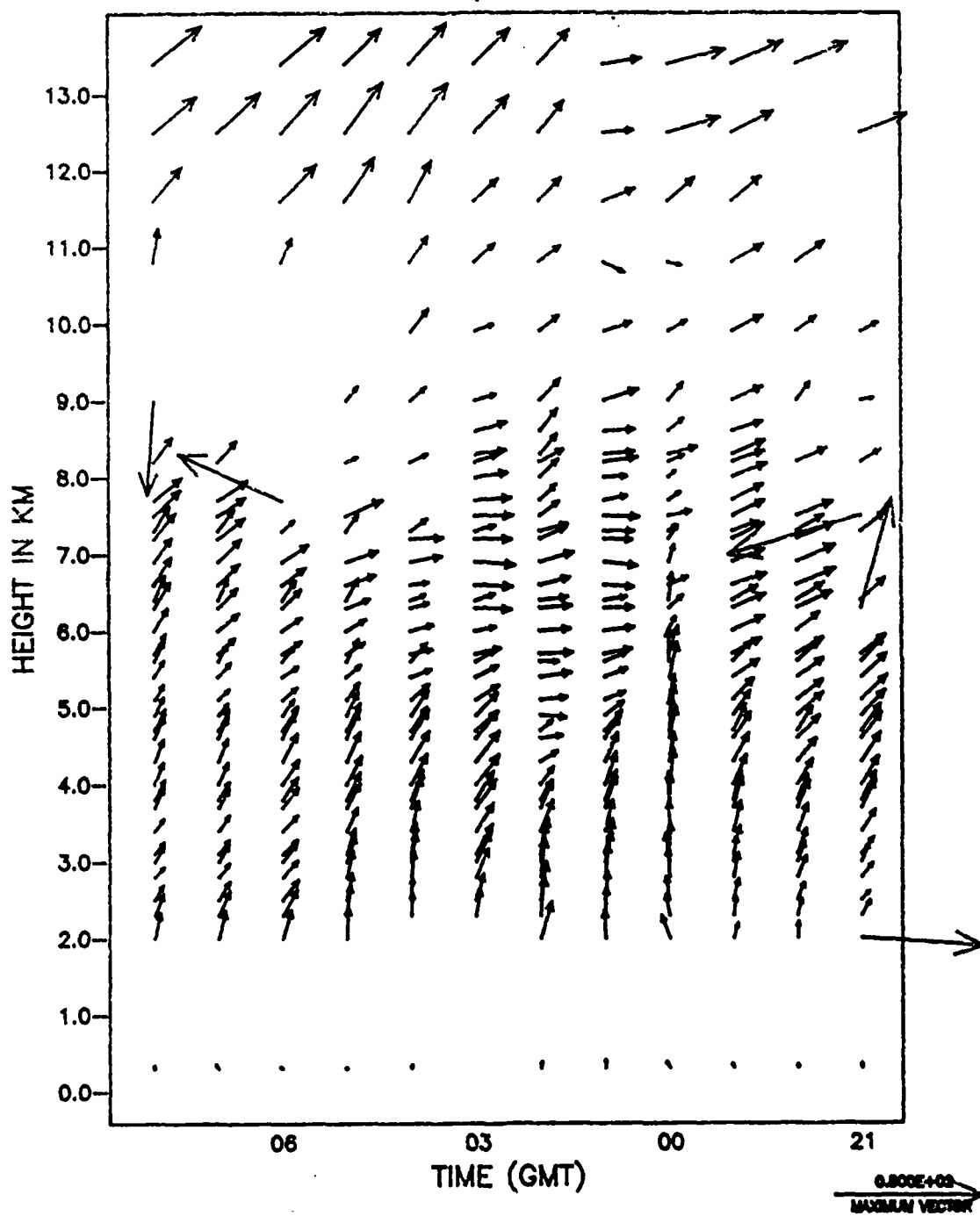


Fig. 2.11. Same as 2.10. but for 12-13 May Norman.

## LIBERAL DATA (12-13 MAY)

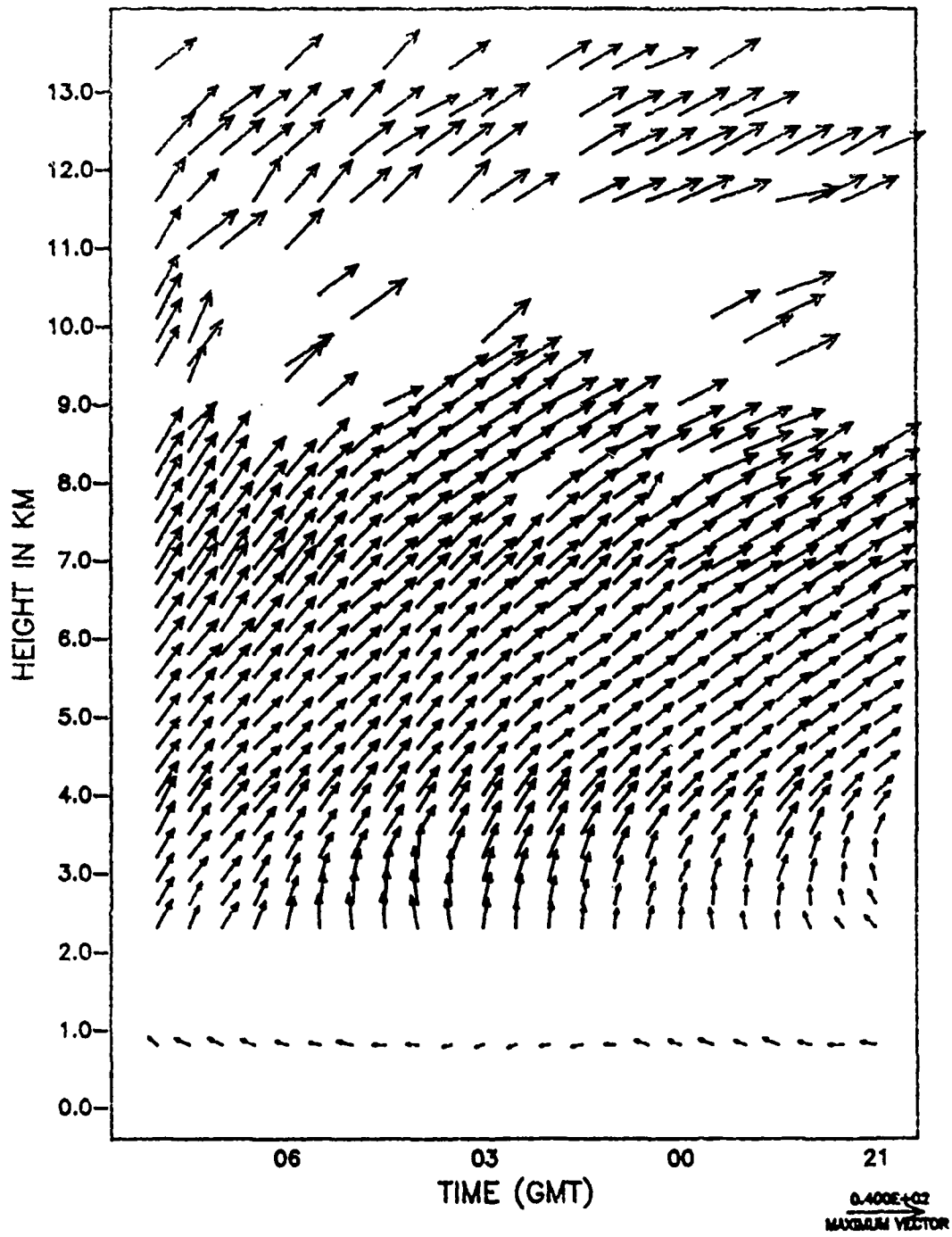


Fig. 2.12. Same as 2.10. but for 12-13 May Liberal.

time series. This data set and the 26-27 June data set are both twelve hours in length.

On Sunday morning, 12 May, a frontal system had stalled across Oklahoma and a surface low was situated in the central Texas Panhandle. A weak stationary front extended south-southwestward from this low into west Texas. Dominating the 500 mb level (Fig. 2.13) in the western two-thirds of the U.S. was a deepening long wave trough extending through the central Rockies and into southwest Arizona. A shortwave trough was indicated in the Texas Panhandle. Profiler data in Figs. 2.10 through 2.12. show that, above about 4.0 km, the flow was predominantly from the southwest over Oklahoma throughout the period. Winds at 850 mb (from NMC analysis not shown in this chapter) were initially from the southwest in Oklahoma and eastern Texas but by mid-afternoon had backed to south and southeasterly directions, allowing deep moisture advection into these regions.

By 2100 GMT, satellite imagery (Fig. 2.14) showed that deep convection had fired along a dryline located east of the stationary front in western Texas. This activity developed further until, by 0000 GMT, 13 May (Fig. 2.15), an area of thunderstorms extended along a rough southwest to northeast line from Abilene, Texas to just northeast of Oklahoma City. Norman profiler data (Fig. 2.11) indicated southerly flow below 4.5 km veering to westerly above 4.5 km. Around this time, two-inch diameter hail was reported

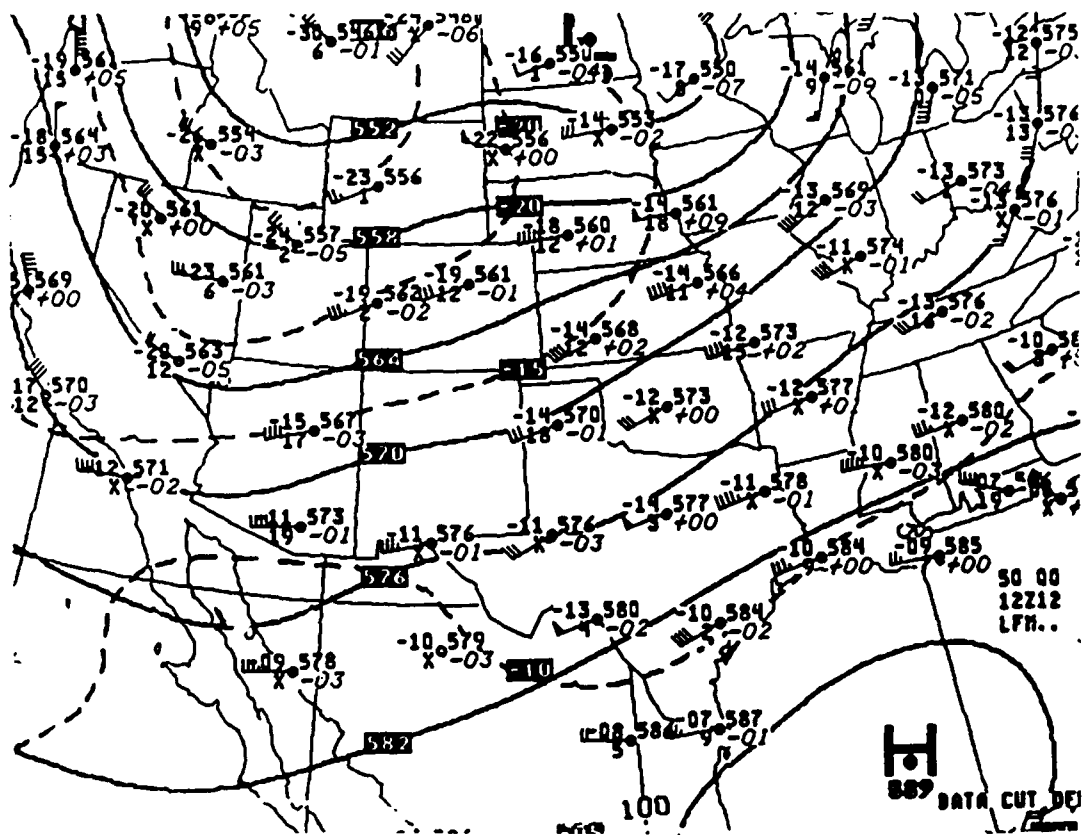


Fig. 2.13. NMC 500 mb analysis for 1200 GMT, 12 May.

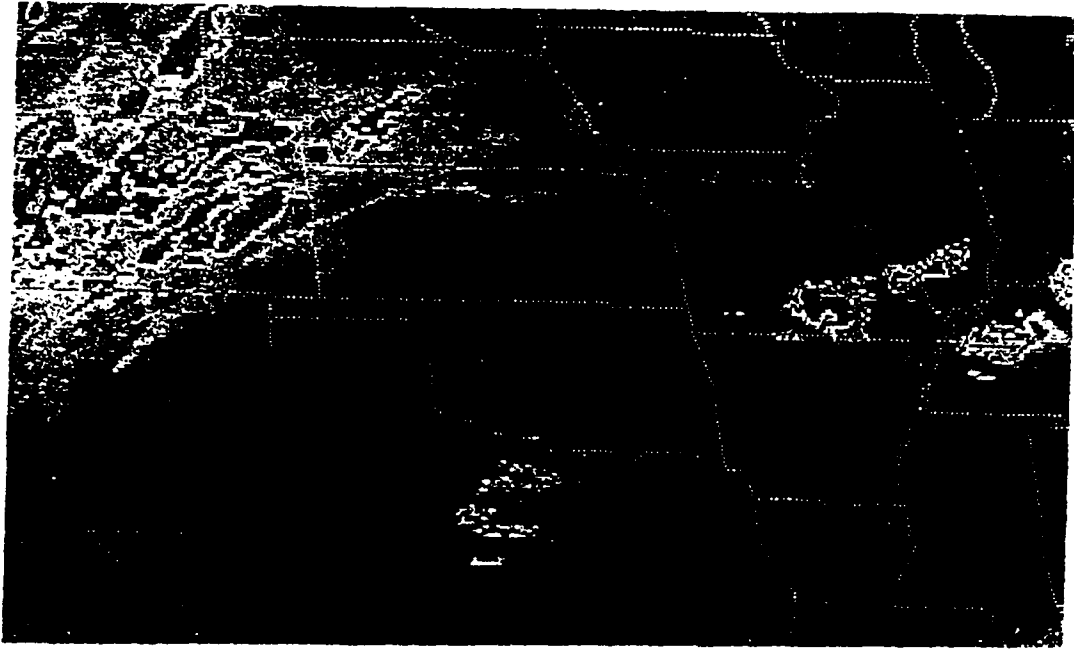


Fig. 2.14. GOES infrared imagery at 2100 GMT, 12 May.

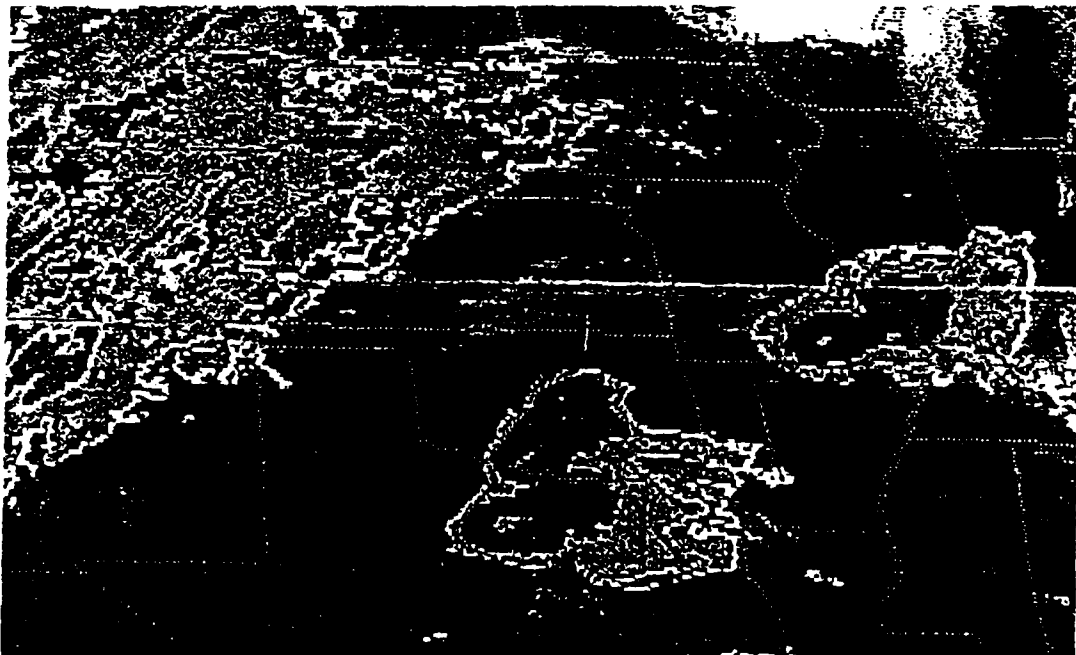


Fig. 2.15. Same as 2.14. but for 0000 GMT, 13 May.

in Moore and a weak (F0) tornado had been spotted two miles south of Seward, Oklahoma. This area moved to the north-northeast as it became more organized until, by 0400 GMT (Fig. 2.16), an MCS had been formed in northeast Oklahoma. Also indicated at this time was the development of thunderstorms in southeastern Colorado and western Kansas. This activity increased in areal coverage as it moved eastward until central Kansas was affected as well by 0830 GMT (Fig. 2.17).

Highly questionable data points exist in the McPherson time series mainly below three kilometers and are most pronounced at 2200Z, 12 May and 0730Z and 0800Z, 13 May. Large gaps exist in these profiles above these data points up to around eleven kilometers ASL.

The time series from the Liberal profiler, as in the 3-4 June data set, is well behaved with no missing profiles and very few data points of questionable quality.

Unlike the other two profilers during the PRE-STORM experiment, the one at Norman used two pulsewidths; 3.7 and 9.7  $\mu$ sec. The former was used to collect data from 1.97 to 8.61 km while the latter was used to collect data from 2.98 to 17.71 km. This resulted in a sizable overlapping of coverage in the vertical (Hermes, 1988). While this "blending" of data created rather smooth profiles in the 3-4 June data set, it is apparent that the short and long pulse data don't mesh well here. This problem is dealt with in Chapter III. No profiles are missing from the Norman time

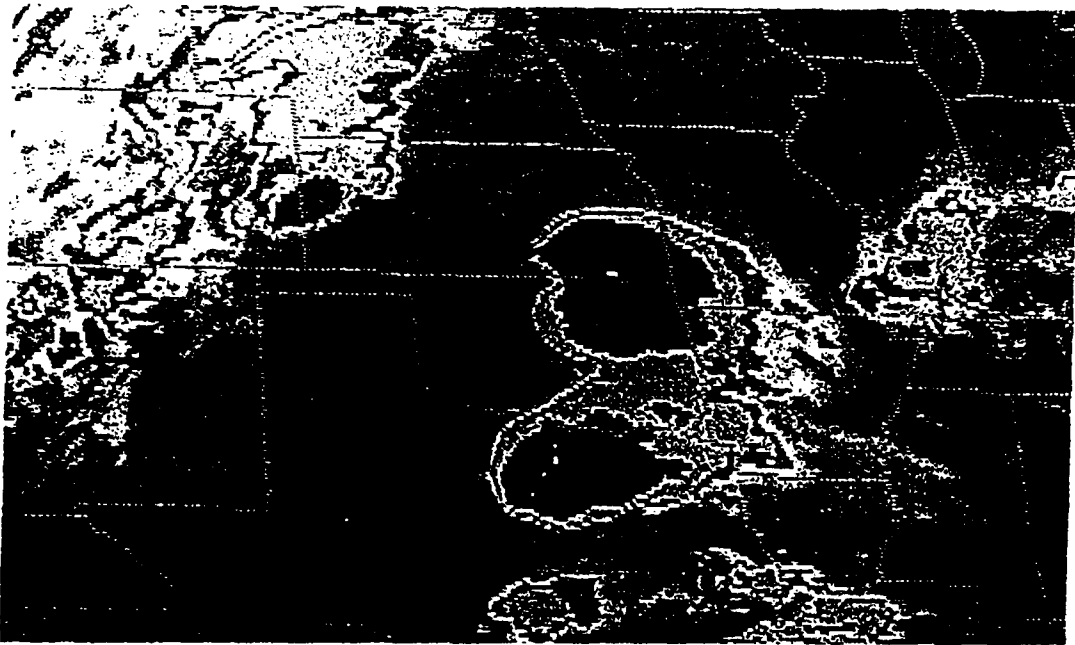


Fig. 2.16. Same as 2.14. but for 0400 GMT, 13 May.

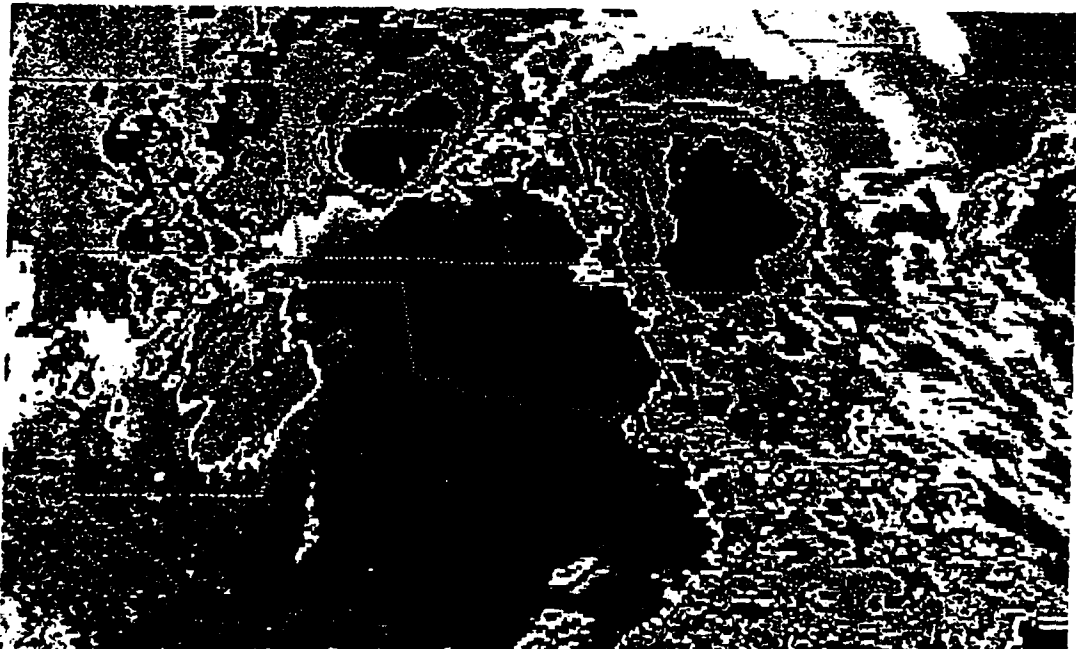


Fig. 2.17. Same as 2.14. but for 0830 GMT, 13 May.

series and, as with the 3-4 June data, the poorest data points clearly stand out against the "good" data field.

#### 2.4 26-27 June

This data set begins at 2200Z, 26 June and ends at 0900Z, 27 June 1985 (Figs. 2.18-2.20). Of the three data sets, this one contains the highest amount of missing profiles, bad data and data gaps. The largest data gap occurs in the Norman time series where three consecutive profiles are missing, 0500Z, 0600Z and 0700Z, 27 June. The 2300Z and 2330Z, 26 June profiles are missing from the McPherson time series as is the 0730Z, 27 June profile. The McPherson time series shows evidence of possible precipitation contamination most notably in the 0030Z and 0100Z, 27 June profiles.

During the afternoon and evening of 26 June, a slow-moving cold front extending from Minnesota to western Texas moved through Oklahoma producing mostly "garden variety" thunderstorms along its convergence zone as it passed. The 2100 GMT surface analysis from NMC (Fig. 2.21) indicated an abundance of surface moisture ahead of this front with southeasterly flow in eastern Texas and southeastern Oklahoma. As one might expect, profiler data in Figs. 2.18 through 2.20 show backing winds with height below four kilometers for the entire period at Liberal,

## MCPHERSON DATA (26-27 JUN)

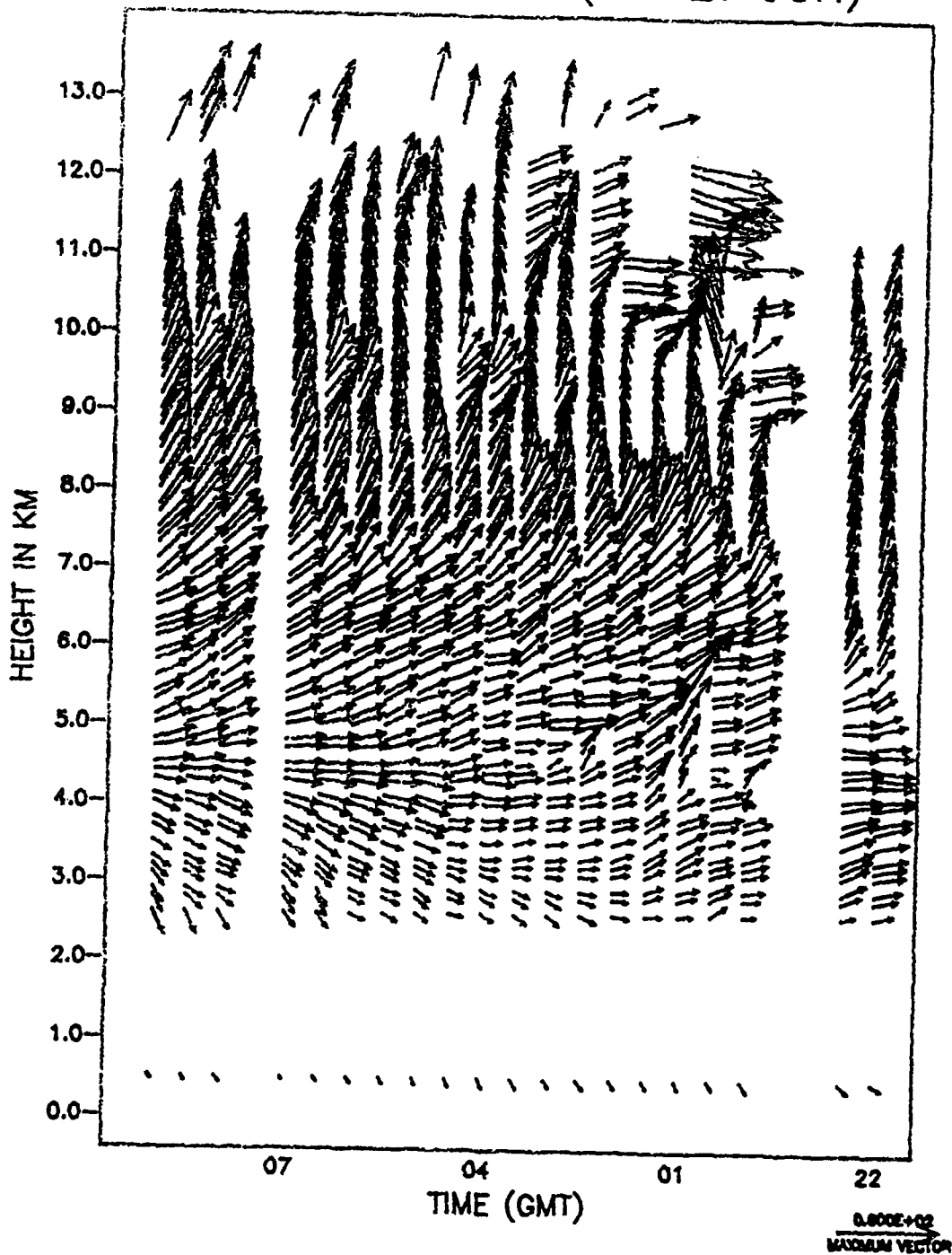


Fig. 2.18. "Raw" McPherson profiler data for 26-27 June.

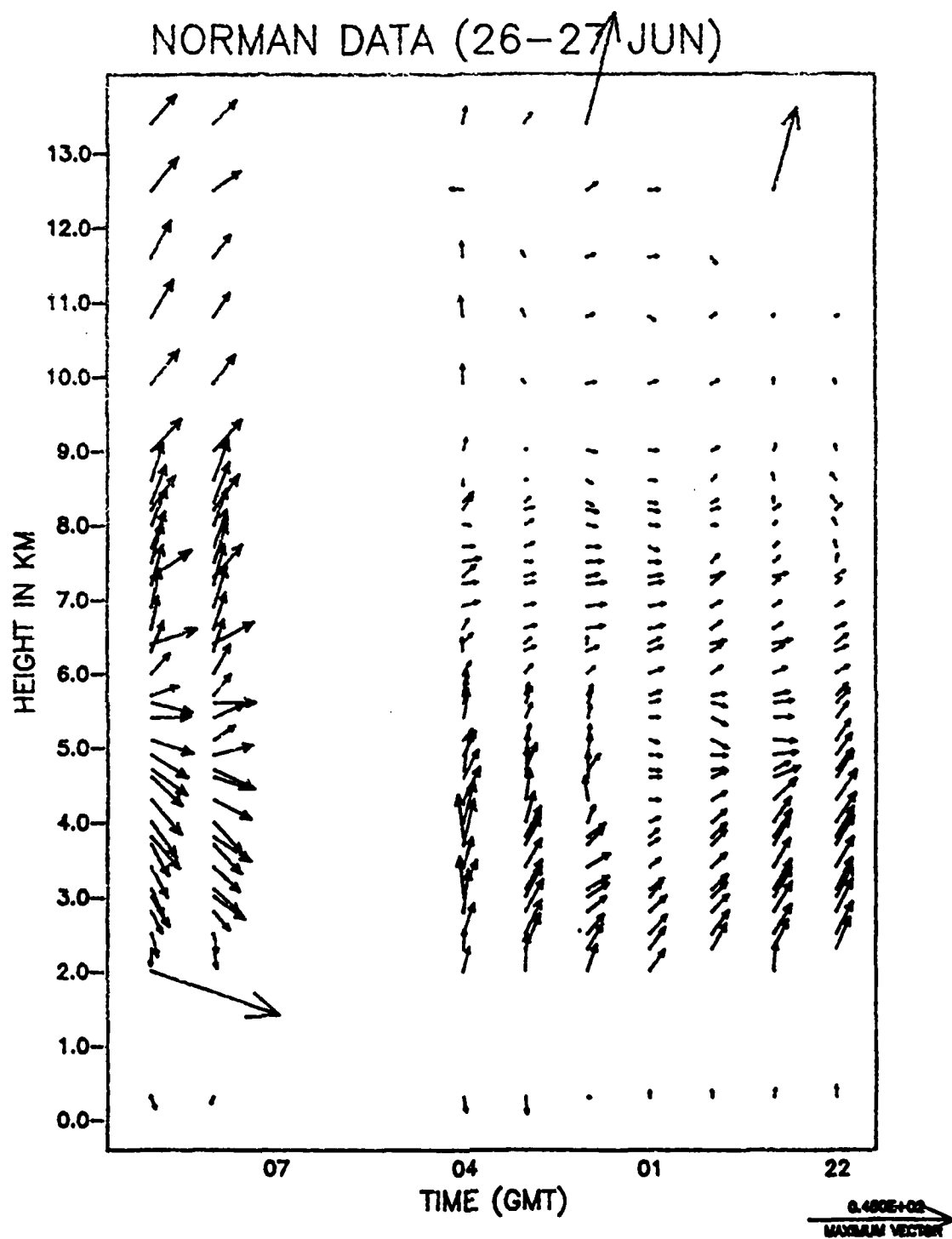


Fig. 2.19. Same as 2.18. but for 26-27 June Norman.

## LIBERAL DATA (26-27 JUN)

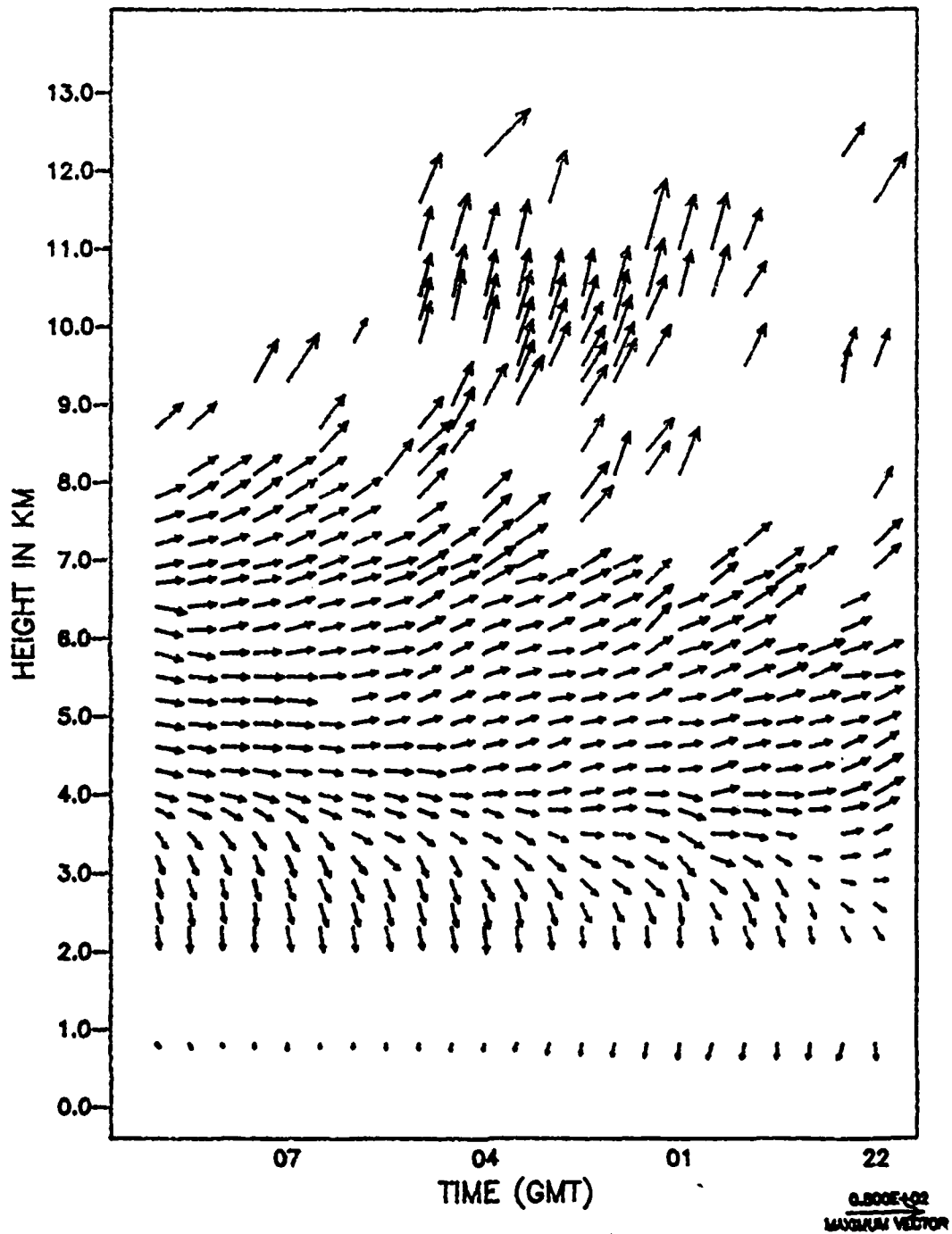


Fig. 2.20. Same as 2.18. but for 26-27 June Liberal.

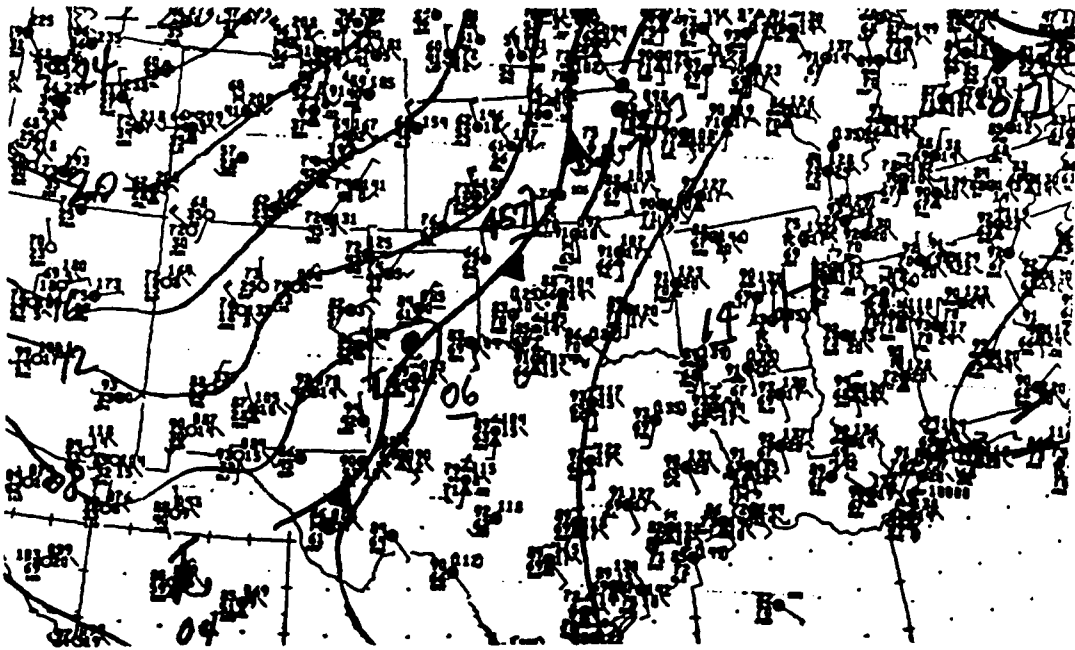


Fig. 2.21. NMC surface analysis for 2100 GMT, 26 June.

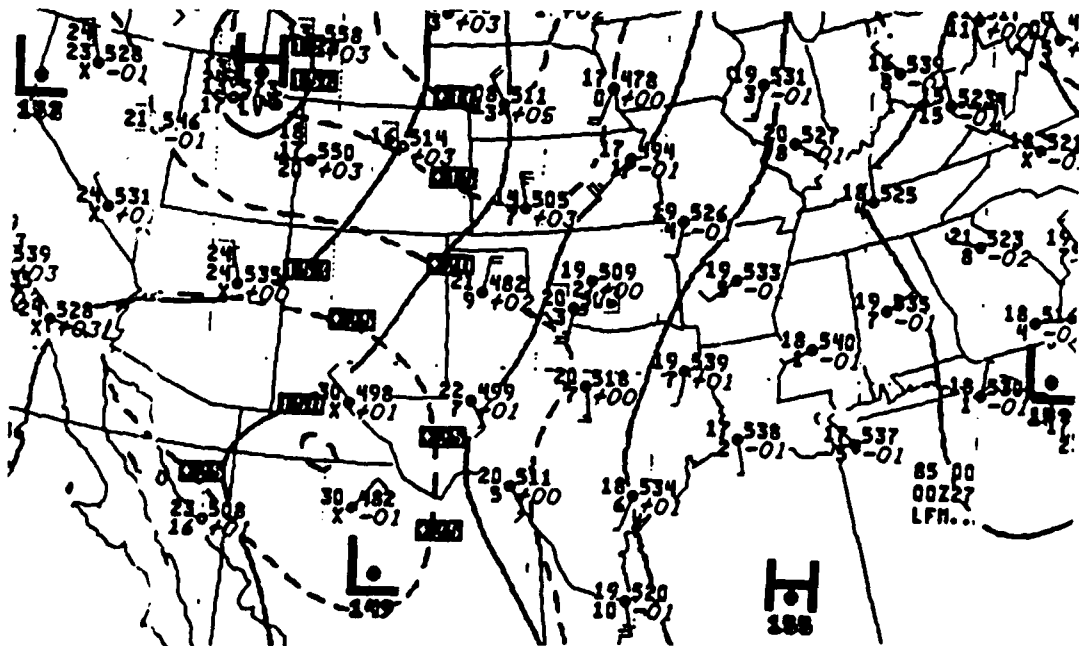


Fig. 2.22. NMC 850 mb analysis for 0000 GMT, 27 June.

after 0100 GMT at McPherson, and after 0400 GMT at Norman (ie. cold air advection behind a cold front moving from northwest to southeast across the region).

The 0000 GMT, 27 June 850 mb analysis (Fig. 2.22) indicated neutral temperature advection in this region along with near-saturation moisture levels. Very weak flow at 500 mb was evident over the southern plains (Fig. 2.23).

At the beginning of this time period, satellite photography indicated thunderstorm activity in central Kansas, western Oklahoma, and central Texas (Fig. 2.24). This activity slowly consolidated into a wide frontal band as it moved southeastward with the front and, by 0100 GMT (Fig. 2.25), virtually dominated the entire profiler triangle. By 0900 GMT (Fig. 2.26), the band-like structure was gone and, except for an area of activity south of Wichita falls, Texas, thunderstorm activity was widely scattered and unorganized along the frontal boundary.

Differences between long and short pulse data in the Norman time series are as evident in this data set as they were in the 12-13 May data set. These differences are most pronounced between five and nine kilometers ASL in the 0800Z and 0900Z, 27 June profiles.

The Liberal time series, again, is well behaved. This is one of the few traits common to all three data sets. Sizable gaps exist, though, above ten kilometers near the end of the time series.

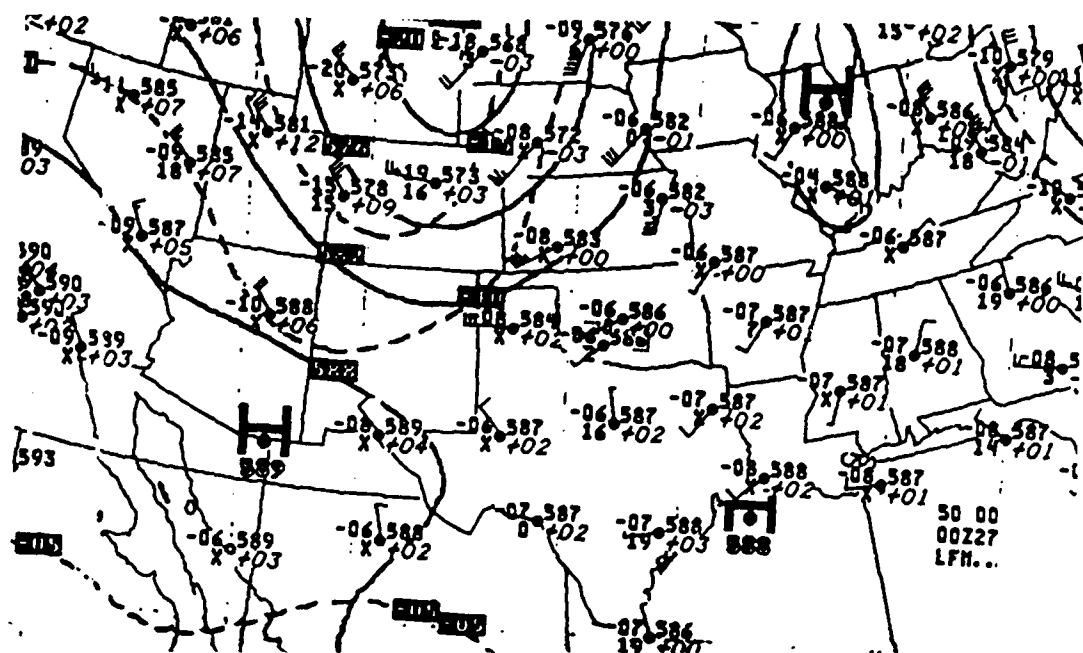


Fig. 2.23. Same as 2.22 but for 500 mb.



Fig. 2.24. GOES infrared imagery at 2200 GMT, 26 June.

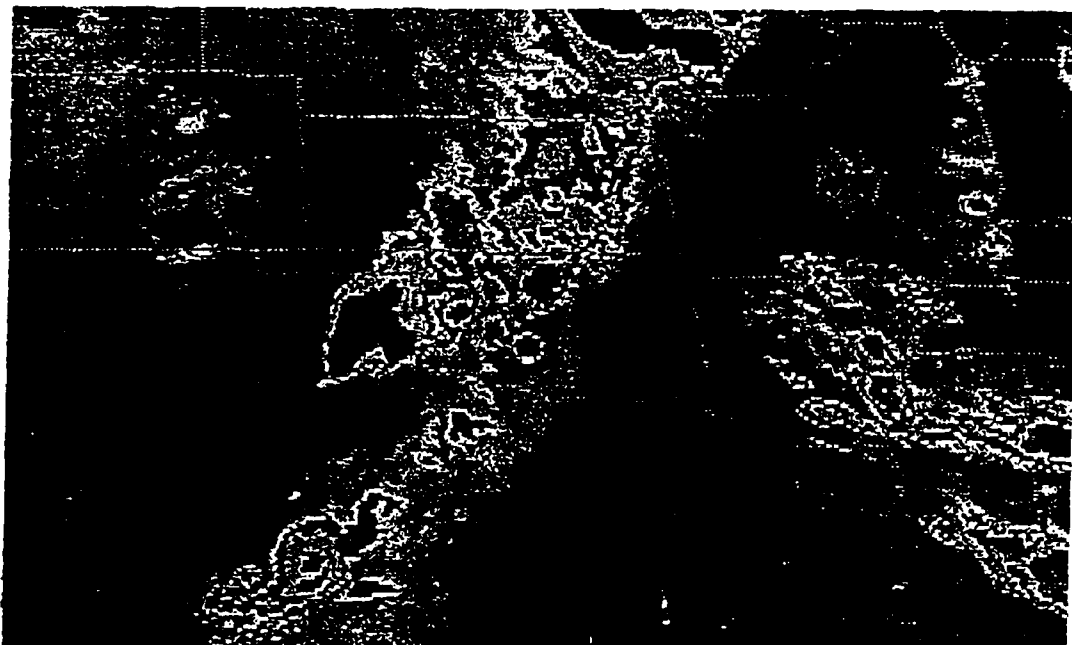


Fig. 2.25. Same as 2.24. but for 0100 GMT, 27 June.



Fig. 2.26. Same as 2.24 but for 0900 GMT, 27 June.

### 2.5 Sources of Error in the Data Sets

While excitement over the many analysis possibilities opened by wind profiler development is high, wind profiler data, like all measurements, are subject to error. Unbiased errors with reasonably small variances around a mean value can effectively be smoothed through objective analysis and can be considered 'acceptable' errors. Of greater concern, however, are the biased error possibilities inherent in the two or three beam wind profiler design. These errors were partially discussed in Chapter I.

The 75 degree elevation angle of the non-vertical profiler radar beams creates a separation between the sample volumes of 0.38 times the height of the volumes. This means that at the top of the profiler data sets used for this study (13 kilometers) the beams are separated by 4.94 km. Non-uniform behavior of the wind across the profiler beams on a scale smaller than five kilometers at a height of 13 kilometers ASL can create non-representative wind measurements at this height. Measuring winds via profilers in a highly convective environment can produce erratic results due to the inherent non-uniformities of such an environment. While it is possible, with appropriate vertical motion adjustment, to obtain accurate wind measurements while precipitation is occurring, non-uniform precipitation across the profiler beams will create

measurement errors. Examples of time series containing these errors are in Van de Kamp's "Principles of Wind Profiler Operation" (1988). In short, a uniform 3-D wind assumption must be made over the beam separation distance during the sample time in order to obtain representative wind measurements.

Spurious targets such as aircraft, birds or even automobile traffic in the main beam or side lobes can show up in a data set. The problem of such targets in a side lobe can be made worse by weak return signals from the main radar beam. Common sense in the selection of a profiler site can help reduce some of these problems. Fortunately, the hour-long consensus averaging technique (see Augustine and Zipser, 1987) helps to eliminate errors of this type.

Other sources of error include internal electronic noise or "ringing" which can occur if transient currents in the profiler antenna array aren't allowed to dissipate after signal transmission before the returned signals arrive. Possible errors due to combining surface meso-network data and profiler data into single data sets have already been discussed.

It should be noted that, although the sources for possible error are recognized, no attempt was made in this study to correct observations through elimination of an "error component" in each observation. If a data point is flagged as spurious during quality control, it is eliminated entirely.

## CHAPTER III

### QUALITY CONTROL

#### 3.1 General Comments

Because of the existence of spurious data in the chosen profiler data sets, a quality control (QC) process is desired. The ultimate goal of this process is to rid ourselves of all bad data. This, in part, would involve comparing a data point with its closest neighbors and, using a set of objective criteria, either retaining or eliminating this point.

Many quality control tests have been developed and used over the years. These tests range from a simple two-standard deviation screen and the various forms of combined median and vertical consistency checks discussed by Brewster and Schlatter (1986) to complex quality control (CQC) as discussed by Gandin (1988). The two-standard deviation screen, while computationally fast, is biased since spurious data and outliers in the data set are included in the calculation of the standard deviation of the data set. This process was thus rejected in favor of one

similar to Brewster and Schlatter (1986).

In a sense, any quality control process acts as a filter of sorts. For example, the nine-point median QC check using a "centered" template is very similar to the non-linear median filter discussed by Brock (1986). The median QC test used here, however, doesn't replace a failed data point with the median value of its neighbors as suggested by Brock (1986). With the median QC check, the "bad" data are simply removed and any spaces or "holes" created by the removal of failed data are filled using an objective analysis or other filling scheme further along in the data processing. The emphasis of the QC process used for this research is data "screening" and not data filtering. Filtering of data for the purpose of removing high frequency oscillations is considered separately and, as will be seen, is inherent in the objective analysis scheme to be used.

### 3.2 Median Check

The median check involves comparing a data point with the median of its eight closest neighbors (Fig. 3.1). If the data point value lies outside an envelope described by a threshold value above and below the median value (Fig. 3.2), the data value is assumed to be bad or unrepresentative and is eliminated from the data set. The template is said to be "centered" because, with historical data, "future" data is

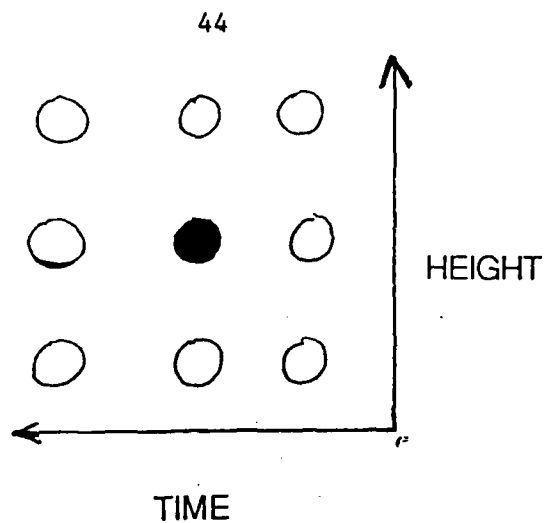


Fig. 3.1. "centered" template for the median quality control check.

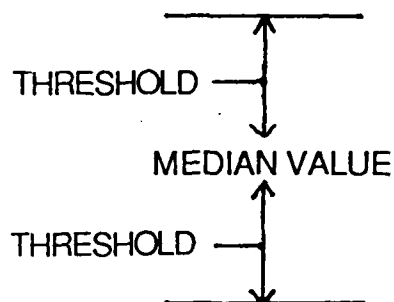


Fig. 3.2. The median quality control check threshold envelope.

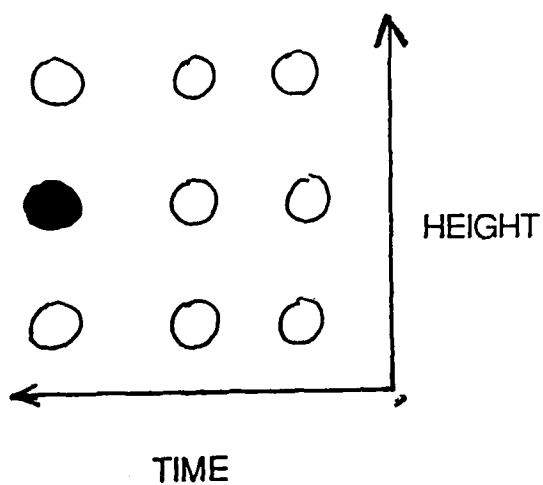


Fig. 3.3. "Non-centered" template for real-time median quality control check.

as readily available as "past" data. A non-centered template would be required for use with real-time data (Fig. 3.3).

The unmodified median check threshold was calculated as follows:

$$\text{Threshold} = Ah^2 + Bh + C \quad (6)$$

where the constants A, B, and C are taken from Brewster (1987) and are given by:

$$A = -7.89 \times 10^{-8} \text{ s}^{-1}\text{m}^{-1}$$

$$B = 1.54 \times 10^{-3} \text{ s}^{-1}$$

$$C = 9.50 \text{ ms}^{-1}$$

Threshold is in units of  $\text{ms}^{-1}$  and h is height above sea level in meters. The above curve is a quadratic fit to the values:

<u>Threshold</u>	<u>Height (MSL)</u>
9.5 $\text{ms}^{-1}$	0 m
17.0 $\text{ms}^{-1}$	9000 m
14.0 $\text{ms}^{-1}$	16000 m

These were designed for use from 2000 m to 18000 m MSL by Brewster as part of his continuing experiments with the

Program for Regional Observing and Forecasting Services (PROFS) quality control system.

This threshold, hereafter called T1, is designed to allow greater differences between median and data values above the boundary layer and allow the greatest differences at jet stream level.

Initial applications of this curve to the data sets in this research failed to eliminate a "satisfactory" amount of spurious data. In order to eliminate more "bad" data but maintain the benefits of the Brewster quadratic threshold equation, T1 was modified for each case by multiplying it by a constant between zero and one beginning with 0.9. This value was decreased in increments of 0.05 until a subjectively determined "balance" was achieved between remaining "bad" data values and eliminated "good" data values. Once this value was found for a given time series, it was used for all three profiler data sets within that time series. The resulting multipliers for each time series are as follows:

<u>Series Date</u>	<u>Multiplier</u>
3-4 June	0.65
12-13 May	0.60
26-27 June	0.60

A threshold based on speed only was calculated as follows:

$$\text{Threshold} = 0.4 \times \text{SPD} \quad (7)$$

where SPD is the average of the observed wind component and the median wind component. This threshold, hereafter called T2, was attached to the median QC check and the final median QC check threshold used was the maximum of T1 and T2 or:

$$\text{THRESH} = \text{MAX} (\text{T1}, \text{T2}) \quad (8)$$

where THRESH is the final median QC check threshold (Brewster, 1987).

Wind data were separated into u and v components and each component was tested independently of the other. If a u component was eliminated, the corresponding v component was eliminated as well and vice versa.

Using the maximum of T1 and T2 versus T1 alone eliminated fewer "good" data points at high levels that were initially rejected by T1. It became apparent, though, that a different test was necessary to eliminate the few remaining spurious data points. Tightening the median QC check threshold further would eliminate an unacceptable number of "good" data points before it would eliminate these last "bad" ones. A vertical consistency check was developed in response to this need.

### 3.3 Vertical Consistency Check

The vertical consistency QC check involves the examination of a single profile for excess directional shear. A data point is compared to the closest neighbor above it. The directional shear between the two points is compared to a threshold value which depends upon the separation between the two data points. If the observed shear is higher than the threshold value, the higher data point is eliminated. The thresholds for different separation ranges are as follows:

<u>Threshold</u>	<u>Data Separation</u>
25 degrees	$D < 200$ meters
30 degrees	$200 < D < 500$ meters
40 degrees	$500 < D < 900$ meters

where  $D$  is the vertical separation between two adjacent data points in a profile in units of meters. The threshold values were arrived at experimentally and, once established, were used for all three profilers in all three time series. This test was not performed where  $D$  was larger than 900 meters.

Initially, each check was performed once for each data set with the median QC check performed first. A small number of spurious data points stubbornly remained, however, but instead of designing a new QC check to deal with these data points, multiple passes of the existing scheme were

performed. Multiple passes compensated for the fact that the vertical consistency check did not work when bad data existed on adjacent height levels (ie. when they were more than one level deep).

Even multiple passes, though, wouldn't clear the Norman profiler time series of spurious data for 12-13 May and 26-27 June unless over ten passes were made, owing to vertically well correlated errors. These errors appear at the heights of overlapping long and short radar pulses (roughly five to eight kilometers). After cross-checking with Oklahoma City rawinsonde data, it was decided that short pulse data be subjectively removed above five kilometers from the 26-27 June time series and long pulse data be removed below eight kilometers from the 12-13 May time series. The resulting profiles then corresponded well with rawinsonde data.

Figures 3.4 through 3.21 show, in alternating order, the final rejected winds and final quality controlled wind fields for each profiler for each time series. The next data processing steps include filling the data gaps, objectively analyzing the quality controlled data onto grids and filtering the data to remove high frequency oscillations. All three steps can be accomplished in one using the technique developed in the next chapter.

## REJECTED MCPHERSON WINDS

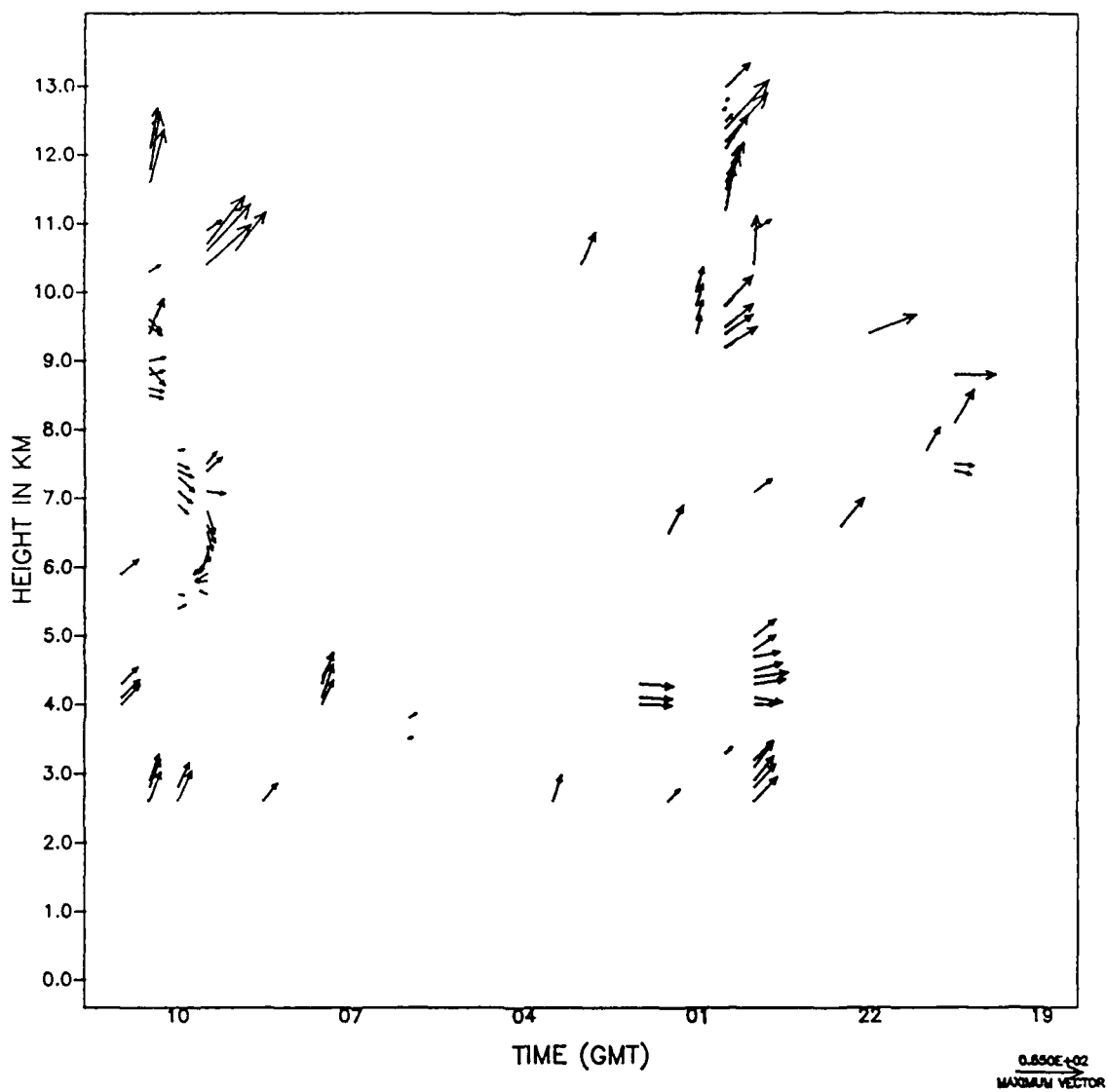


Fig. 3.4. Rejected wind data from the 3-4 June McPherson profiler data after application of the quality control technique.

## QCD MCPHERSON DATA

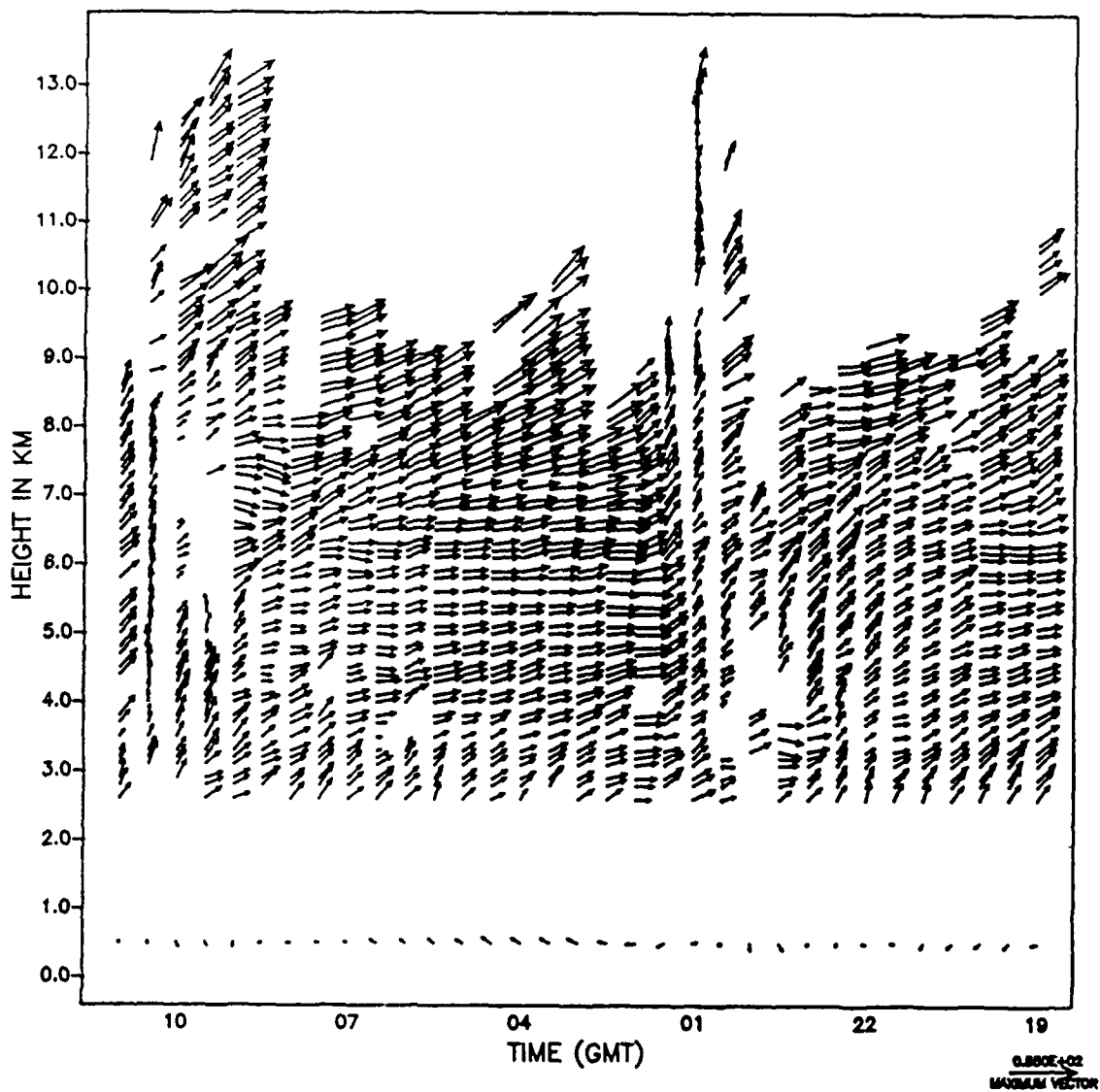


Fig. 3.5. Quality controlled 3-4 June McPherson profiler data.

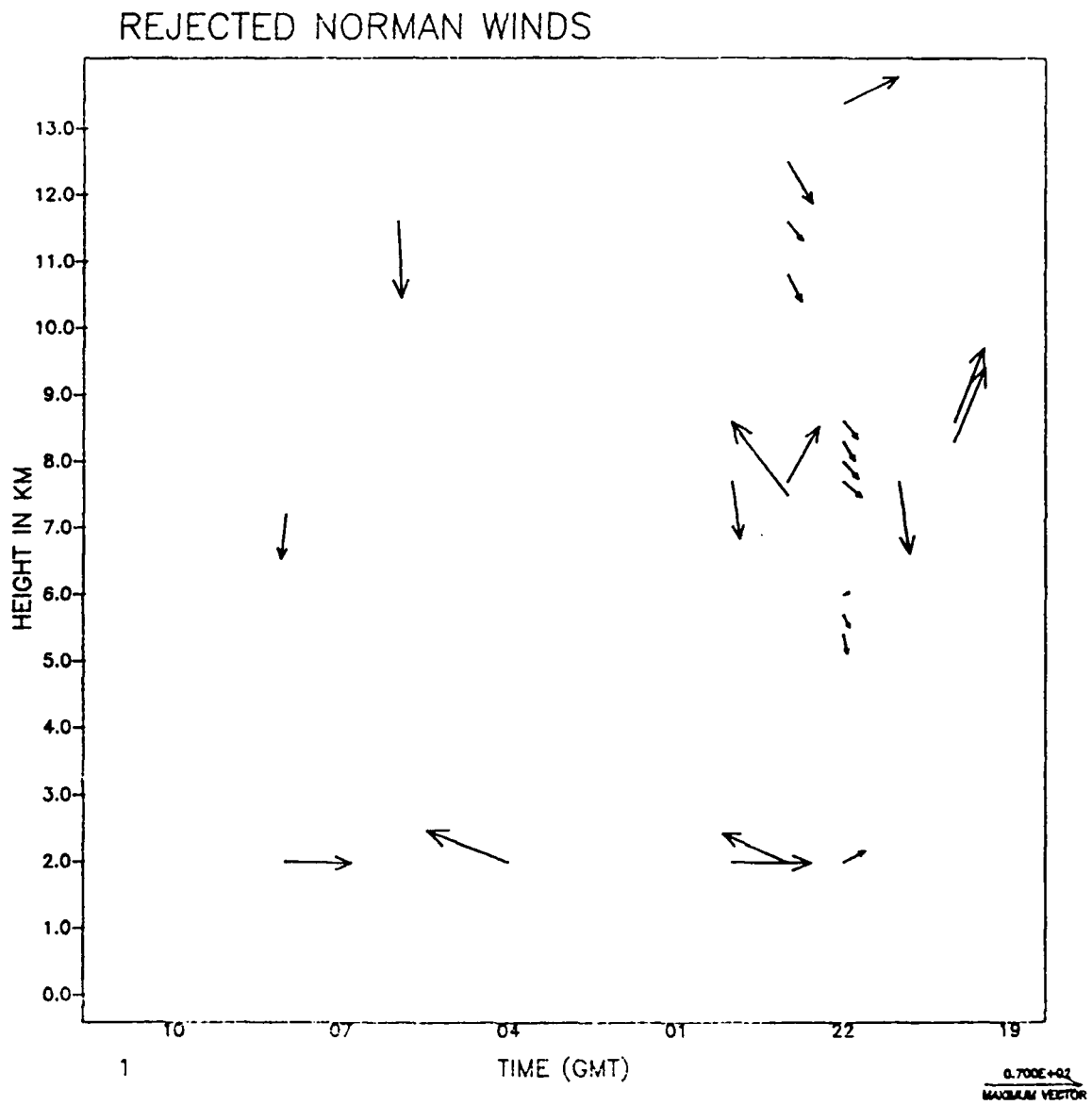


Fig. 3.6. Same as 3.4. but for 3-4 June Norman.

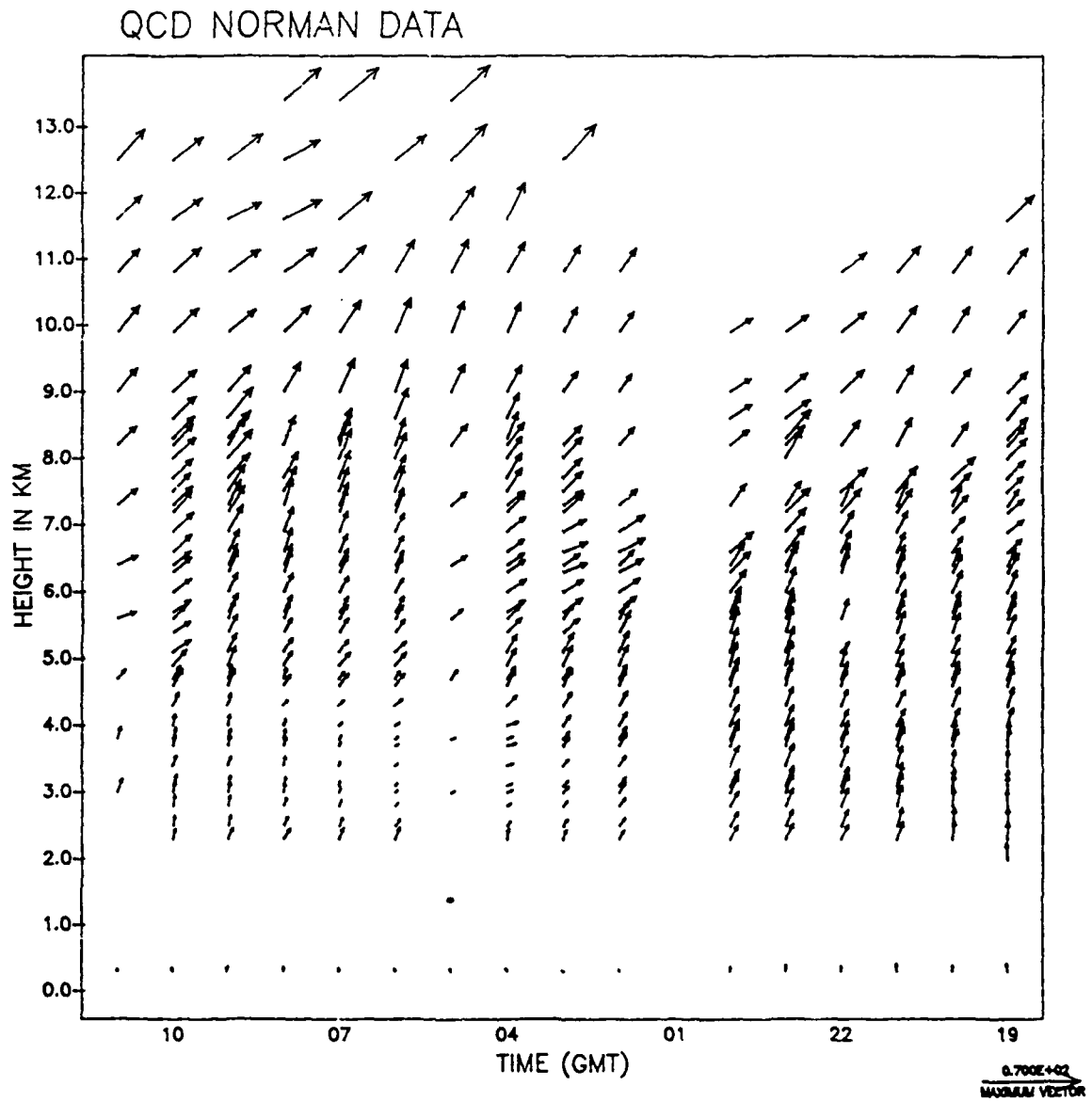


Fig. 3.7. Same as 3.5. but for 3-4 June Norman.

## REJECTED LIBERAL WINDS

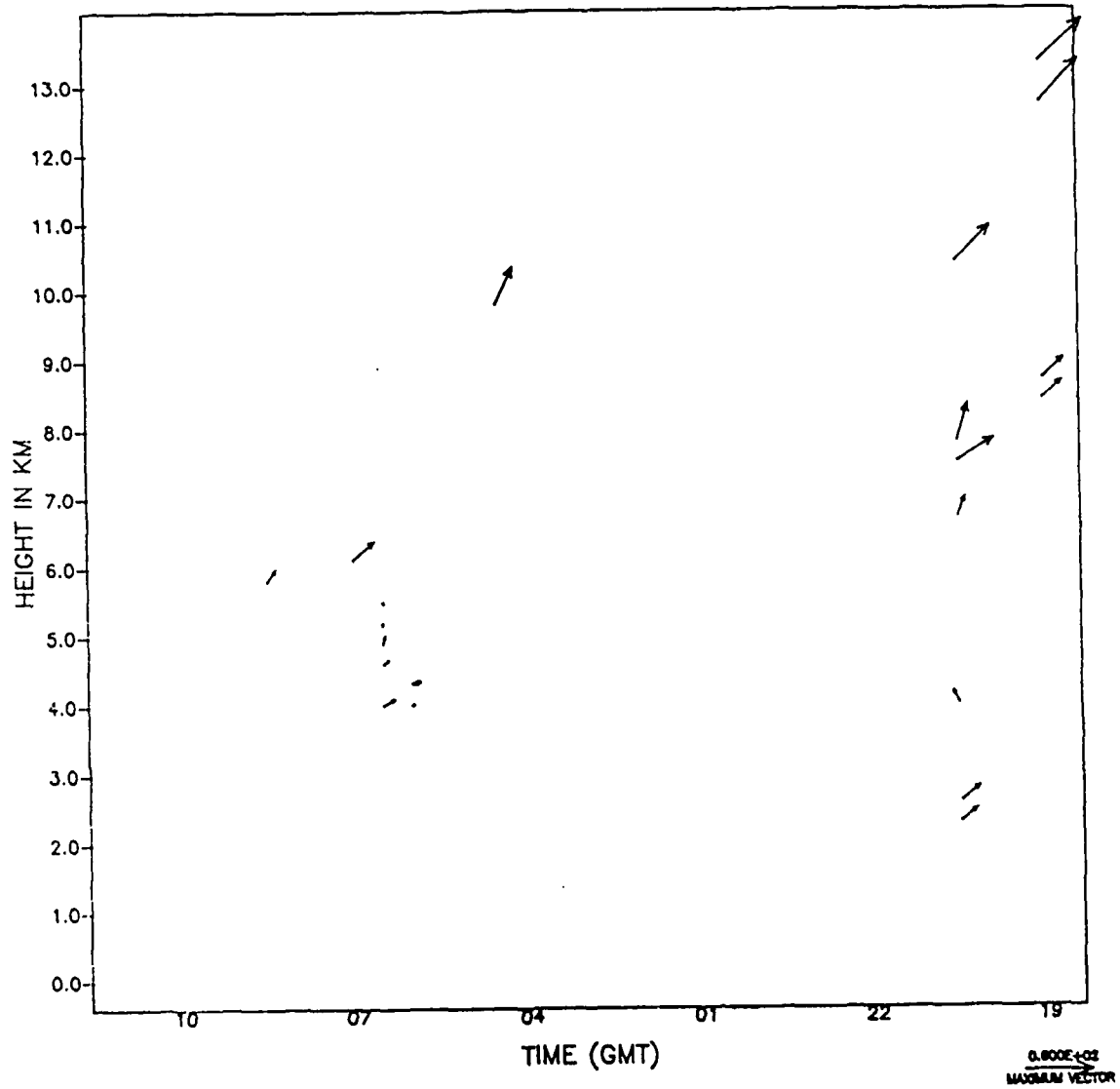


Fig. 3.8. Same as 3.4. but for 3-4 June Liberal.

## QCD LIBERAL DATA

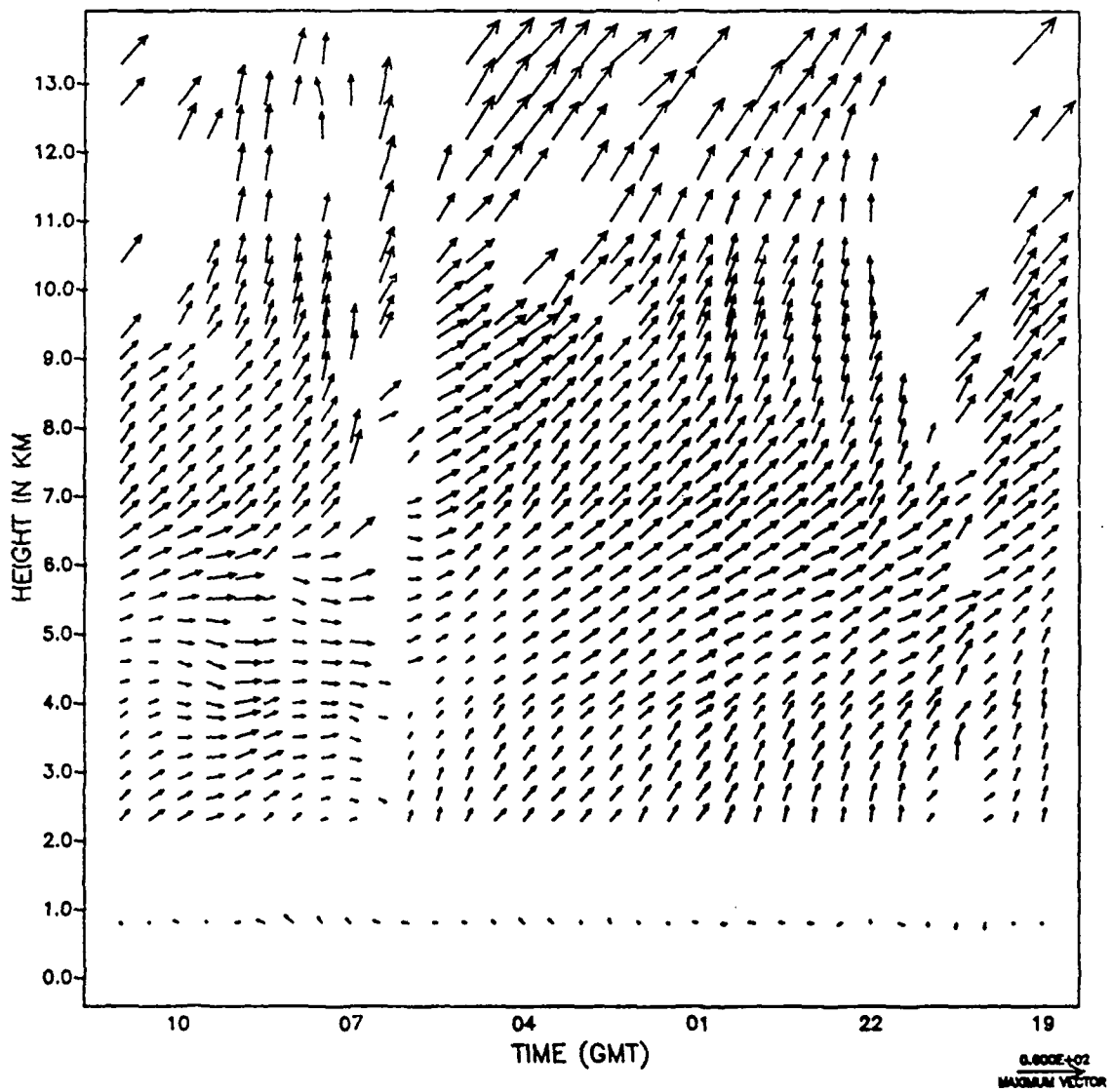


Fig. 3.9. Same as 3.5. but for 3-4 June Liberal.

## REJECTED MCPHERSON WINDS

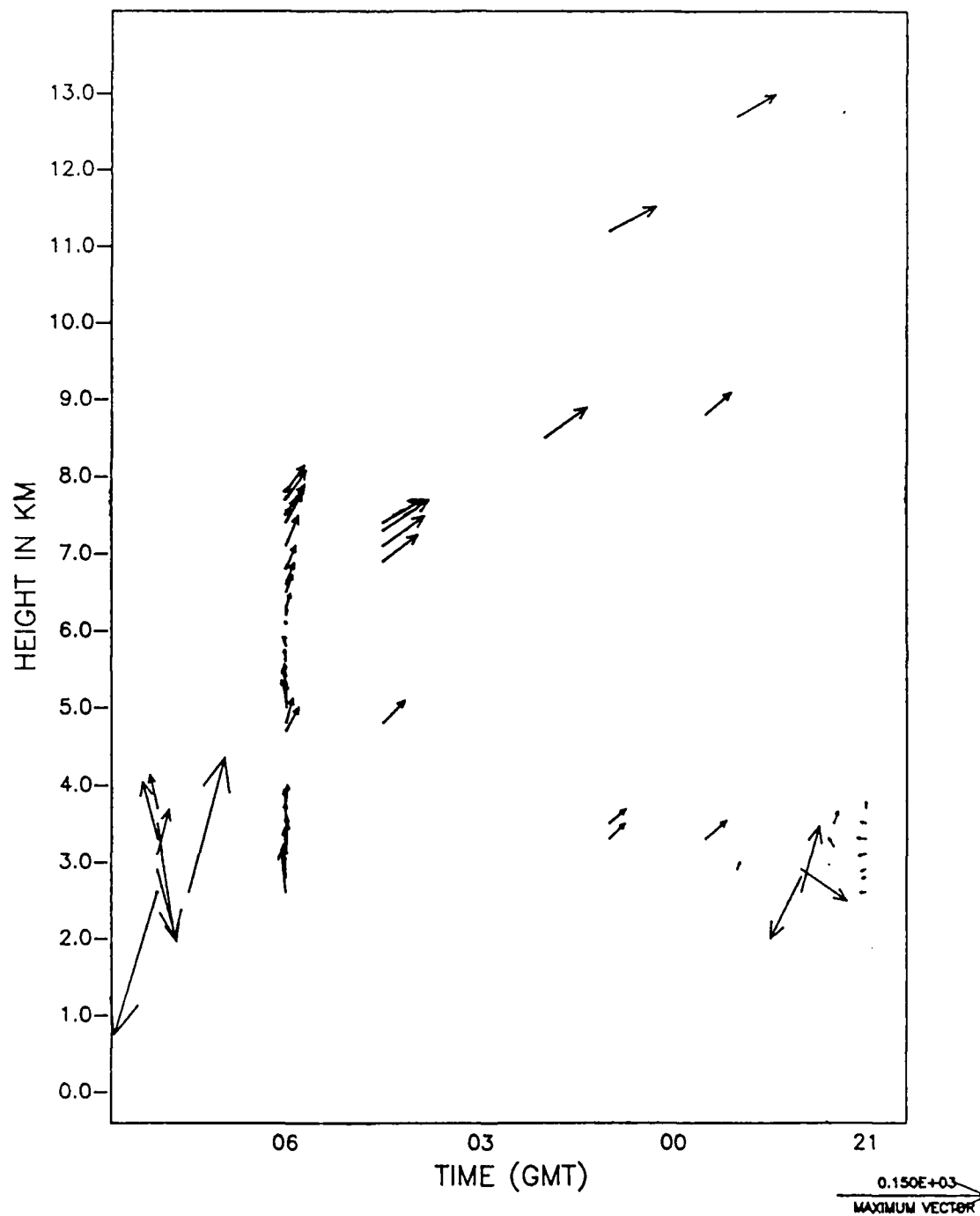


Fig. 3.10. Same as 3.4. but for 12-13 May McPherson.

## MCPHERSON QCD (12-13 MAY)

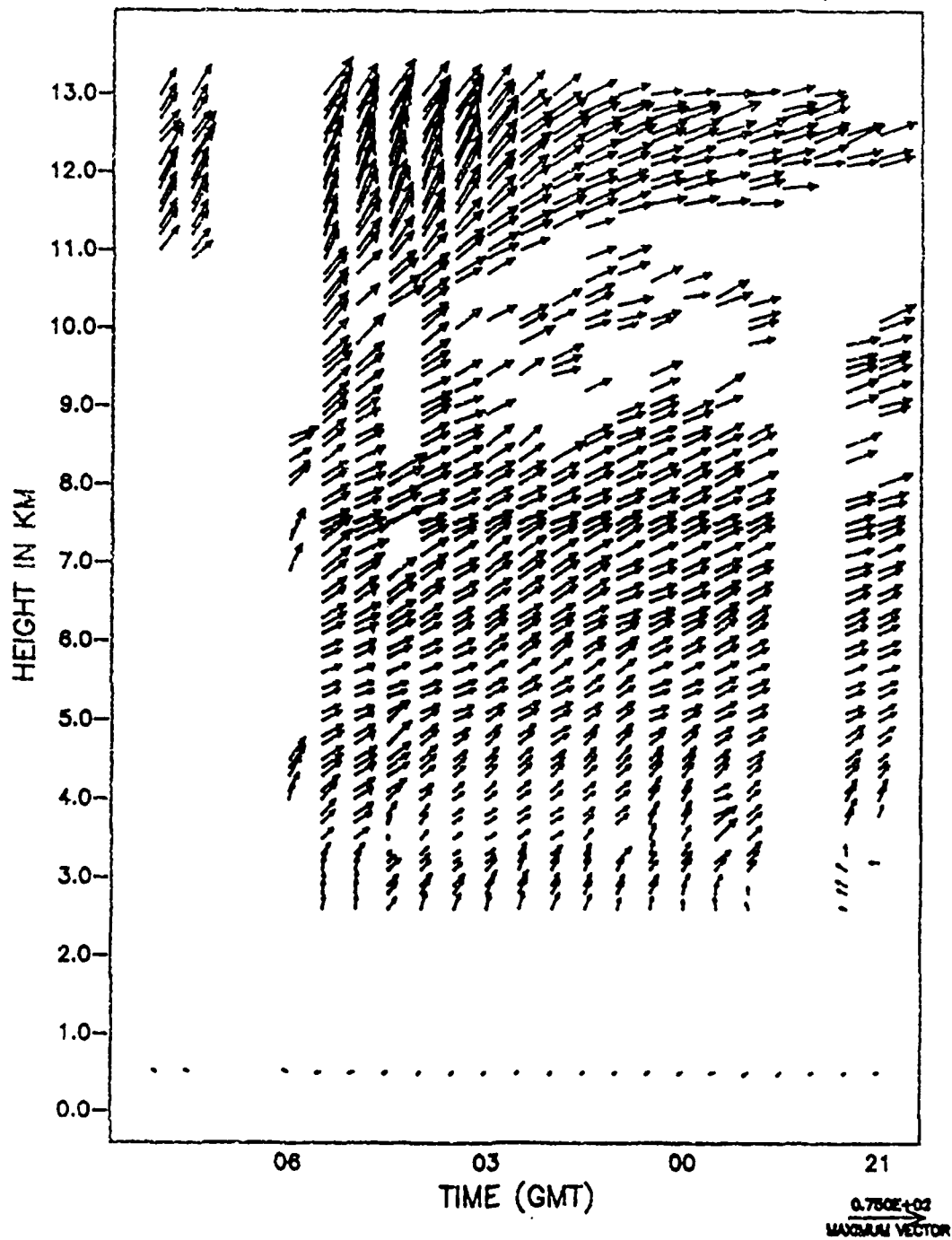


Fig. 3.11. Same as 3.5. but for 12-13 May McPherson.

## REJECTED NORMAN WINDS

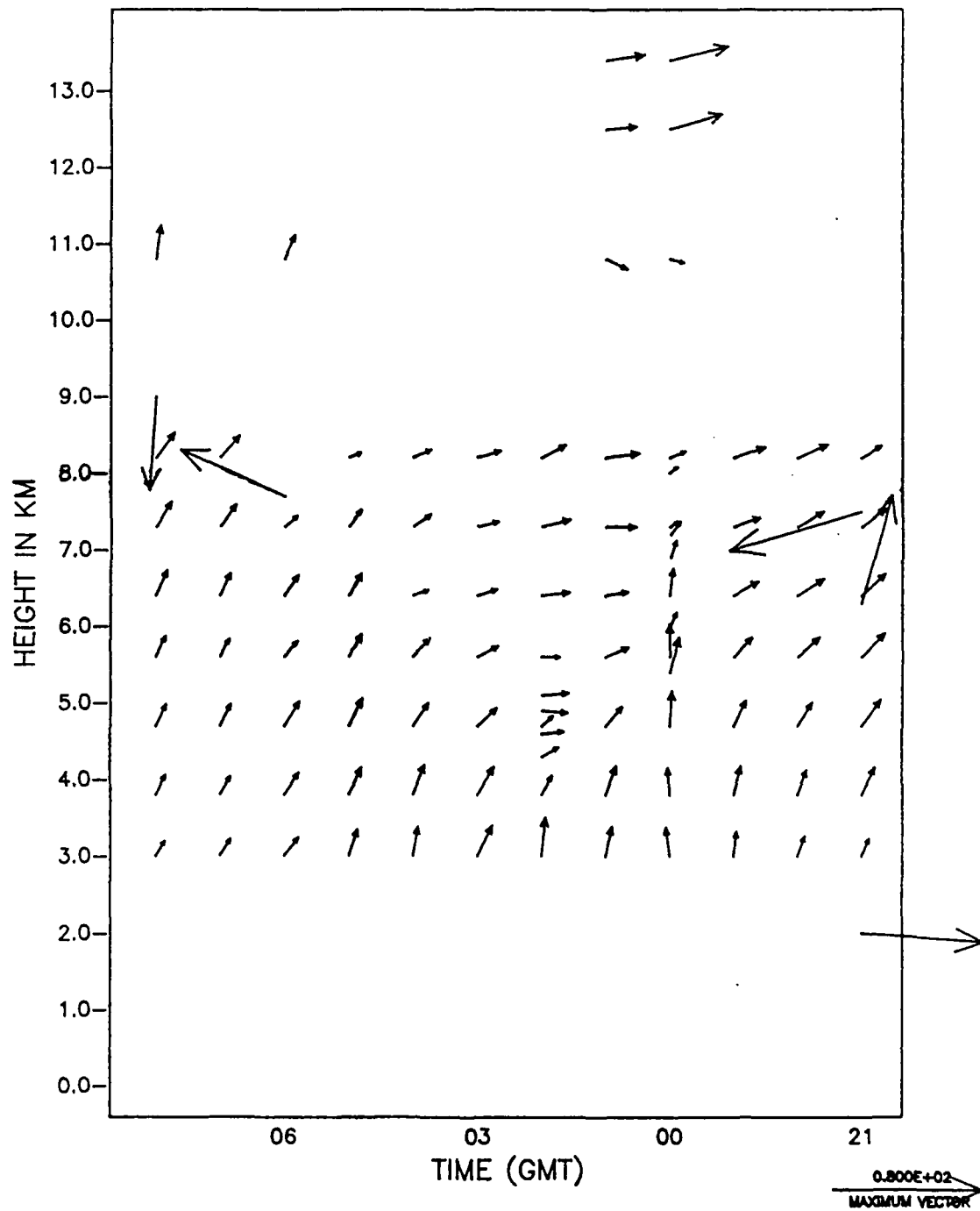


Fig. 3.12. Same as 3.4. but for 12-13 May Norman.

## NORMAN QCD (12-13 MAY)

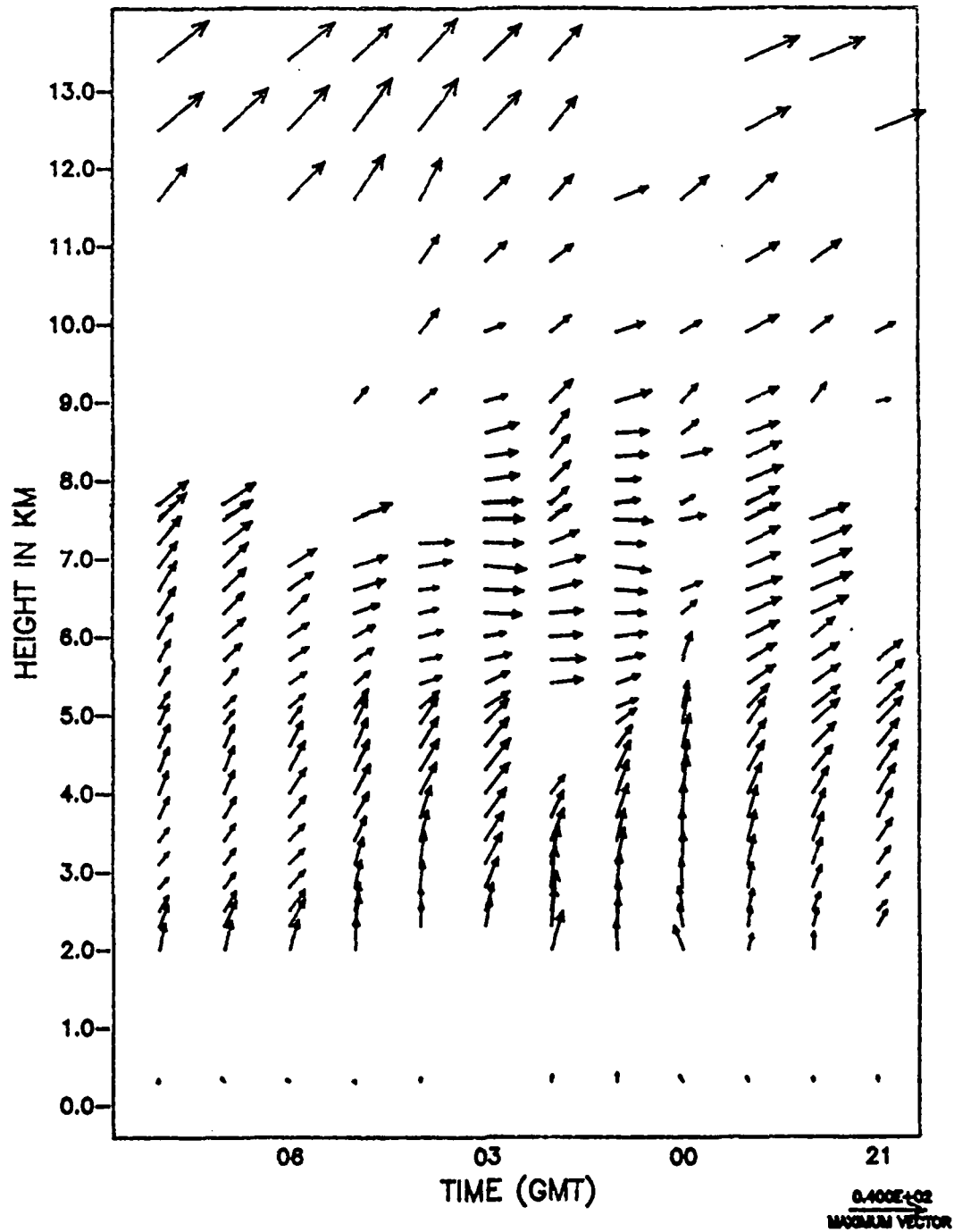


Fig. 3.13. Same as 3.5. but for 12-13 May Norman.

## REJECTED LIBERAL WINDS

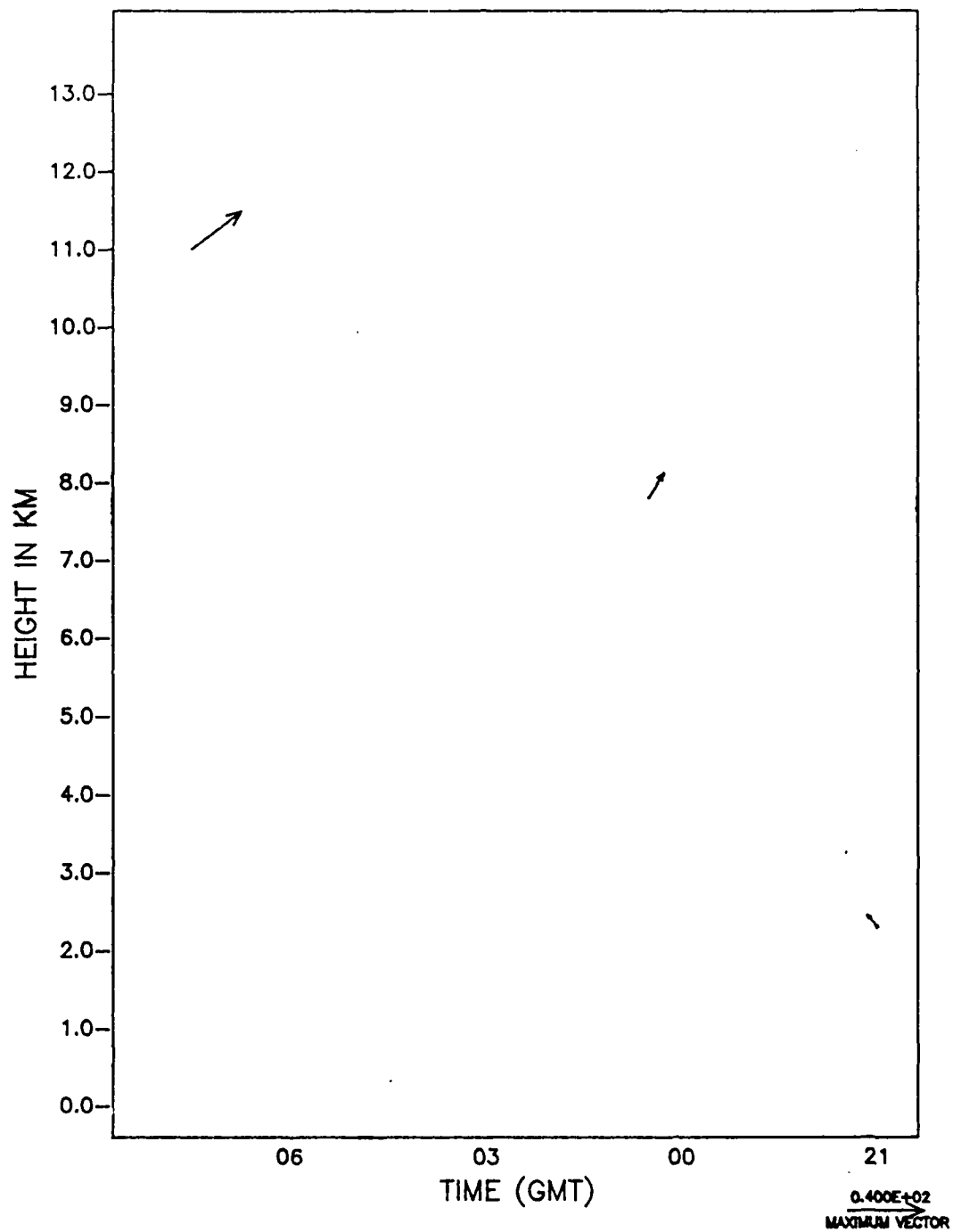


Fig. 3.14. Same as 3.4. but for 12-13 May Liberal.

## LIBERAL QCD (12-13 MAY)

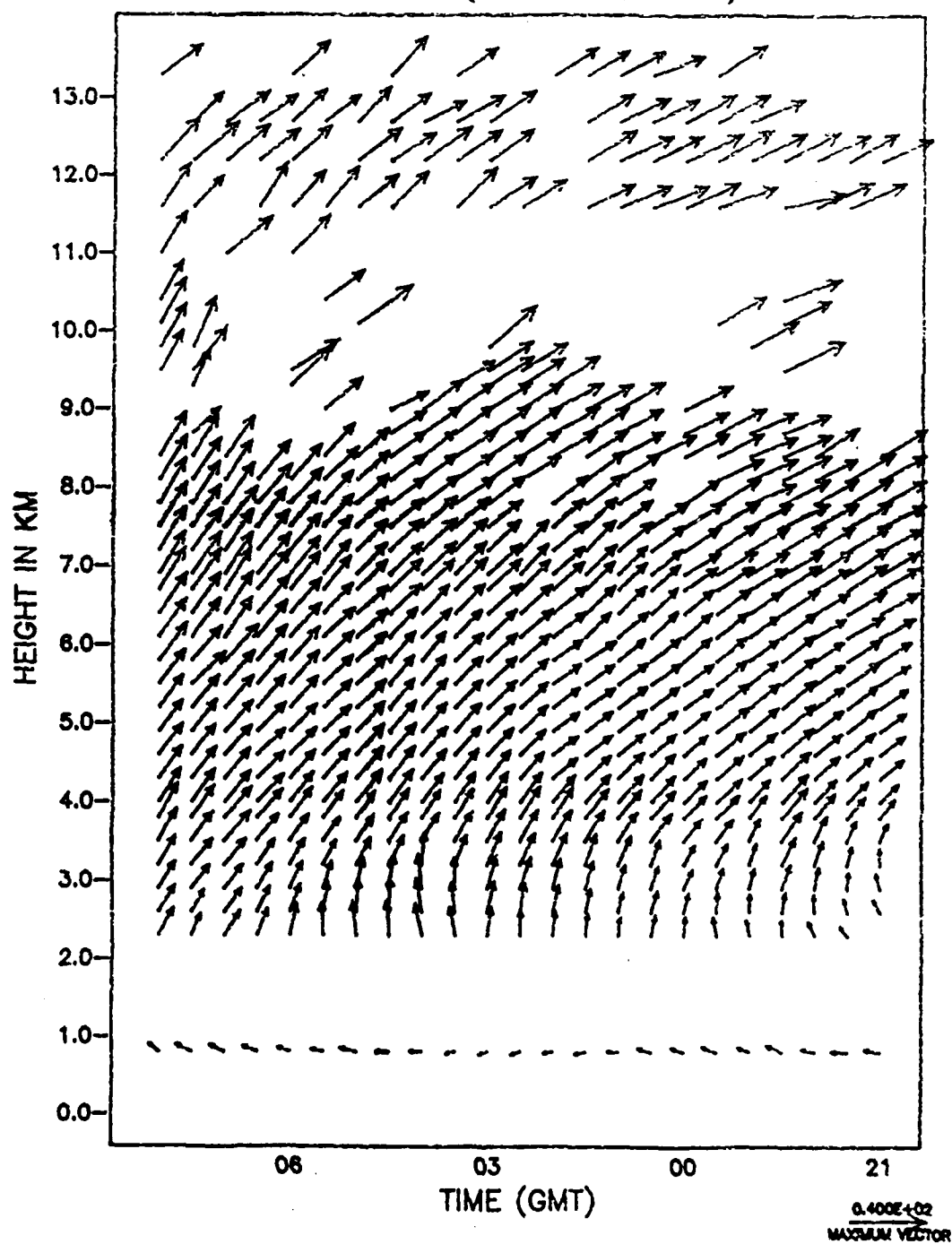


Fig. 3.15. Same as 3.5. but for 12-13 May Liberal.

## REJECTED MCPHERSON WINDS

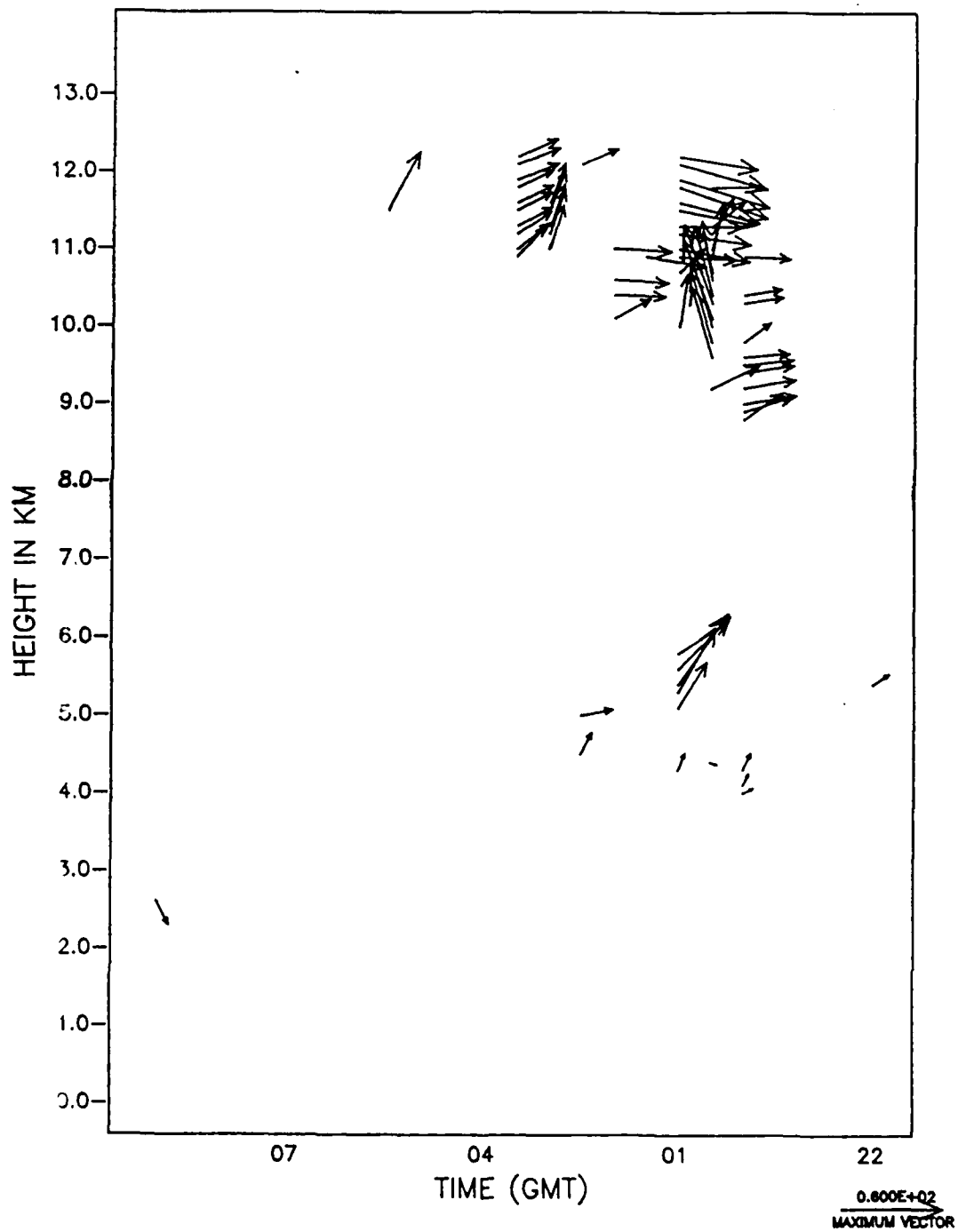


Fig. 3.16. Same as 3.4. but for 26-27 June McPherson.

## MCPHERSON QCD (26-27 JUN)

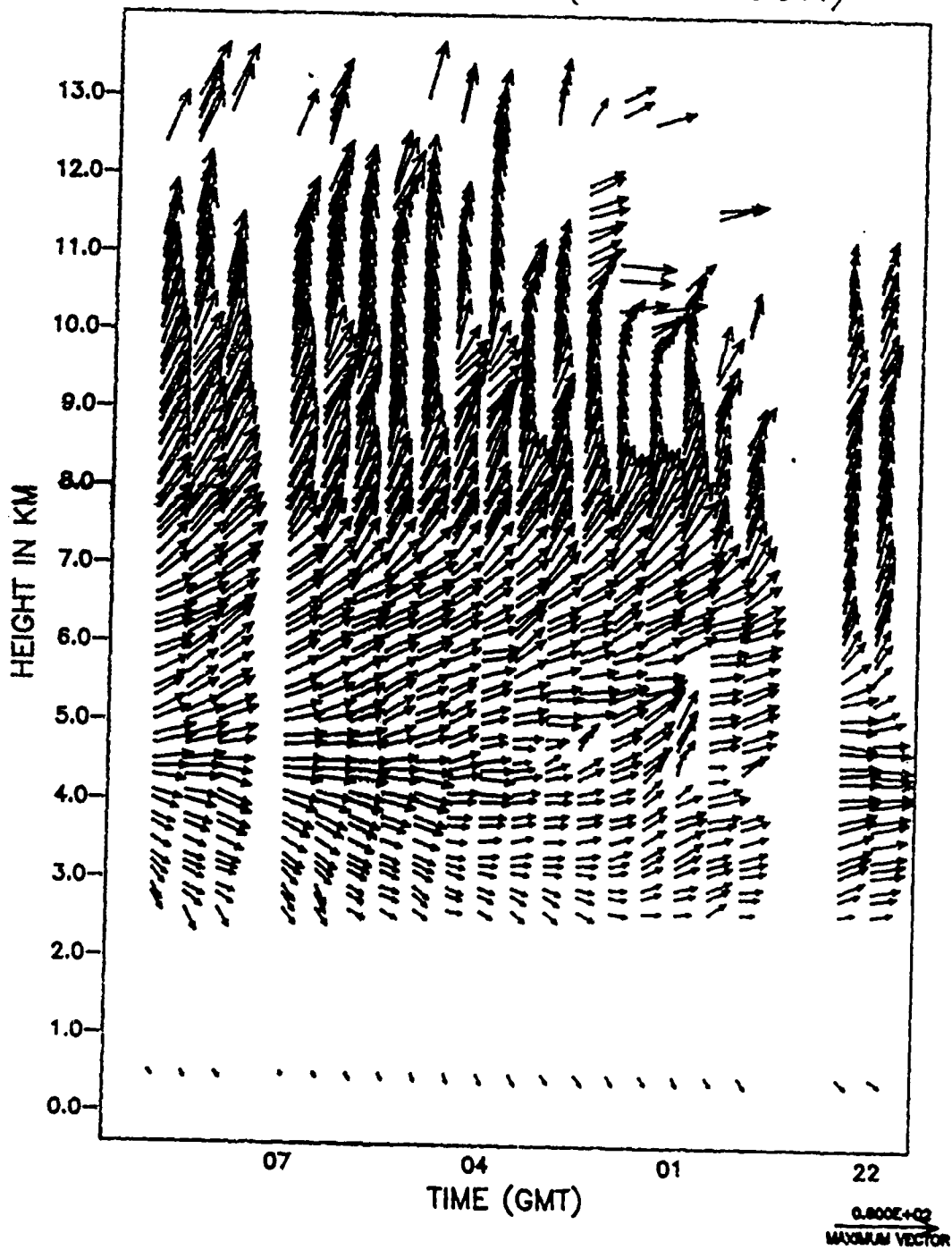


Fig. 3.17. Same as 3.5. but for 26-27 June McPherson.

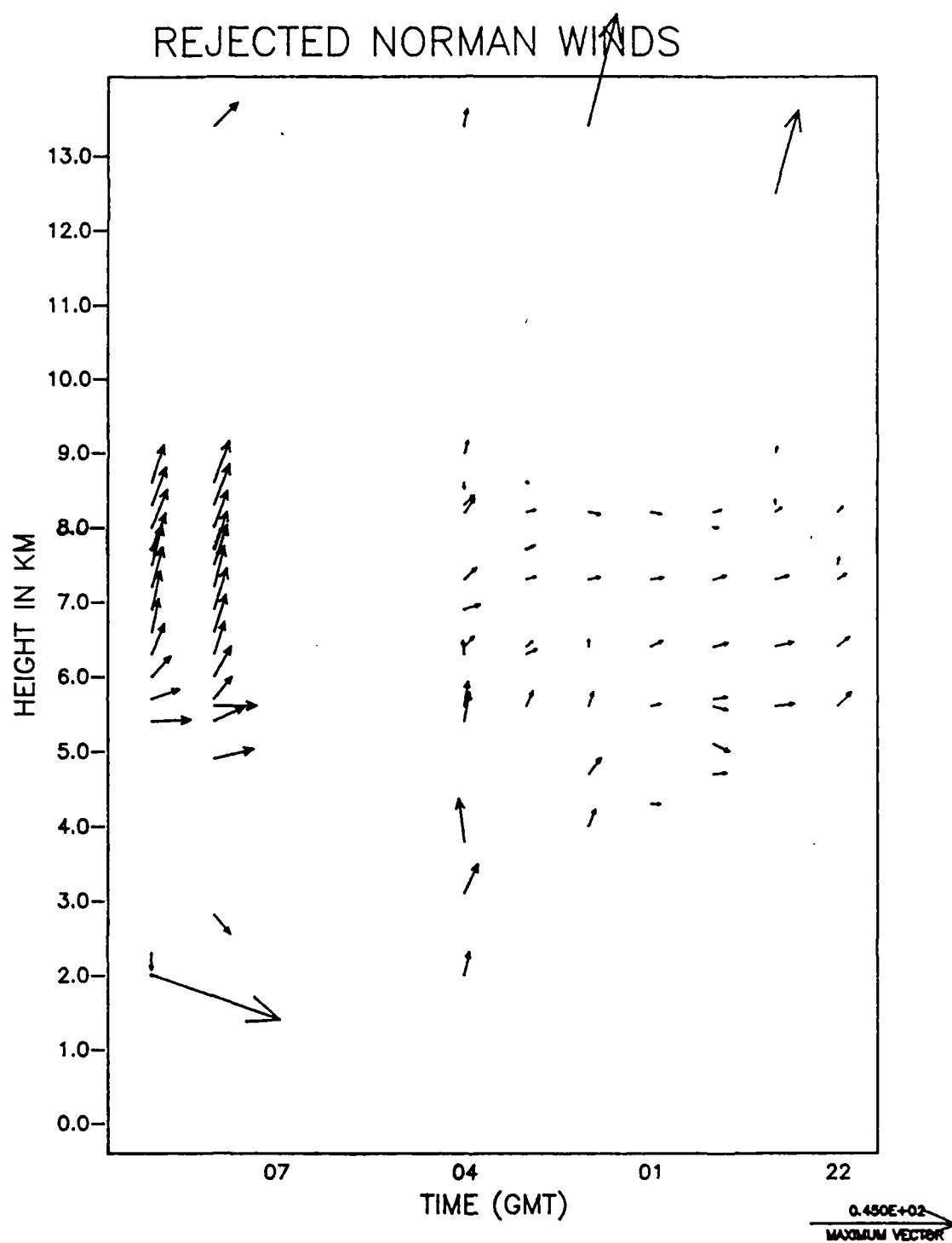


Fig. 3.18. Same as 3.4. but for 26-27 June Norman.

## NORMAN QCD (26-27 JUN)

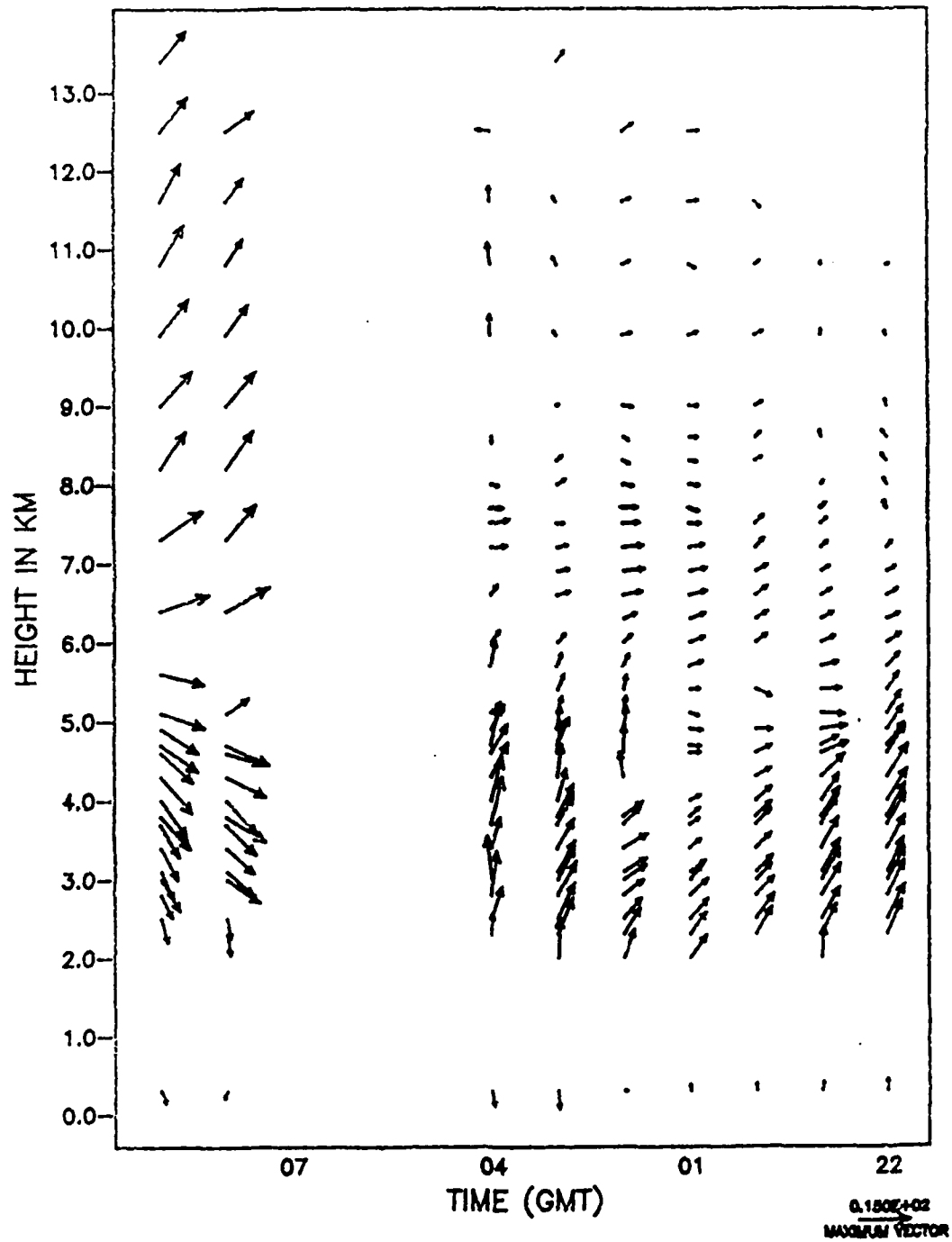


Fig. 3.19. Same as 3.5. but for 26-27 June Norman.

## REJECTED LIBERAL WINDS

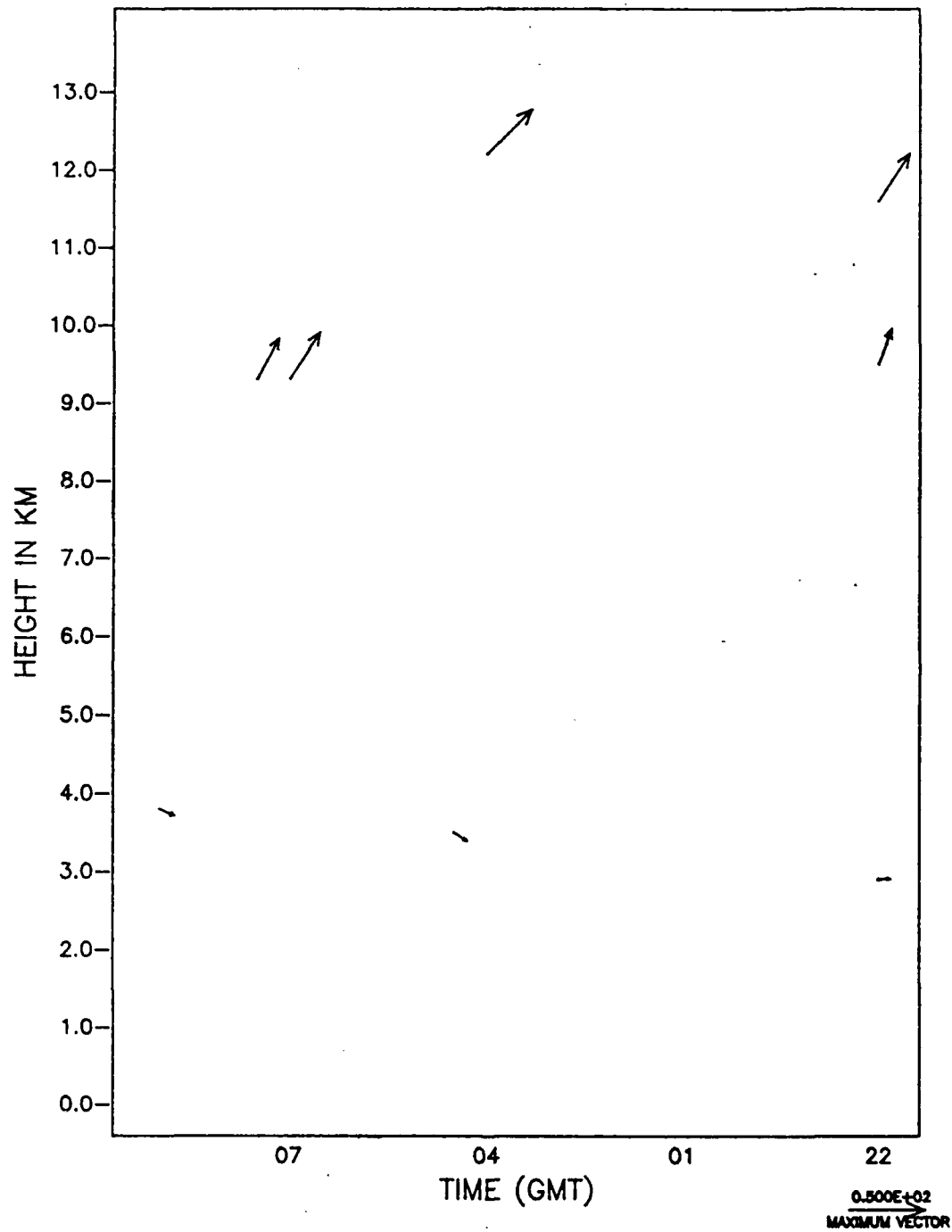


Fig. 3.20. Same as 3.4. but for 26-27 June Liberal.

## LIBERAL QCD (26-27 JUN)

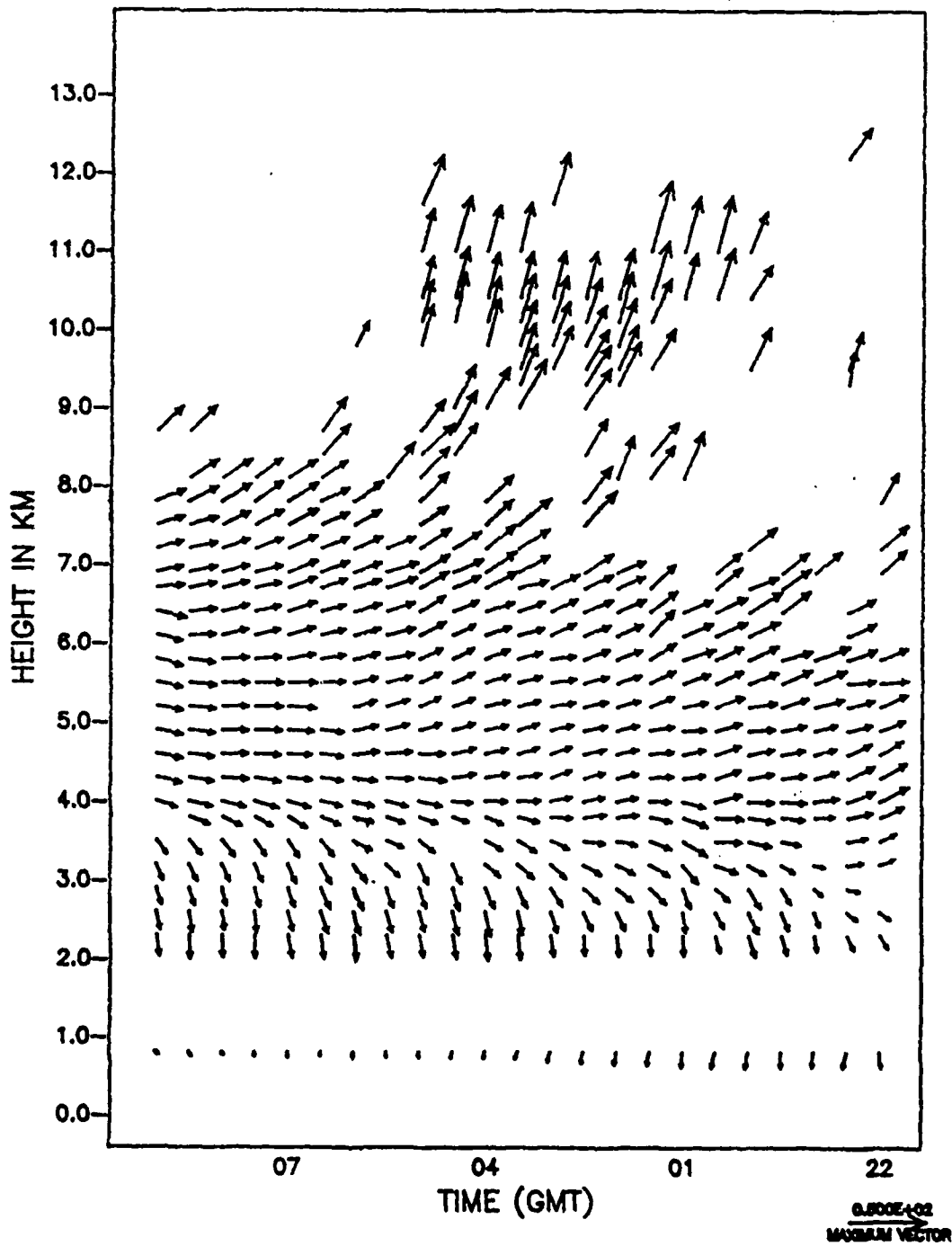


Fig. 3.21. Same as 3.5. but for 26-27 June Liberal.

## CHAPTER IV

### OBJECTIVE ANALYSIS AND KINEMATIC FIELD CALCULATIONS

#### 4.1 A Barnes Objective Analysis Review

At this point, all of the profiler time series within the selected data sets have been quality controlled and are ready for the subsequent processing steps of filling, interpolation and filtering. These three steps can be performed separately within a time series (e.g. Hermes, 1988) or all at once through objective analysis (OBAN).

Barnes (1964) developed an OBAN scheme which is an empirical weighting scheme similar to Cressman (1959) but with a weight function that only asymptotically approaches zero. The main concept of the former method is the assignment of Gaussian weights ( $w$ ) to data points based entirely on the distance,  $r$ , between these data points and the desired grid points as follows:

$$w = \exp(-r^2/k_0) \quad (9)$$

where  $k_0$  is a parameter which determines the shape of the

response function. The value at a grid point ( $g$ ) is the weighted average of all ( $M$ ) data points ( $f_m$ ) within a fixed radius ( $R_c$ ) of the grid point:

$$g = \frac{\sum_{m=1}^M w_m f_m}{\sum_{m=1}^M w_m} \quad (10)$$

$R_c$  is usually chosen such that data points at that distance are assigned very small weights (e.g.  $1 \times 10^{-6}$ ). The spectral response of this weight function (which acts as a set of filter weights) after one pass is:

$$D_0 = \exp[-k_0 (\pi/L)^2] \quad (11)$$

where  $L$  is the horizontal wavelength. The shape parameter,  $k_0$ , is chosen only after consideration of the raw data distribution and the desired detail of the final gridded field.

While the filter inherent in the Barnes scheme introduces a degree of amplitude loss to the analyzed field, this amplitude can be recovered (or, in other words, response can be increased) by multiple passes through the subsequent difference fields. Barnes (1973) developed a method to reduce the number of passes that are necessary to recover this desired amplitude at small wavelengths to two by the

introduction of a convergence factor, gamma ( $\gamma$ ). Instead of using the same shape parameter,  $k_0$ , for each OBAN pass, this improved method uses a new shape parameter,  $k_1$ , where:

$$k_1 = k_0 \gamma \quad (12)$$

Gamma could theoretically be between zero and one but the range  $0.2 \leq \gamma \leq 0.4$  is recommended. Smaller values would introduce unwanted, small wavelength noise to the gridded field. Larger values wouldn't appreciably improve the response from a second pass. It is by virtue of this smaller shape parameter,  $k_0$ , that the analysis converges to the desired detail after only two passes. The second pass weight function would be:

$$w = \exp(-r^2/k_1) \quad (13)$$

with a subsequent second pass response of:

$$D_1 = \exp[-k_1 (\pi/L)^2] = \exp[-k_0 \gamma (\pi/L)^2] = D_0^\gamma \quad (14)$$

The final response after two passes would be:

$$D^*_1 = D_0 (1 + D_0^{\gamma-1} - D_0^\gamma) \quad (15)$$

Koch et al. (1983) utilized the Barnes OBAN technique with an interactive computer graphic program (GEMPAK). Their development of an equation designed to recommend a first pass shape parameter based on distance between observations was used for this study. Koch et al. selected a first pass response,  $D_0$ , of 0.0064 at the  $L = 2\Delta n$  (twice the average station separation) wavelength, and the smallest recommended value for a convergence factor,  $\gamma$ , of 0.2. Plugging  $D_0$  and  $\gamma$  into equation (15) we get an e-folding ( $e^{-1}$  or 0.37) value as the final response for the  $2\Delta n$  wavelength. Plugging  $D_0 = 0.0064$  and  $L = 2\Delta n$  into equation (9):

$$0.0064 = \exp[-k_0(\pi/2\Delta n)^2]$$

and solving for  $k_0$  we obtain:

$$k_0 = 5.052(2\Delta n/\pi)^2 \quad (16)$$

All one has to do now is define  $\Delta n$ .

For the McPherson and Liberal profiler time series in each data set, a grid resolution of 200 meters by one-half hour throughout each domain was chosen. Norman grids were also chosen with vertical resolution of 200 meters, but a time resolution of one hour was chosen to match the temporal

resolution of this profiler.

At this point, it is important to remind the reader that, in this study, objective analysis is used within an individual profiler time series only and not across the PRE-STORM profiler triangle. This process puts the data on uniform height levels and time intervals at each profiler in order to compute kinematic quantities via a three-point line integral method to be discussed in the Appendix.

It was decided that the maximum amount of useable detail was desired from the OBAN of each time-height cross section. For the second pass, then, the minimum recommended convergence factor was chosen (0.2).

#### 4.2 Time to Space Conversion

Determining  $\Delta n$ , the "average station separation", was non-trivial owing to the time versus height nature of profiler time series. Doswell (1977) suggests a method for performing an objective analysis without time to space conversions. This involves the development of a second shape parameter in the exponent of the Barnes weight function corresponding to the time separation from data to grid point. While this method was demonstrated successfully by Doswell (1977), an alternative analysis technique was sought which would eliminate the need for the second weight parameter. The use of a single weight parameter

necessitates the derivation of only one response function.

An additional motivation to use just one weighting term (ie. to perform a time to space conversion before performing the OBAN) was the work by Brewster and Schlatter (1988) where they discussed wind data correlation as functions of height separation and time separation. Figure 4.1 shows the correlation field for the u component of the Fleming, Colorado profiler. Correlations are based on deviations from a 24 hour running mean for the month of June, 1987. The ordinate gives height, in meters, ASL and the abscissa gives vertical separation between observations (in meters). Figure 4.2 shows u-component correlations with time separation, in hours, along the abscissa. The v-component correlations, being very similar, are not shown. Correlation contours in both figures are in tenths. Numerous data gaps in the PRE-STORM profiler archives prevented the calculation of correlation statistics for these locations.

Using the above climatologically-derived correlation tables, it is possible to design a Barnes weight function which assigns equal weight to equally correlated data in the vertical and in time. For example, using a correlation factor of 0.7, a data point 1600 meters above or below a grid point at 5600 meters ASL would receive the same weight as a data point plus or minus 2.4 hours removed from the same grid point. In effect, at 5600 meters ASL, 1600 vertical meters is equated to 2.4 hours in time. To

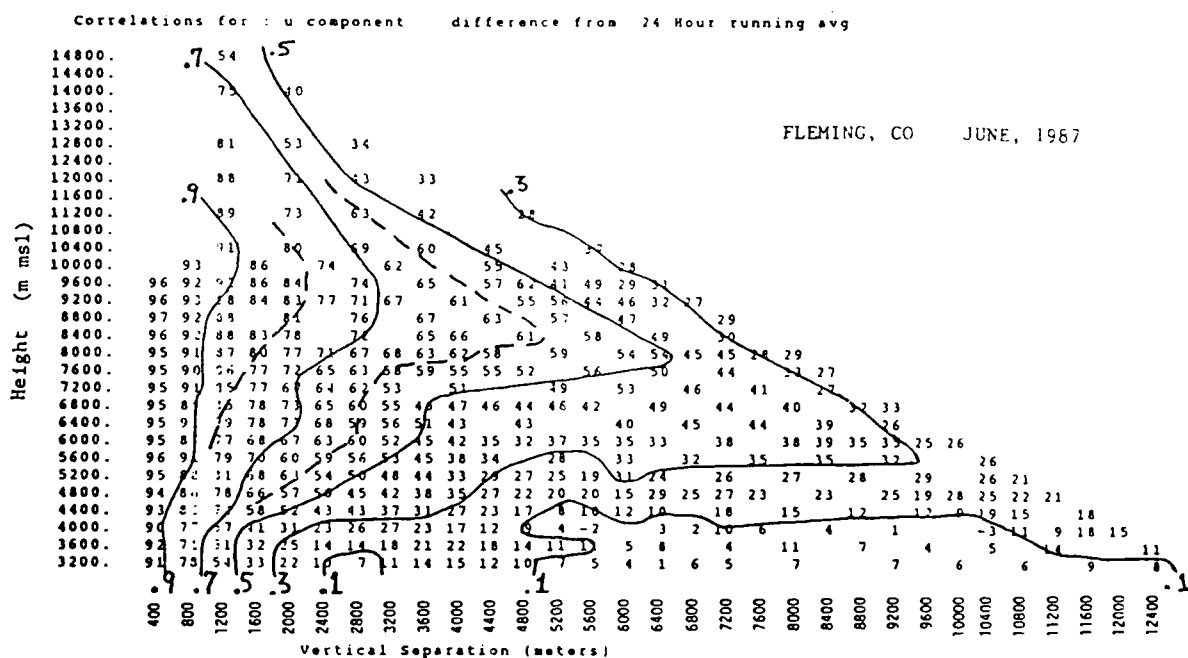


Fig. 4.1. U-component correlations ( $\times 100$ ) for the Fleming CO profiler during June 1987 as a function of height and vertical separation. Differences are from a 24-hour running mean. Contours are in tenths (Brewster and Schlatter, 1988).

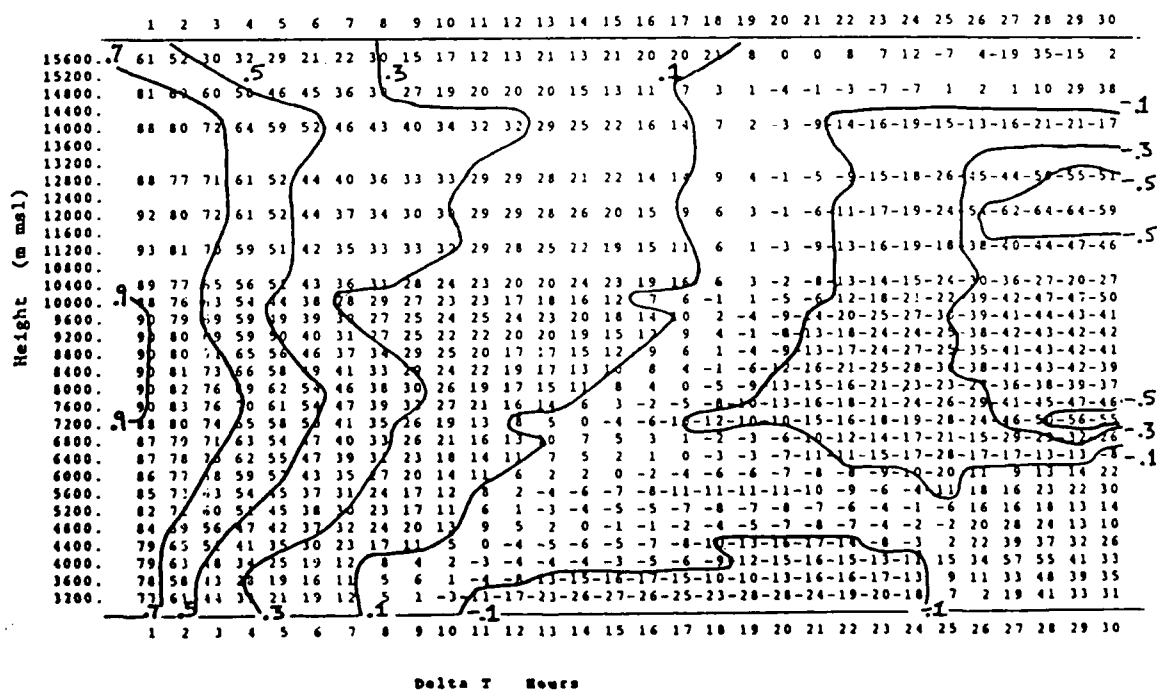


Fig. 4.2. Same as 4.1. but as a function of height and time separation (Brewster and Schlatter, 1988).

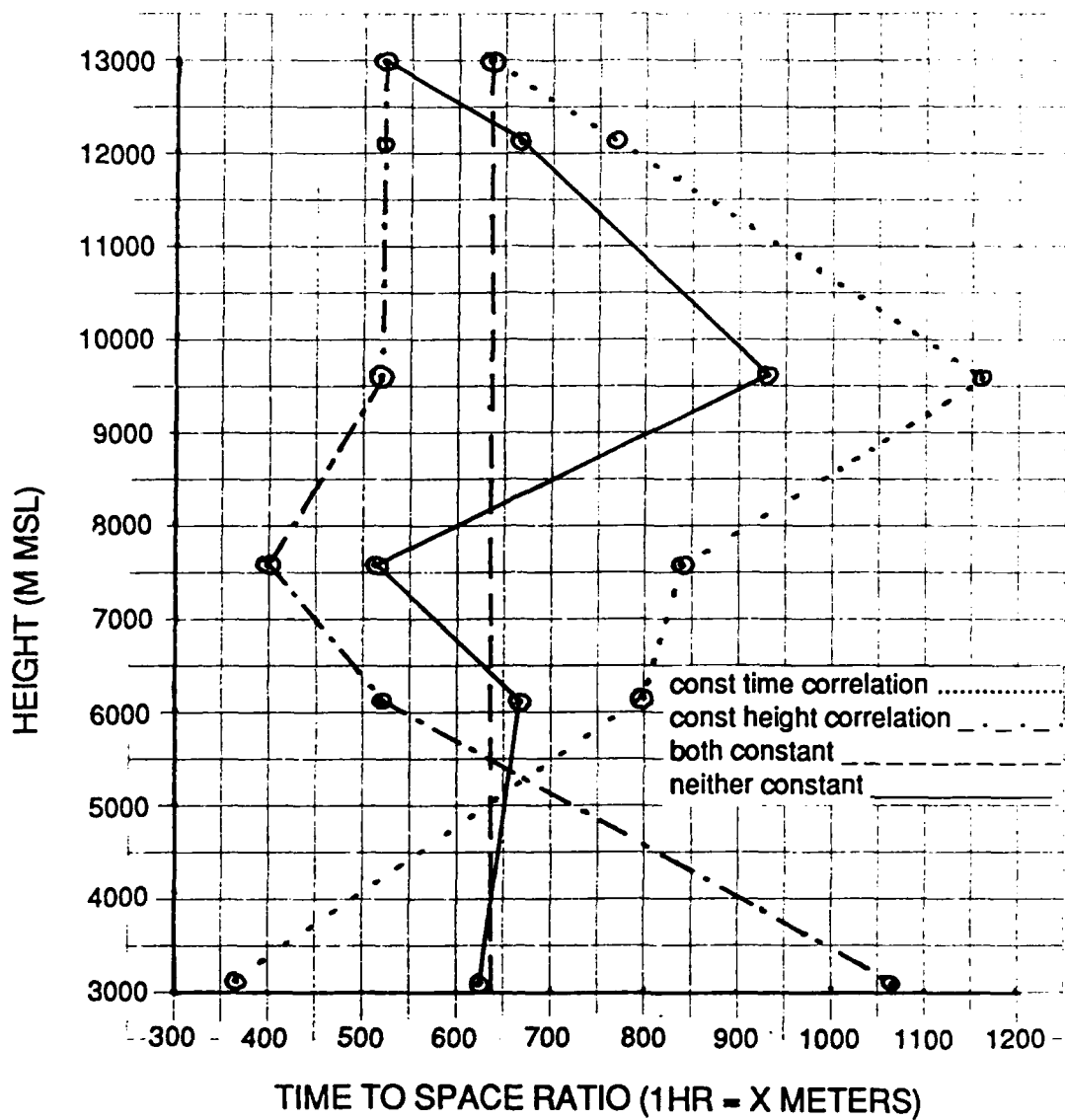


Fig. 4.3. Graphs of the various calculated time to space conversion factors as functions of height.

normalize, one hour is equal to about 660 meters at this level. Computing this normalized time to space conversion factor on a continuous basis for all heights in the domain would be cumbersome. This factor is calculated at selected heights, though, and is shown in graphical form in figure 4.3 as the solid line. A linear variation of the conversion factor is assumed between the selected heights. The ordinate in figure 4.3 gives the height ASL and the abscissa gives the normalized conversion factor in meters. For simplicity, it is possible to compute an average 0.7 correlation height separation for all heights. The same can be done for the time lag. This "straightening" of the 0.7 correlation contours on one or both of figures 4.1 and 4.2 results in the other graphs shown in Figure 4.3. For the dotted line, the 0.7 time correlation is held constant at 2.5 hours for all heights while the 0.7 height separation correlation is varied as before. The alternating dashed and dotted line shows the result of holding the 0.7 height separation correlation contour constant at 1600 meters for all heights while varying the 0.7 time correlation as before (with the solid line). The dashed line shows the result of holding both 0.7 correlation contours constant at 2.5 hours and 1600 meters giving us a normalized time to space conversion factor of 640 meters for all height levels. This value for the conversion factor was used in the calculation of  $\Delta n$  (and, therefore, the Barnes weights).

### 4.3 Final Parameter Decisions

A glance at the quality controlled McPherson profiler time series for the 3-4 June data set (Fig. 2.1) will remind the reader that large gaps do exist in the data. Care must be taken to select a grid length,  $\Delta n$ , that takes the possibility of data clustering into account. Koch et al. (1983) offer a few guidelines for this selection. At one extreme, when one has a fairly even distribution of data within the domain, the average minimum distance from one data point to its neighbor would be appropriate for  $\Delta n$ . Let's call this value  $\Delta n_c$ . At the other extreme, in the case of clustered data, the "random" data separation,  $\Delta n_r$ , would be more appropriate. This latter value is defined as the distance from one data point to another if the severely clustered data were spread out evenly (or "randomly") within the data domain. It would be computed as follows:

$$\Delta n_r = A^{1/2} [(1 + M^{1/2}) / (M - 1)] \quad (17)$$

where  $A$  is the area of the data domain and  $M$  is the number of data points within this domain. When  $M$  is large, this formula approaches:

$$\Delta n_r = (A/M)^{1/2} \quad (18)$$

The final value for  $\Delta n$  is subjectively chosen to be close to but less than  $\Delta n_r$  (but always greater than  $\Delta n_c$ ).

In order to simplify the OBAN process further by deriving a single first pass and final response curve for each data set, a single "conservative" value of 600 meters for  $\Delta n$  was selected for the 3-4 June data set after inspection of  $\Delta n_c$  and  $\Delta n_r$  for all profiler time series in all data sets. Tables 4.1 and 4.2 contain these values in units of meters. Given these values, 600 meters for  $\Delta n$  is considered "conservative" because it creates a smoother (or less detailed) analysis of the data set than if a smaller value for  $\Delta n$  were chosen. As the result of an omega field comparison (Chapter VI), a value of 1200 meters for  $\Delta n$  was used to derive the 12-13 May and 26-27 June omega fields. This choice for  $\Delta n$  will give an even smoother analysis.

Plugging  $\Delta n = 600$  meters into equation (16) gives us:

$$k_0 = 5.052(1200/\pi)^2 = 7.37 \times 10^5 \text{ m}^2$$

Similar, for  $\Delta n = 1200$  meters:

$$k_0 = 2.95 \times 10^6 \text{ m}^2$$

With these selections for  $k_0$ , the Barnes parameter space has been determined and all weight and response functions can be

	<u>LIBERAL</u>	<u>MCPHERSON</u>	<u>NORMAN</u>	<u>COMBINED</u>
12-13 May	295	121	363	260
03-04 Jun	290	120	229	213
26-27 Jun	291	120	258	223
COMBINED	292	120	283	232

(units of meters)

Table 4.1. Values of average station separation,  $\Delta n_c$ .

	<u>LIBERAL</u>	<u>MCPHERSON</u>	<u>NORMAN</u>	<u>COMBINED</u>
12-13 May	406	321	677	468
03-04 Jun	390	314	578	427
26-27 Jun	463	290	635	462
COMBINED	420	308	630	452

(units of meters)

Table 4.2. Values of "random" station separation,  $\Delta n_r$ .

derived.

Figure 4.4 shows the first pass weight function while figure 4.5 shows the second pass weight function using the above derived parameters. Both are derived using  $\Delta n = 600$  meters. Figures 4.6 and 4.7 show the same with  $\Delta n = 1200$  meters. Figure 4.8 shows the first pass and final response functions. An example of the effect of the small correction pass convergence factor on the response function is the increase in amplitude response from 0.3 to 0.86 at the  $4\Delta n$  wavelength.

Finally the McPherson and Liberal half-hour grids were converted into hour grids to match the Norman hourly profile resolution. This was accomplished by averaging hourly and subsequent half-hourly values and assigning these averages to the beginning of each hour. Data from the last profile in each time series were not manipulated since that profile always appeared on the hour. The final objectively analyzed fields, in height coordinates, are shown in Figures 4.9 through 4.17.

One test of an objective analysis scheme is the degree of "fit" between the final analyzed fields and the original quality controlled data fields. The root mean square (RMS) vector difference is used here to measure the OBAN fit. The standard RMS formula is:

$$RMS = \left[ \frac{1}{N} \sum_{m=1}^N (v_{om} - v_{om})^2 \right]^{1/2} \quad (19)$$

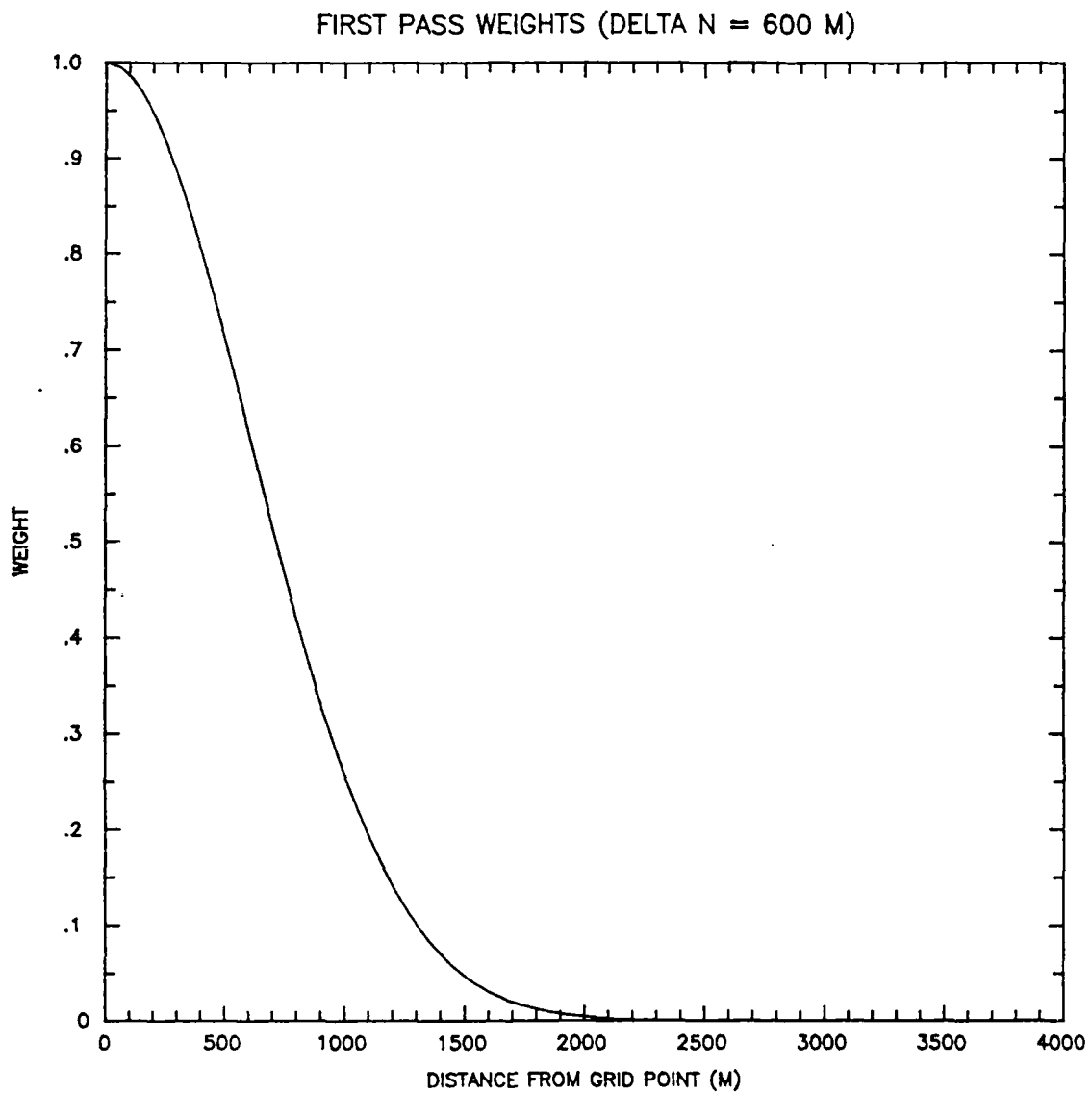


Fig. 4.4. Barnes first pass weight function using  $\Delta n = 600$  meters.

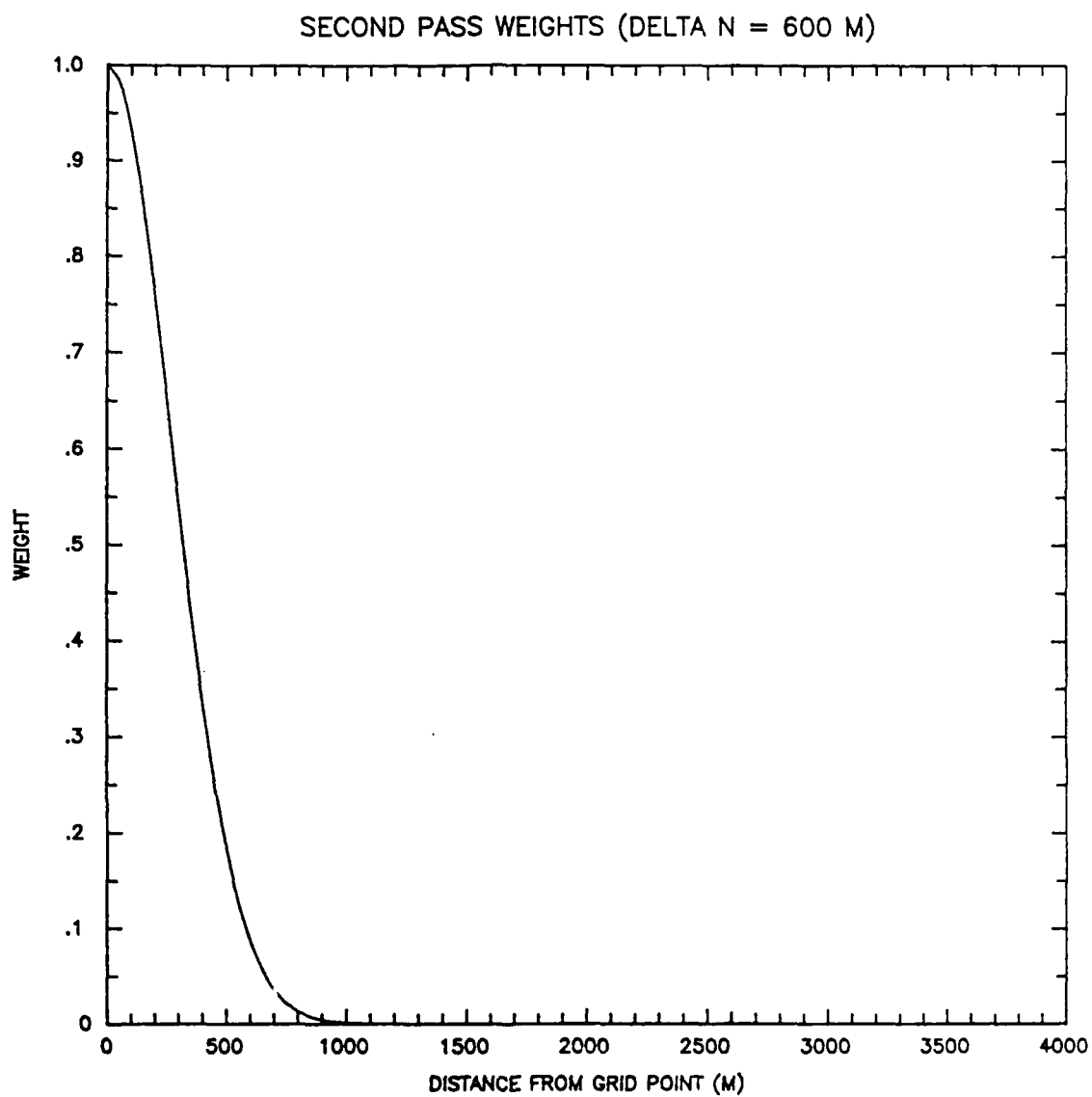


Fig. 4.5. Barnes second pass weight function using  $\Delta n = 600$  meters and  $\gamma = 0.2$ .

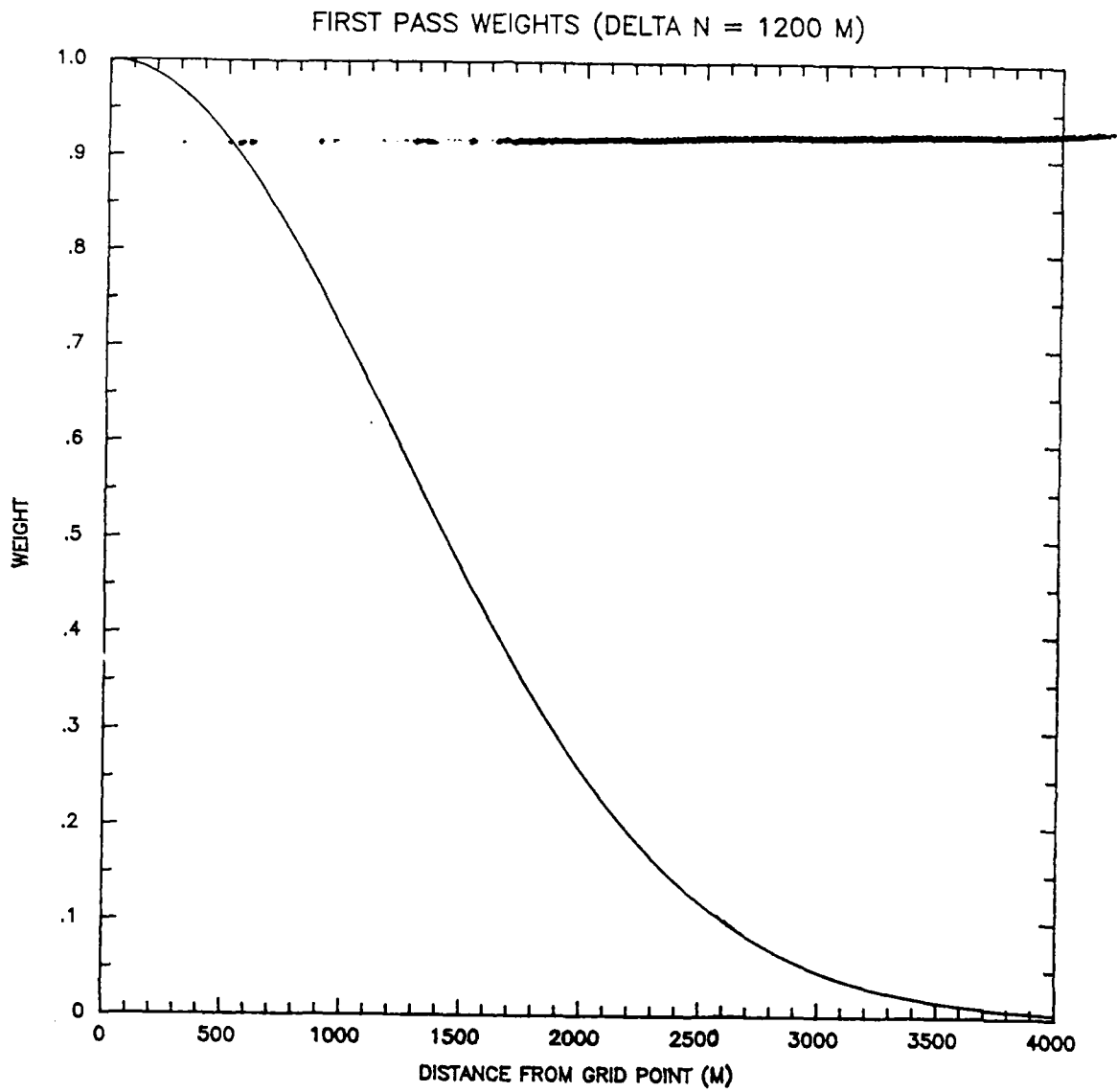


Fig. 4.6. Same as 4.4. but for  $\Delta n = 1200$  meters.

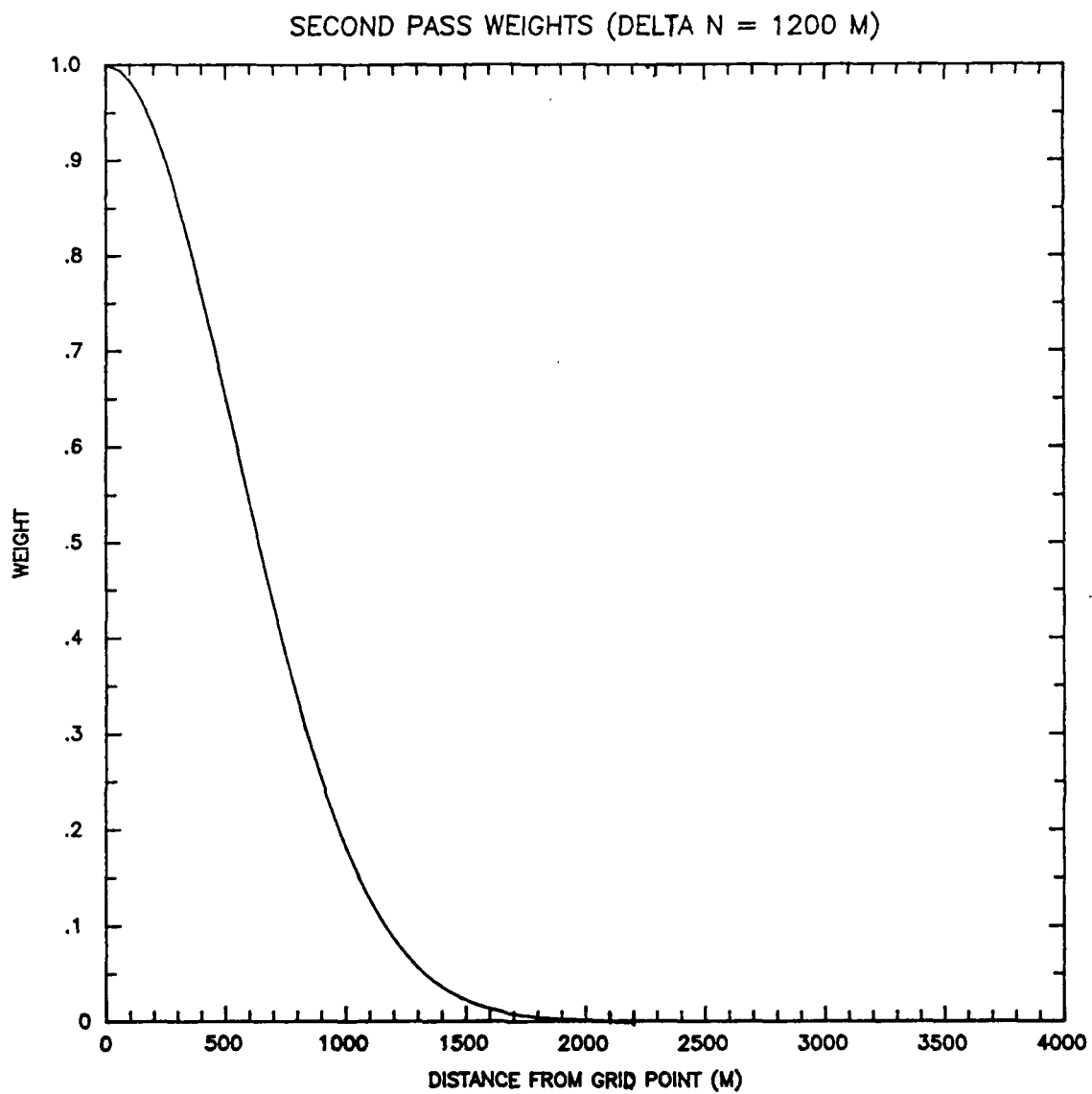


Fig. 4.7. Same as 4.5. but for  $\Delta n = 1200$  meters.

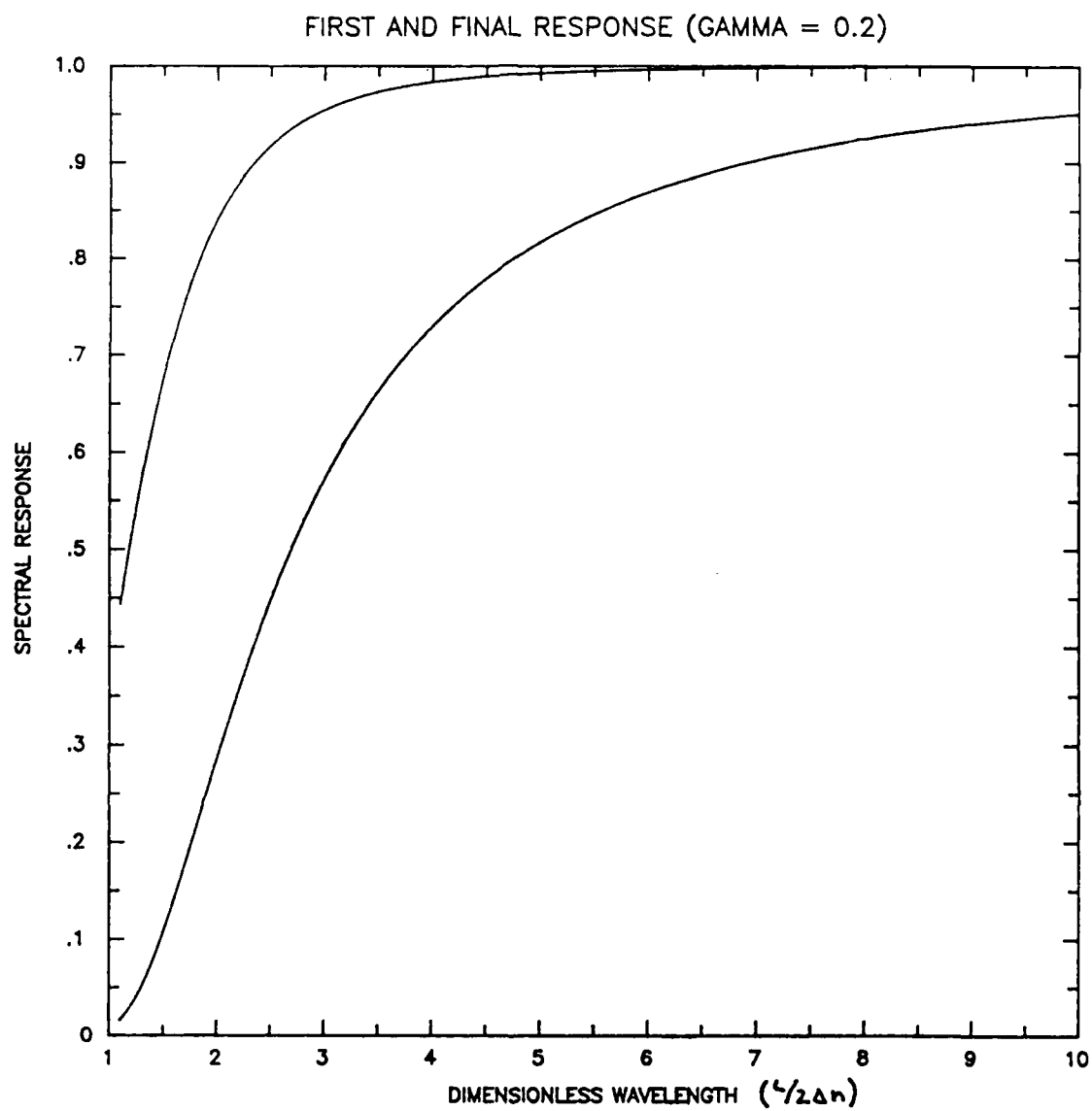


Fig. 4.8. Barnes first and second pass response functions.

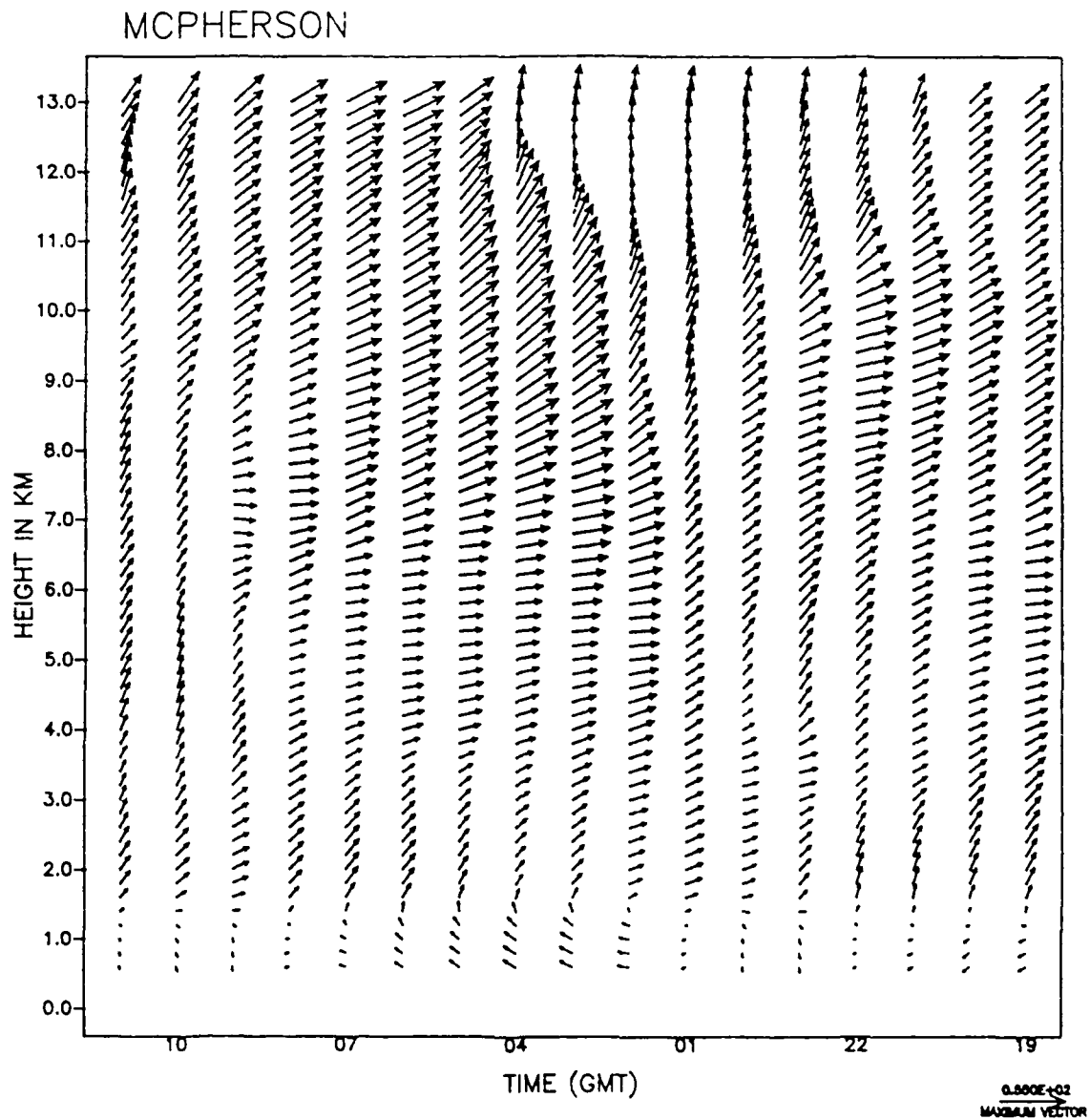


Fig. 4.9. Analyzed wind field for the 3-4 June McPherson profiler data. height interval is 200 meters.

. NORMAN

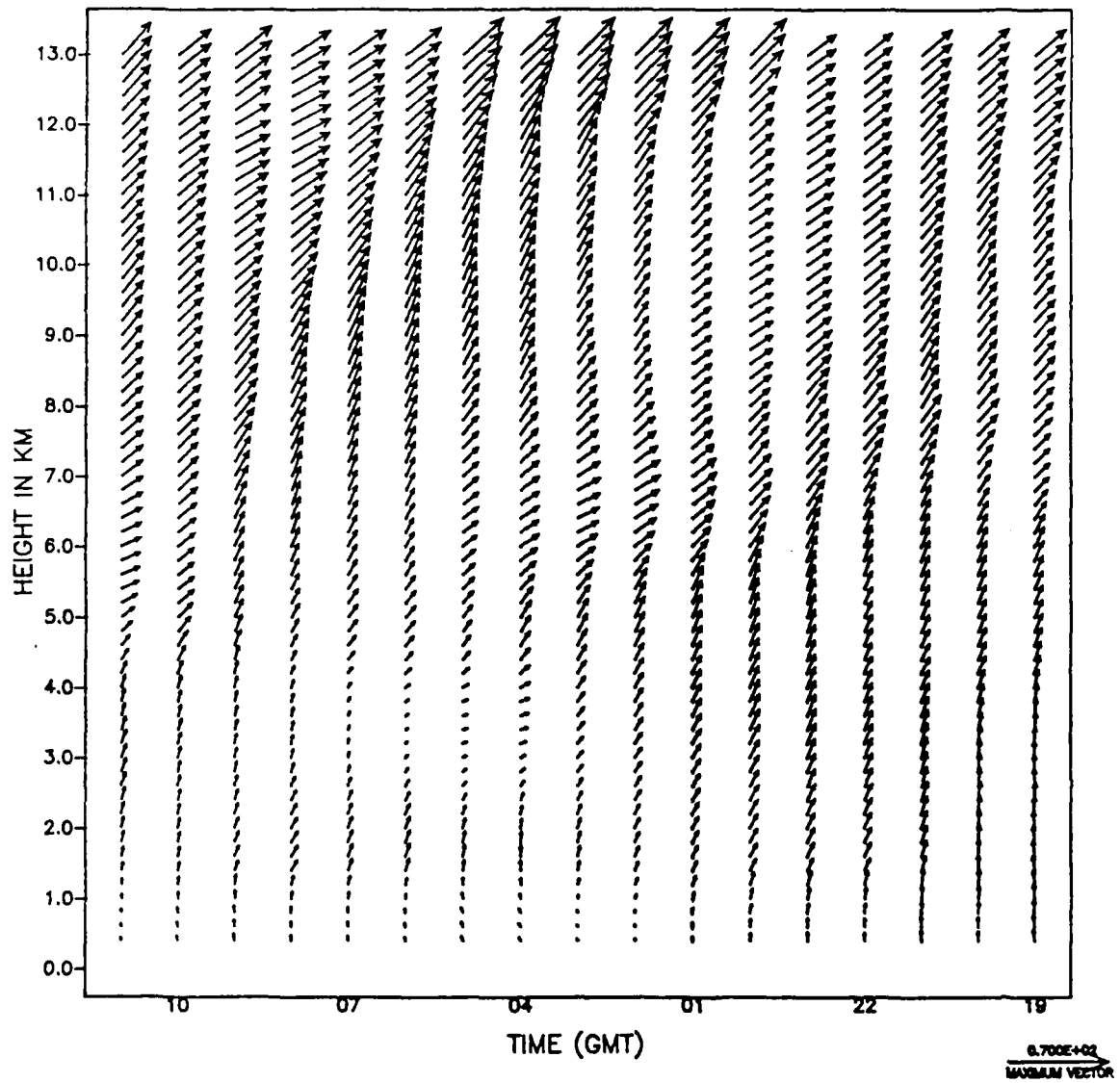


Fig. 4.10. Same as 4.9. but for 3-4 June Norman.

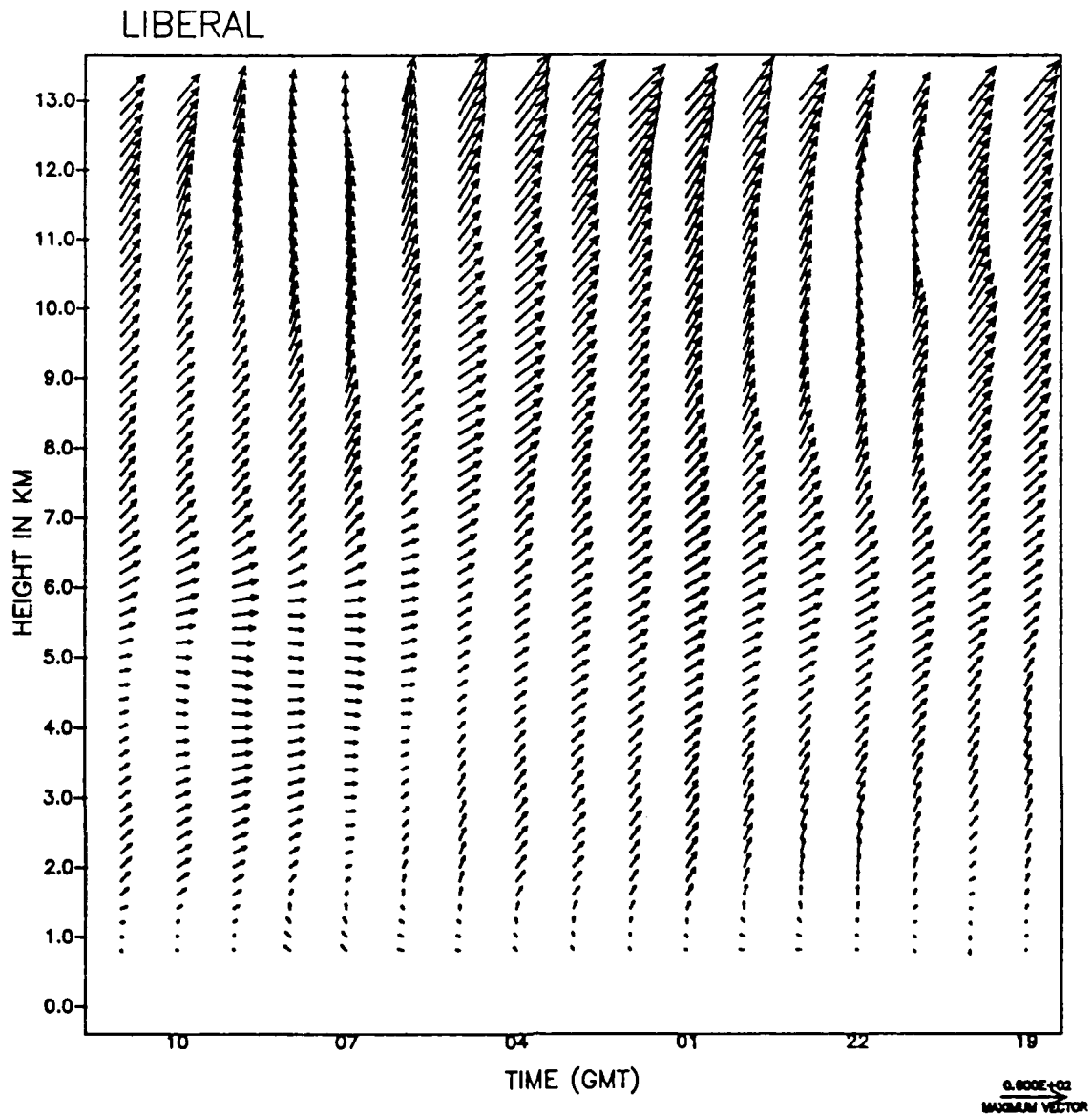


Fig. 4.11. Same as 4.9. but for 3-4 June Liberal.

## MCPHERSON

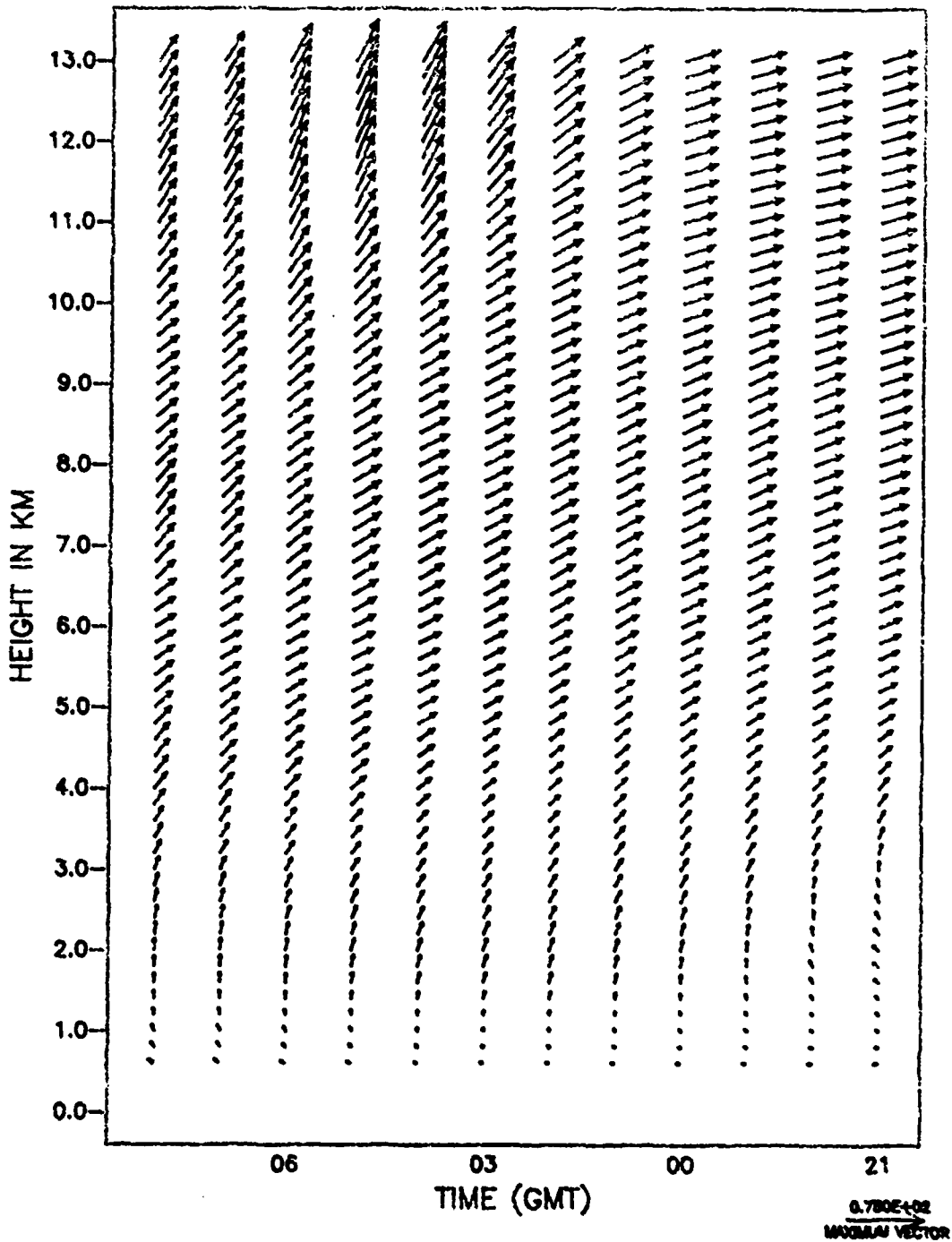


Fig. 4.12. Same as 4.9 but for 12-13 May McPherson.

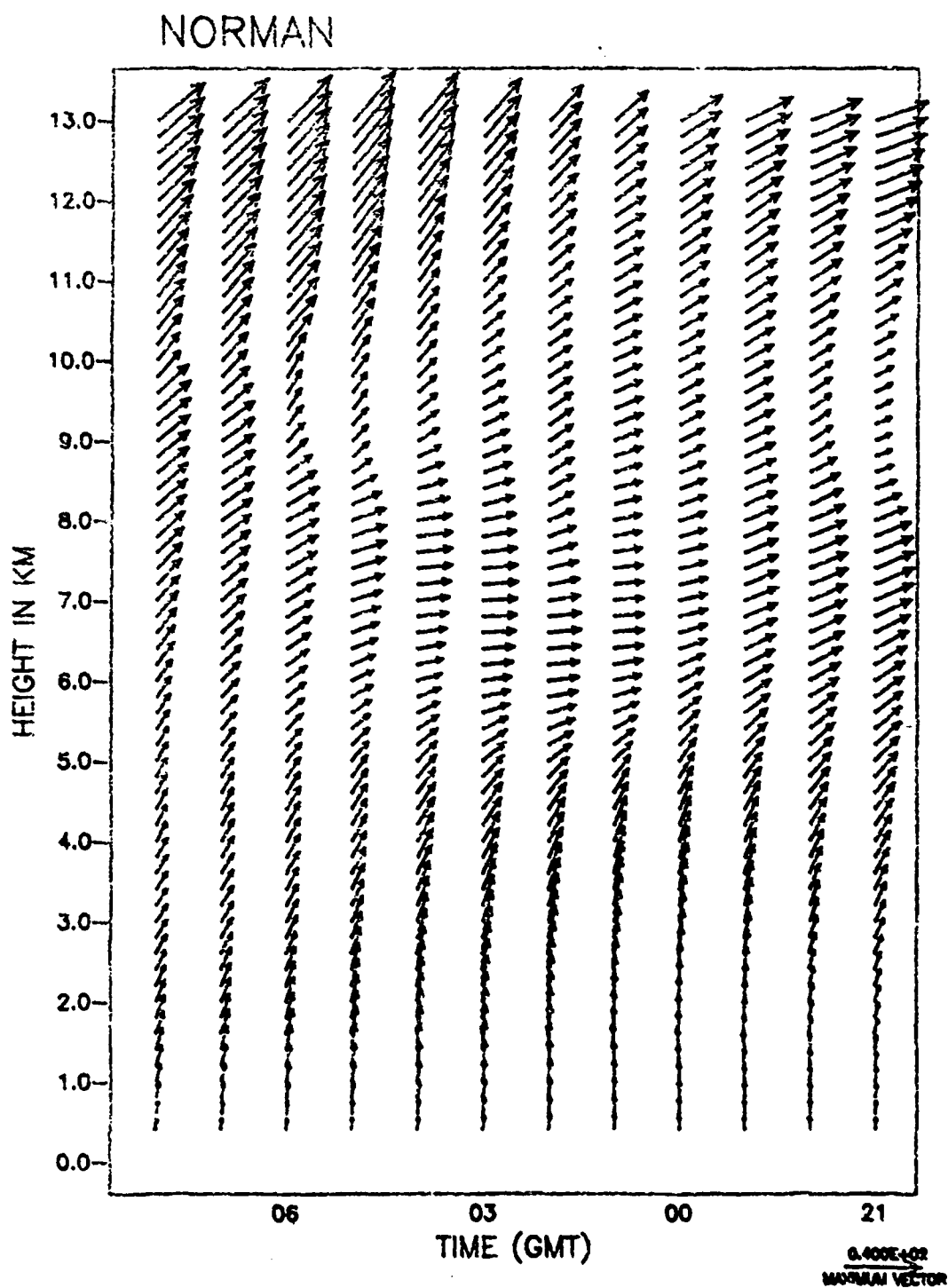


Fig. 4.13. Same as 4.9. but for 12-13 May Norman.

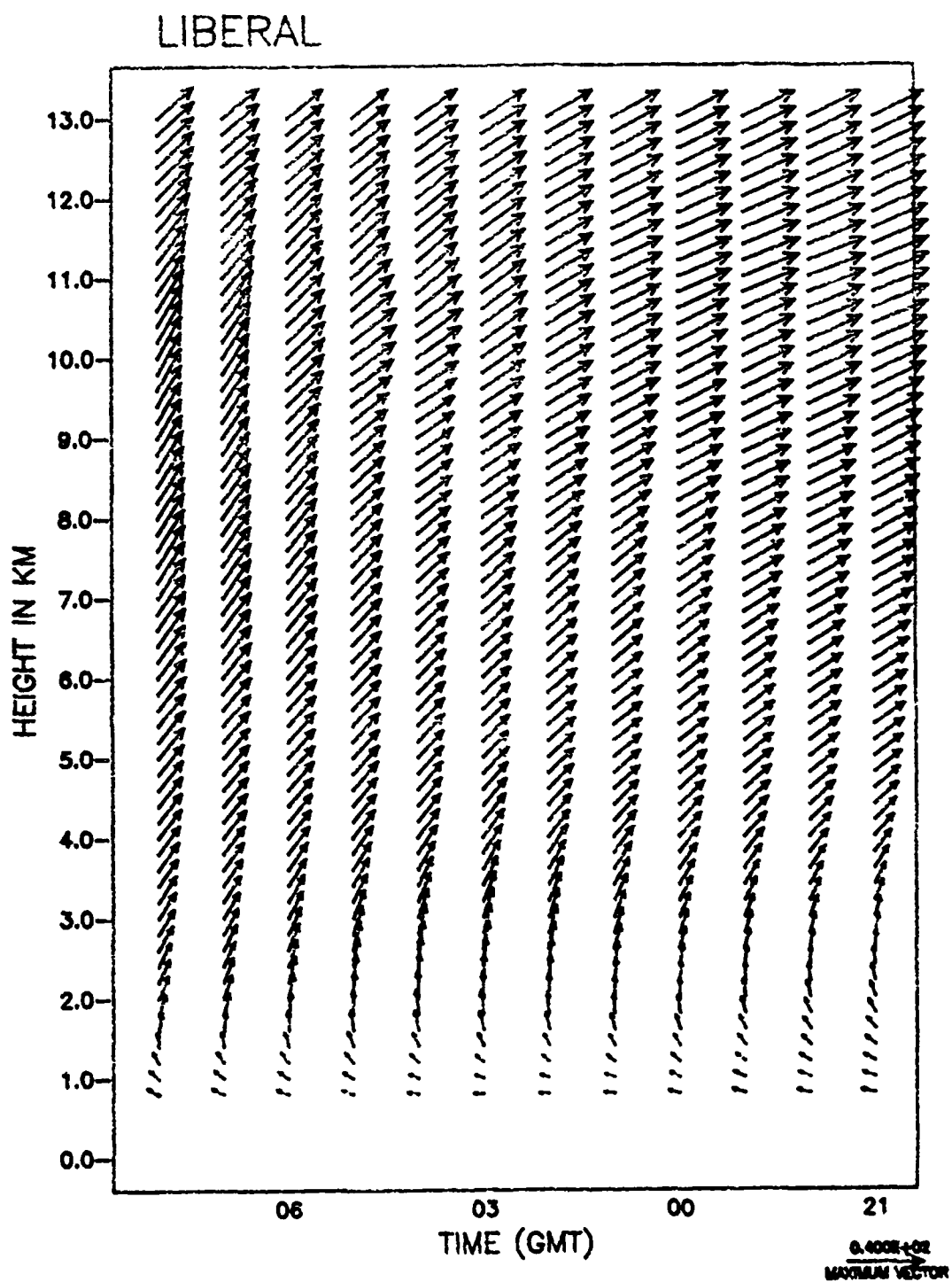


Fig. 4.14. Same as 4.9. but for 12-13 May Liberal.

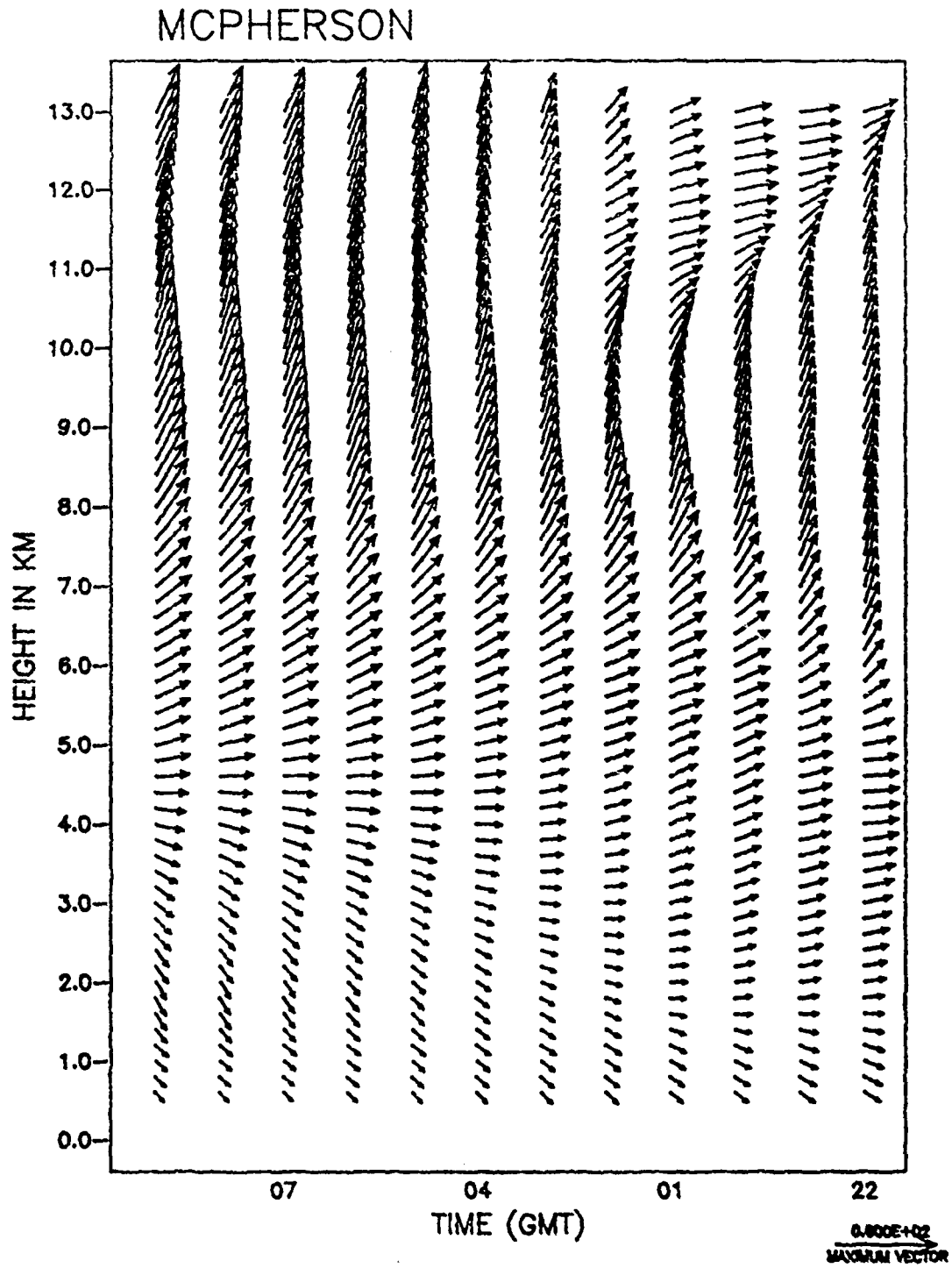


Fig. 4.15. Same as 4.9 but for 26-27 June McPherson.

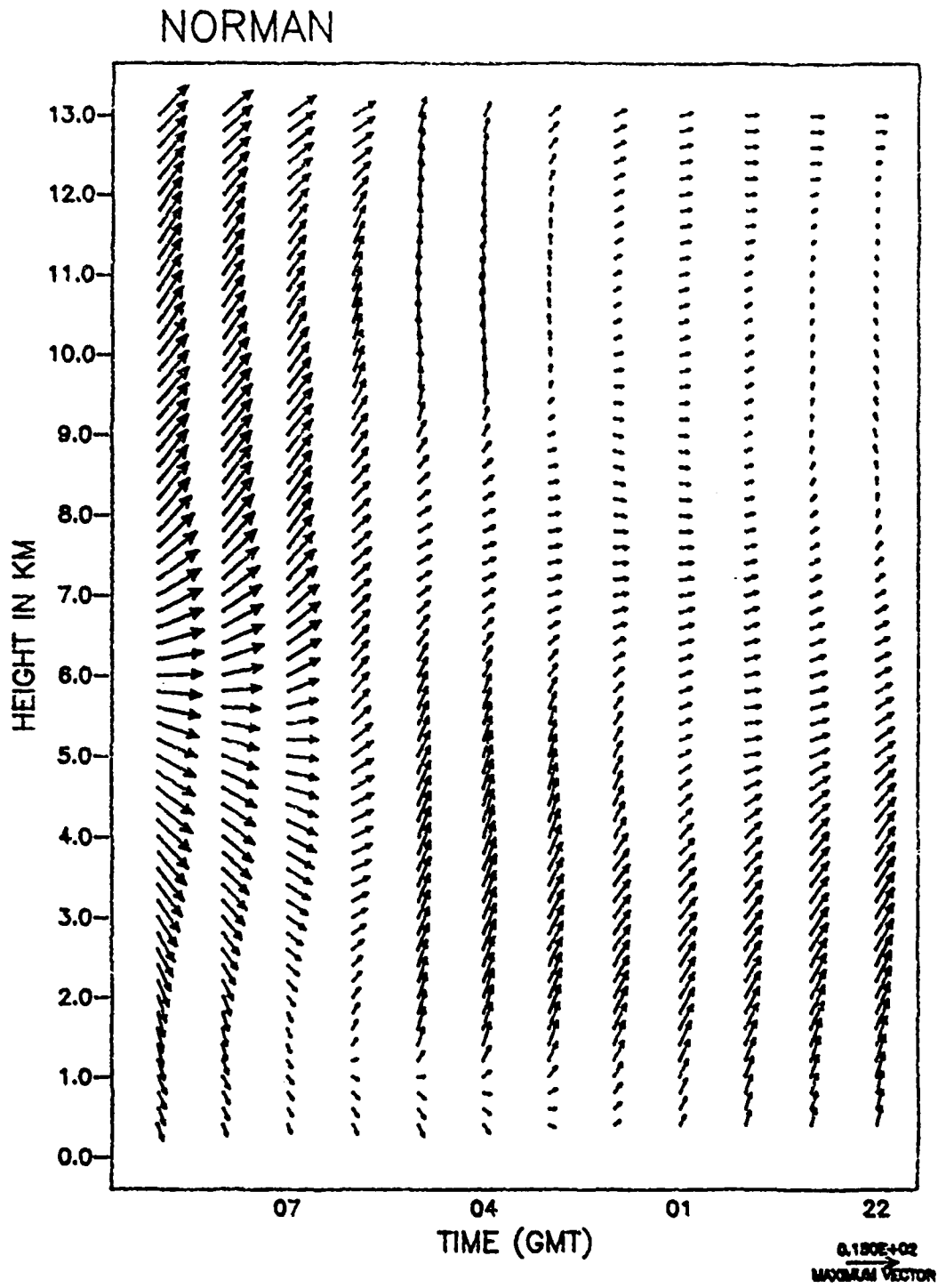


Fig. 4.16. Same as 4.9 but for 26-27 June Norman.

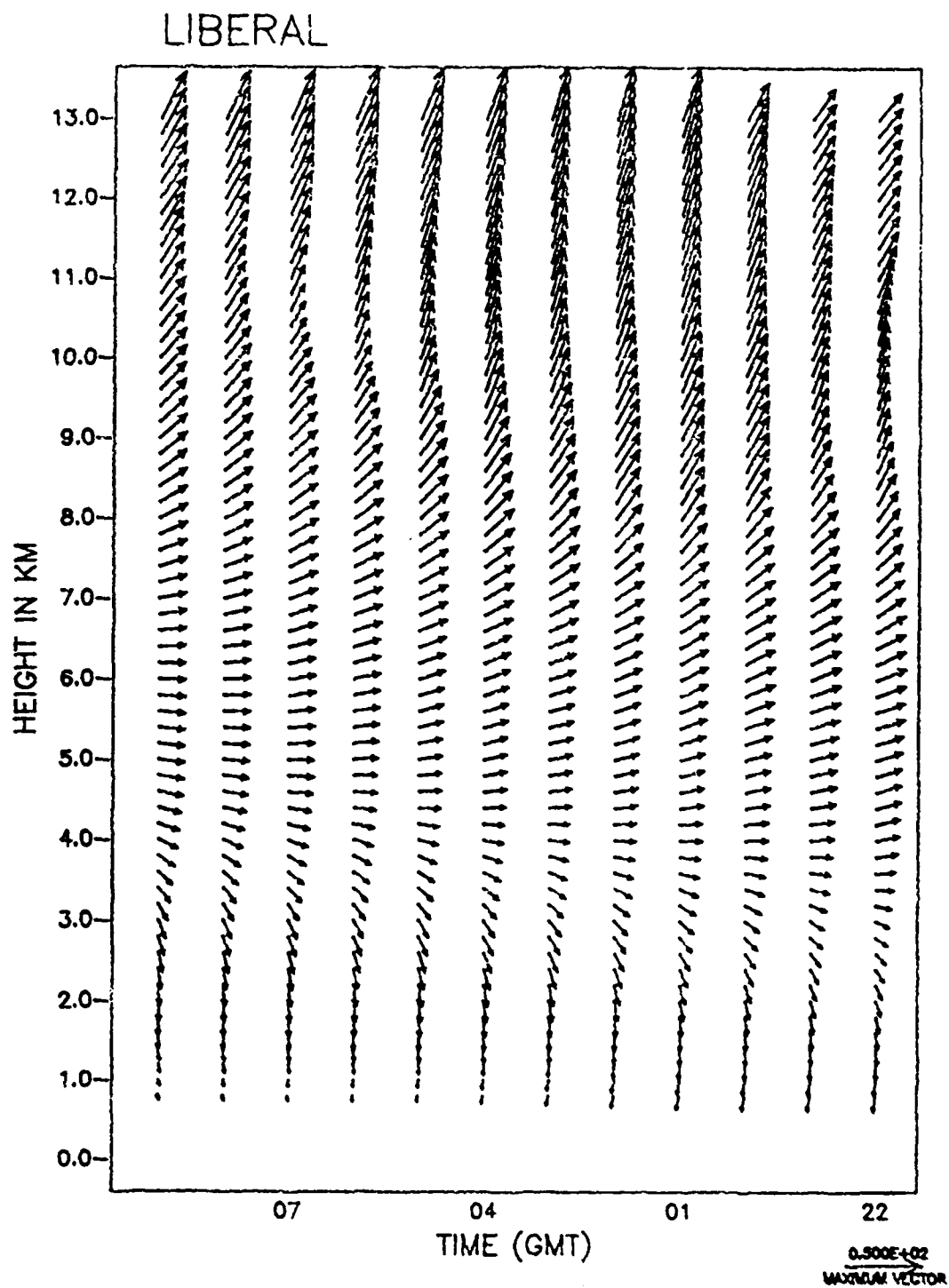


Fig. 4.17. Same as 4.9. but for 26-27 June Liberal.

where  $U_{Om}$  represents the  $m^{th}$  OBAN field value and  $U_{Dm}$  represents the  $m^{th}$  quality controlled data point.  $M$  is the total number of data points.

The OBAN grid values were bilinearly interpolated to the original data locations in order to perform the above calculation. The RMS values for each data set, based on an OBAN scheme using  $\Delta n = 1200$  meters, are shown in Tables 4.3 through 4.5. Table 4.6 shows the RMS values for the 3-4 June data set using  $\Delta n = 600$  meters in the OBAN scheme.

The OBAN grids were interpolated onto pressure surfaces utilizing either real rawinsonde data from the closest station (for 3-4 June) or a standard atmosphere modified for surface conditions (for 12-13 May and 26-27 June). Interpolation was performed via a cubic spline method.

#### 4.4 Kinematic Fields Calculations

A line integral method of computing divergence and vorticity in two-dimensional regions, discussed by Schaefer and Doswell (1979), is the method used in this study to calculate these kinematic fields within a triangle of wind profilers. A divergence value is calculated for the triangle at each grid point in the  $p$ - $t$  time series domain. The line integral method is discussed in the Appendix.

Once divergence values were obtained for each interpolated grid point within a profiler time series, the

## RMS VECTOR DIFFERENCES 3-4 JUNE

( $\Delta n = 1200$  m)

<u>PROFILER</u>	<u>COMP</u>	<u>DIFFS (m/s)</u>
Liberal	U	1.81
	V	1.70
McPherson	U	2.49
	V	2.92
Norman	U	1.10
	V	1.07

Table 4.3. RMS vector differences between analyzed and quality controlled wind fields for 3-4 June.

## RMS VECTOR DIFFERENCES 12-13 MAY

( $\Delta n = 1200$  m)

<u>PROFILER</u>	<u>COMP</u>	<u>DIFFS (m/s)</u>
Liberal	U	1.38
	V	1.24
McPherson	U	2.43
	V	2.49
Norman	U	1.89
	V	1.86

Table 4.4. Same as 4.3. but for 12-13 May.

## RMS VECTOR DIFFERENCES 26-27 JUNE

 $(\Delta n = 1200 \text{ m})$ 

<u>PROFILER</u>	<u>COMP</u>	<u>DIFFS (m/s)</u>
Liberal	U	1.36
	V	2.02
McPherson	U	2.67
	V	2.97
Norman	U	1.29
	V	1.81

Table 4.5. Same as 4.3. but for 26-27 June.

## RMS VECTOR DIFFERENCES 3-4 JUNE

 $(\Delta n = 600 \text{ m})$ 

<u>PROFILER</u>	<u>COMP</u>	<u>DIFFS (m/s)</u>
Liberal	U	1.32
	V	1.30
McPherson	U	1.96
	V	2.40
Norman	U	0.91
	V	0.79

Table 4.6. Same as 4.3. but for  $\Delta n = 600$  meters.

vertical velocity ( $W$ , where  $W = dp/dt$ ) was calculated for the same using an integrated form of the continuity equation in pressure coordinates:

$$W_p = W_{p+\Delta p} + \int_{p+\Delta p}^p (DIV) dp \quad (20)$$

which, by an assumption of linear variation of divergence within a layer  $\Delta p$  becomes:

$$W_p = W_{p+\Delta p} + \overline{DIV}_{\Delta p} \Delta p \quad (21)$$

The second term on the right hand side is the product of the average divergence within a layer and its thickness. Upward integration (from 900 to 200 mb) was used in this study.

Inserting surface wind data from the closest surface meso-network station into the profiler data sets, as discussed in Chapter II, allowed the simulation of boundary layer winds through objective analysis. Unfortunately, the upward sloping terrain towards the west throughout the triangle placed the Liberal profiler (the highest of the three) more than 500 meters higher than the Norman profiler (the lowest of the three). When the wind data for all three profilers were interpolated onto pressure surfaces, it became apparent that a sizable portion of the Norman boundary layer would have to be neglected when calculating kinematic fields over the triangle. This is due to the fact

that the lowest level for the three non-colinear wind observations required by the line integral method was determined by the lowest 25 mb pressure increment above Liberal, 900 mb. Fortunately, while setting omega to zero at 900 mb as a lower boundary condition seems a bit unrealistic, this level is actually not far from the surface and the features in the derived omega fields shouldn't be rendered invalid.

A data set submitted to the most rigorous known quality control checks will still contain measurement errors. Filtering can diminish unbiased errors further but the final fields will contain biased errors to some degree. Unfortunately, a 10% error in wind measurement can result in a 100% error in divergence estimates. When computing vertical motion via integrated divergence, these divergence errors can accumulate so that, for upward integration, extremely large vertical motion values can be computed in the lower stratosphere where they should be small.

The effect of accumulated divergence errors can be reduced by specifying zero vertical velocity at the top of the troposphere or at the top of the data domain through adjustment of the divergence at each level (O'Brien, 1970). Various adjustments can be performed but the simplest one, linear adjustment, was used for this study. A constant correction factor,  $C$ , was calculated for each profile and subtracted from the divergence,  $Div_k$ , at each level within

that profile to obtain an adjusted divergence,  $\text{Div}'_k$  where:

$$C = \frac{W_{\text{top}} - W_0}{P_0 - P_{\text{top}}} \quad (22)$$

with  $W_{\text{top}}$  equal to the unadjusted vertical motion at the top of the data domain,  $W_0$  denotes vertical motion at the bottom of the domain (usually set to zero), and  $p_0$  and  $p_{\text{top}}$  denote pressure at data domain bottom and top, respectively. So:

$$\text{Div}'_k = \text{Div}_k - C. \quad (23)$$

Adjusting the divergence fields necessitates adjusting the original wind field only if an adjusted wind field is needed for further calculations. Therefore, in this study, no adjustments of this type were applied.

## CHAPTER V

### KINEMATIC FIELD RESULTS AND DISCUSSION

After the three omega fields (one for each data set) are calculated and adjusted as discussed in Chapter IV, they are compared with satellite imagery and weather charts from the data set time frames.

#### 5.1 3-4 June

The derived and adjusted omega field for this data set is shown in Fig. 5.1. Values in the field are in units of  $10^2 \mu\text{bs}^{-1}$ . For example, the omega value at 1900 GMT at the 700 mb level is  $2.4 \mu\text{bs}^{-1}$ .

At 1900 GMT, the omega field indicates downward vertical motion at all levels except for a shallow layer of weak rising motion at the lowest domain levels. This seems to correspond well with the 1900 GMT visible satellite imagery (Fig. 5.2) which shows no evidence of deep upward vertical motion (ie. no thunderstorm activity) within the profiler triangle. Note that widespread shallow convection is evident in the form of small cumulus cloud elements within

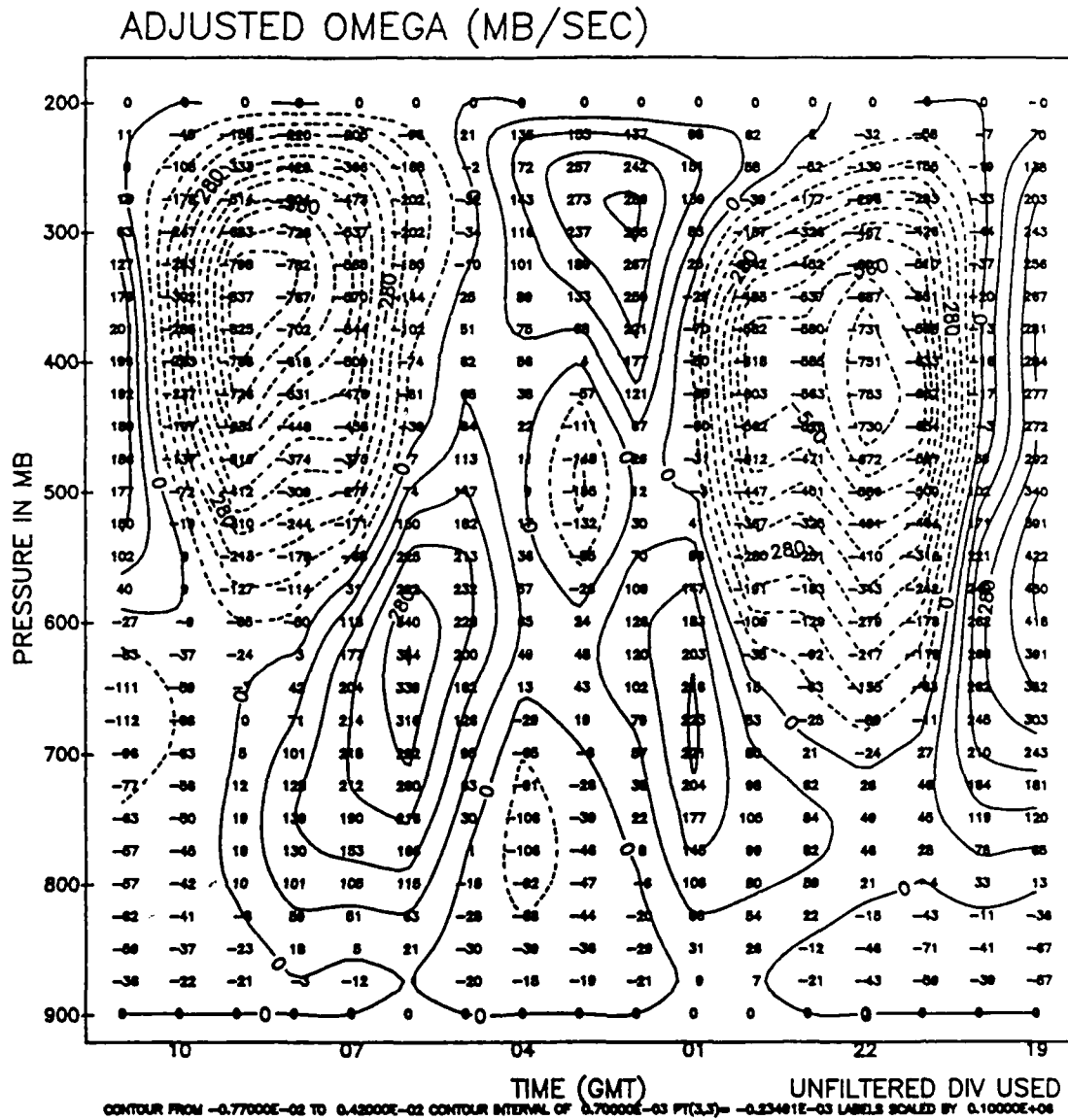


Fig. 5.1. Kinematically derived omega field for 3-4 June. Values are in units of  $10^2 \mu\text{bs}^{-1}$ .

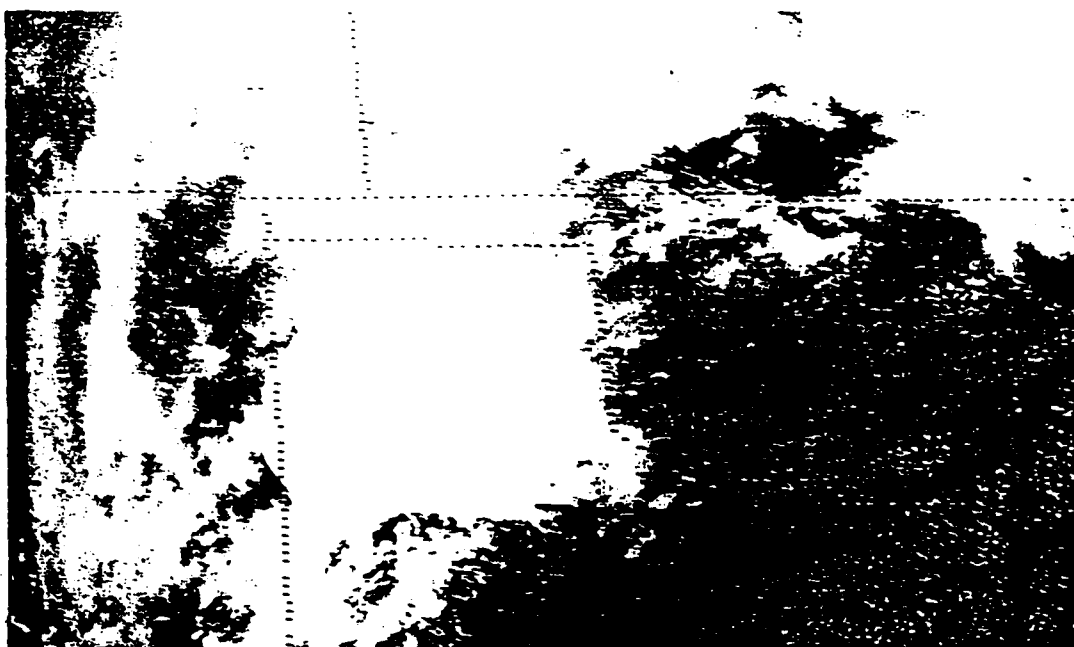


Fig. 5.2. GOES visible imagery at 1900 GMT, 3 June.



Fig. 5.3. Same as 5.2 but at 2230 GMT.



the triangle domain.

Widespread thunderstorm activity begins to develop rapidly in western portions of the triangle and, by 2230 GMT, dominates the northern half of the triangle as seen in Fig. 5.3. Protruding thunderstorm tops are visible above the cirrus shield near the triangle centroid. The 1935 GMT NMC radar summary (Fig. 5.4) verifies the absence of thunderstorm activity within the triangle within the first half-hour of this data set. It is apparent from the 2235 GMT radar summary (Fig. 5.5) that the protruding cloud tops, seen in Fig. 5.3 within the triangle, are intense thunderstorms. The rapid development of widespread deep convection corresponds well with the steep omega gradient seen between 2000 and 2100 GMT in the mid and upper troposphere and the vertical velocity maximum of  $-7.5 \mu\text{bs}^{-1}$  in Fig. 5.1 at 2200 GMT at the 425 mb level.

This first area of thunderstorm activity, by now organized into an MCS, moved to the east-northeast along the ridgeline. By 0300 GMT this MCS had moved out of the profiler triangle (Fig. 5.6). The second MCS in the southern Texas Panhandle hadn't reached the triangle by 0300 GMT, indicating that the triangle could have been in an area of subsidence between the two MCS's. Indeed, the omega fields show that deep downward vertical motion dominated most of the troposphere for about a four hour time period between 0100 and 0500 GMT.

The omega field shows a rapid return to rising motion in

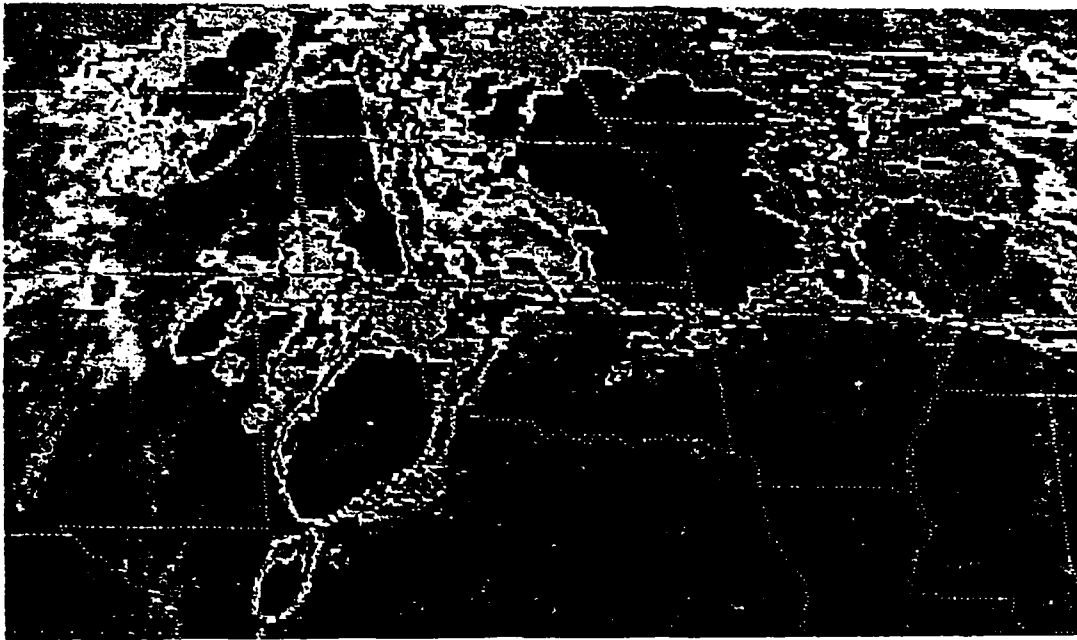


Fig. 5.6. GOES infrared imagery at 0300 GMT, 4 June.

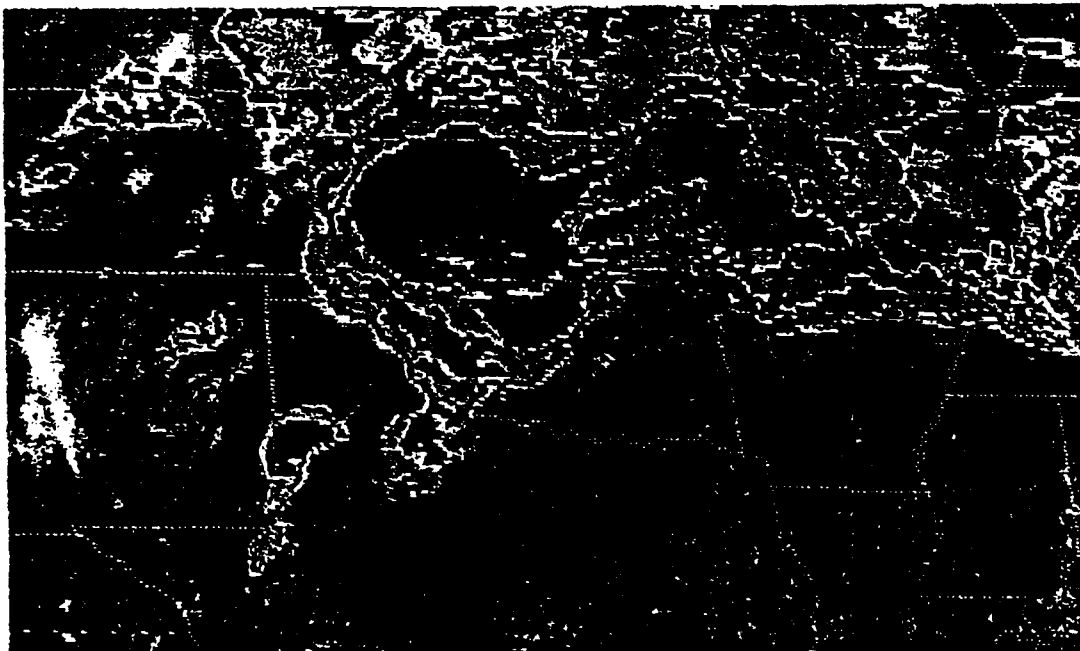


Fig. 5.7. Same as 5.6. but at 0800 GMT.

[illegible]

Fig. 5.9. Same as 5.8. but for 0835 GMT

the mid and upper troposphere by 0700 GMT. Omega values of  $-8.4 \mu\text{bs}^{-1}$  at 0900 GMT are indicated at 325 mb. Satellite imagery at 0800 GMT (Fig. 5.7) shows that the second MCS is well within the profiler triangle. The echo patterns seen on the 0335 and 0835 GMT radar summaries (Figs. 5.8 and 5.9) support the satellite evidence (Figs. 5.6 and 5.7) for these vertical motion features.

Note that as the second MCS moved into the triangle near the end of the time frame, the omega field suggests that low level rising motion was much weaker and shallower than with the first MCS. A possible explanation for this is offered by Maddox (1983). The genesis region for the first MCS was within the profiler triangle while the genesis region for the second MCS was the southwest Texas Panhandle. The second MCS, therefore, was many hours old before it moved into the triangle. The MCS composite study by Maddox states that the typical MCS is characterized by low level convergence (and rising motion) in its genesis region and by weak divergence (and downward motion) at low levels during its mature stage. The omega field for this data set would seem to be consistent with these results. It is important to remember, however, that boundary layer winds are crudely approximated by the objective analysis technique (ie. no profiler data exists within about 1.5 km AGL). While the analysis provides good wind field continuity throughout the gap, important boundary layer dynamics may not be represented. As a result, meteorological interpretation of

omega field features at low levels may be misleading.

Subsequent satellite imagery (not shown) shows that the second MCS begins to decay as it moves east-northeastward out of the profiler triangle. A rapid decrease in upward vertical motion is seen in the omega field by 1100 GMT, the end of this data set.

### 5.2 12-13 May

The adjusted omega field for this 12-hour data set is shown in figure 5.10. As before, omega values are in units of  $10^2 \mu\text{bs}^{-1}$ .

The clear sky conditions prevalent over Oklahoma through 2200 GMT (Fig. 5.11) verify the deep downward vertical motion apparent in the derived omega field during this time. With the onset of rising motion at mid-tropospheric levels after 2300 GMT, organized deep convection becomes evident along the southeastern boundary of the profiler triangle (Fig. 5.12).

In contrast to circumstances which occurred during the 3-4 June time period, the main area of thunderstorm activity developed just outside and east of the triangle and never entered into it. The omega field, however, indicates that the layer of rising motion within the triangle deepened vertically and intensified rapidly until a maximum of  $-6.3 \mu\text{bs}^{-1}$  was reached at 525 mb at 0400 GMT. Rising motions

## ADJUSTED OMEGA (MB/SEC)

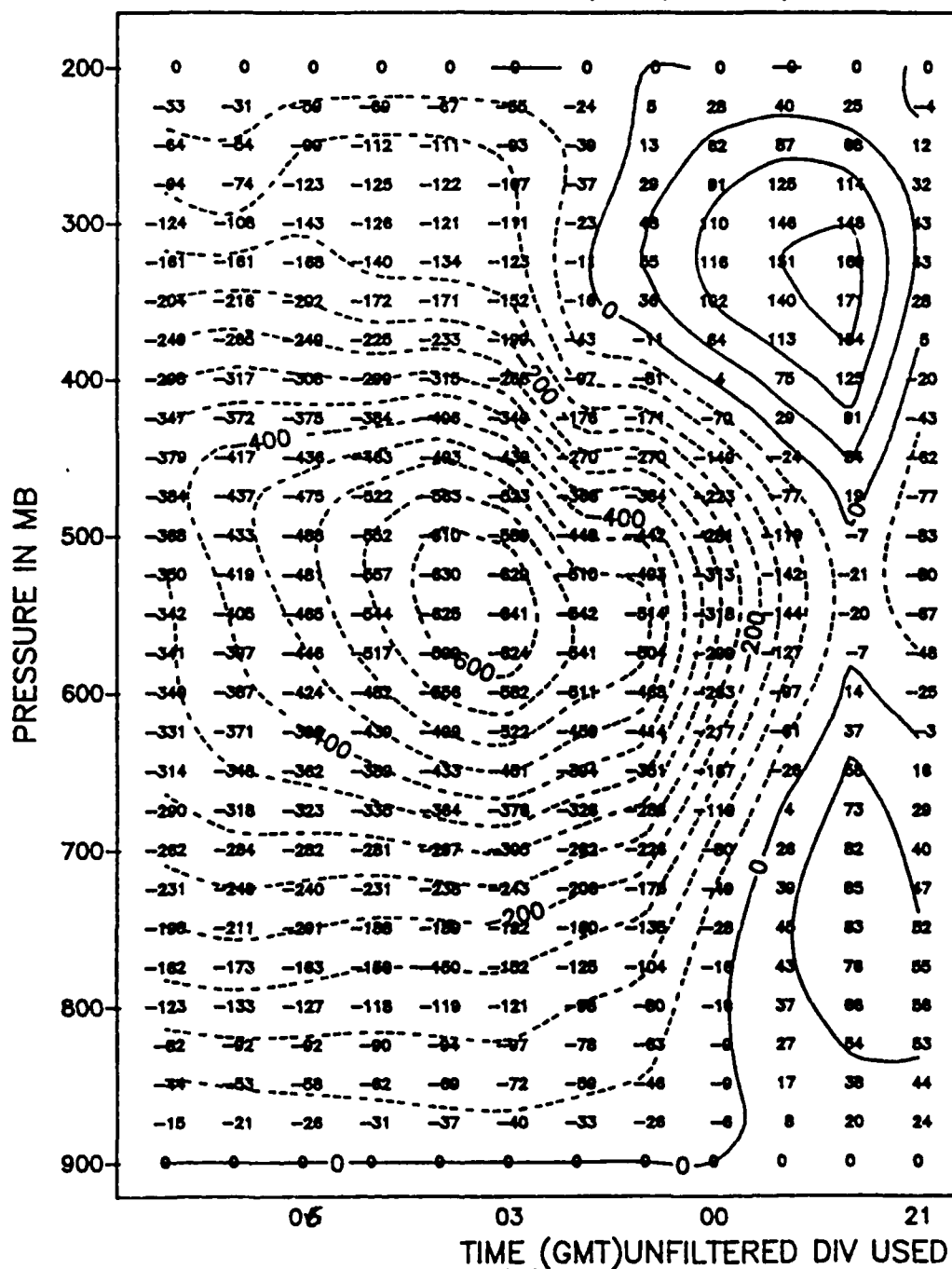


Fig. 5.10. Kinematically derived omega field for 12-13 May. Values are in units of  $10^2 \mu\text{bs}^{-1}$ .

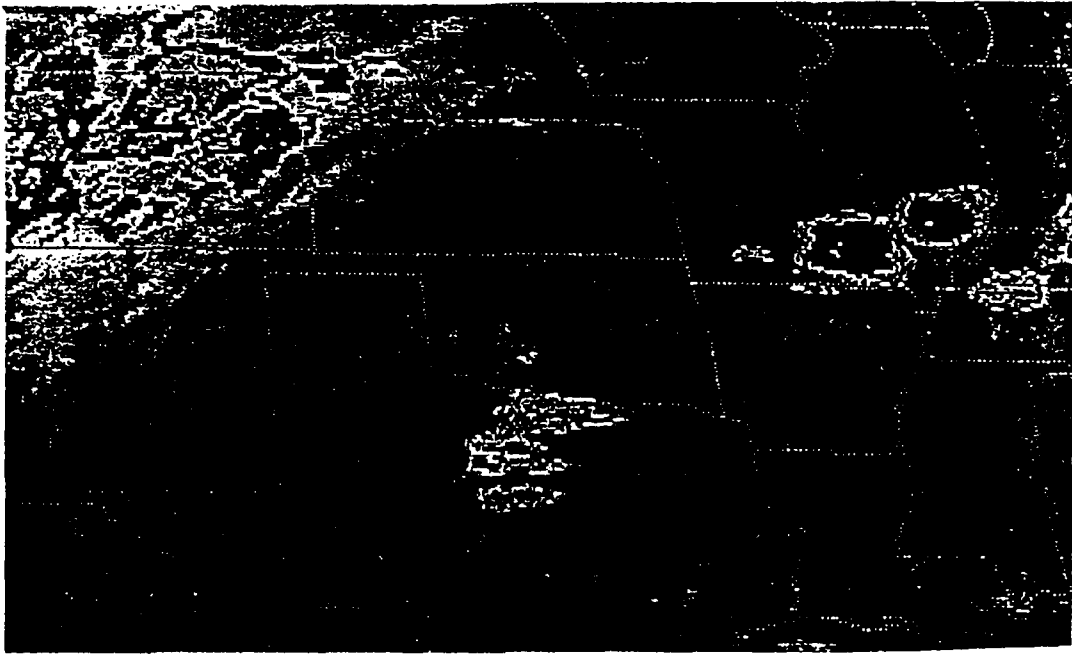


Fig. 5.11. GOES infrared imagery at 2200 GMT, 12 May.

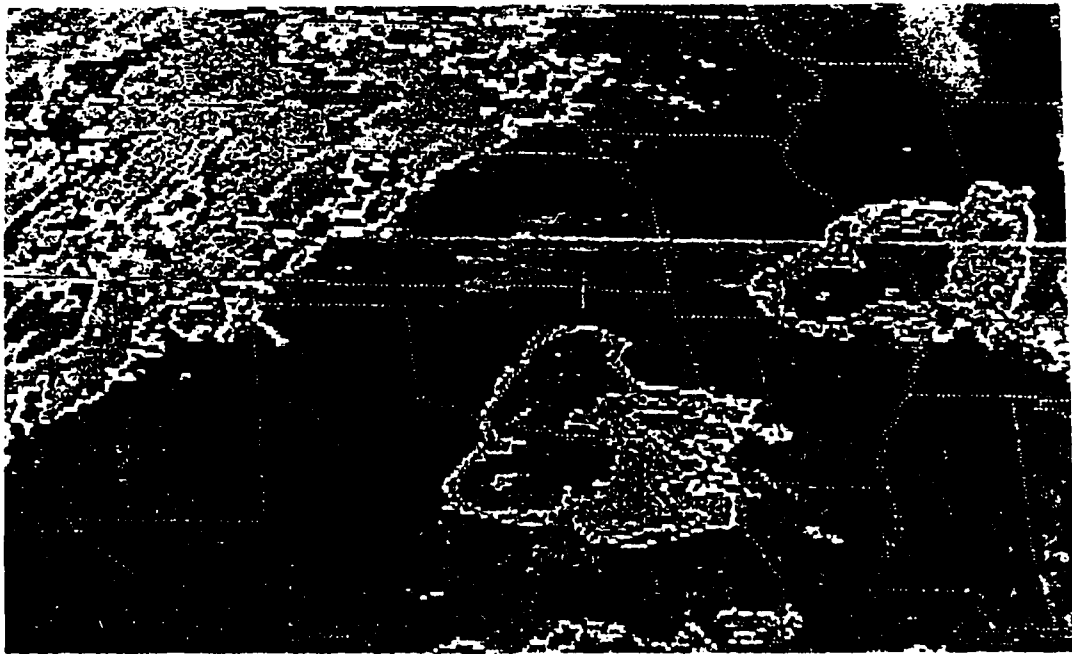


Fig. 5.12. Same as 5.11. but at 0030 GMT, 13 May.

then began to decrease slowly with time at all levels but, even at 0800 GMT (the end of this data set), rising motion dominated all pressure levels in the domain. The triangle remained clear of thunderstorm activity (Fig. 5.13).

A possible explanation for the presence of negative omega values with no visible evidence of such within the triangle is offered by Carr and Millard (1985) with their composite study of comma cloud characteristics. Re-inspection of satellite imagery for this data set reveals the development of a large comma-like crescent of thunderstorm activity around the profiler triangle by 0630 GMT (Fig. 5.14) whereas this feature wasn't noticeable through the first several hours. The profiler triangle is located within the northern end of the dry slot of this comma cloud. Figure 5.15 is a schematic diagram of the composite comma cloud from the Carr and Millard study on the 317 K isentropic surface. The dotted lines represent isobars and the values to the upper right of each station circle are the pressures at this isentropic surface. A major conclusion of the Carr and Millard study was that the area of maximum rising motion within a comma cloud structure is within the clear northern end of the dry slot. This rising air has a previous history of descent and drying and has not yet become saturated as it surges northeastward around the vorticity center located in northeastern New Mexico.

The highest upward vertical velocity value seen in Fig. 5.10 is  $-6.3 \mu\text{bs}^{-1}$ . This corresponds well with the

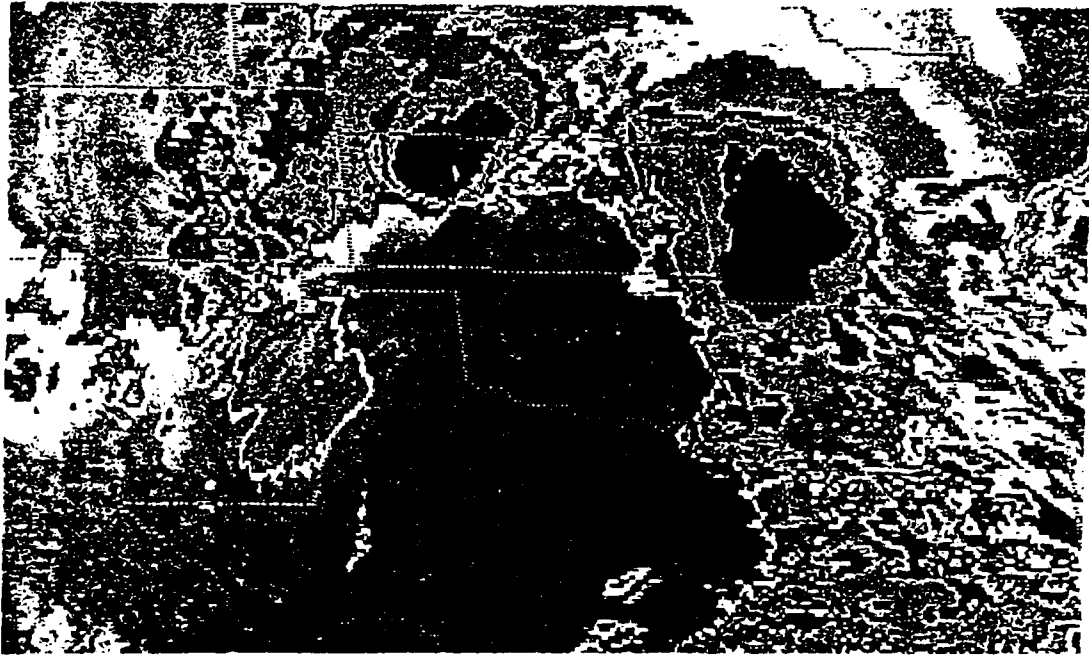


Fig. 5.13. Same as 5.11. but at 0800 GMT.

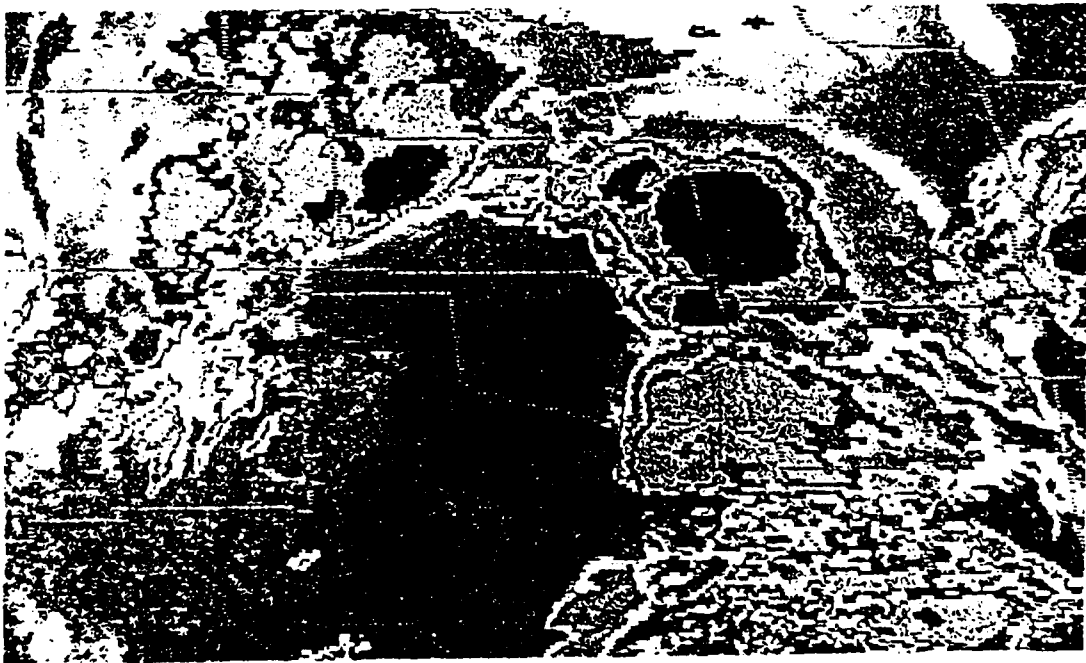


Fig. 5.14. Same as 5.11. but at 0630 GMT.

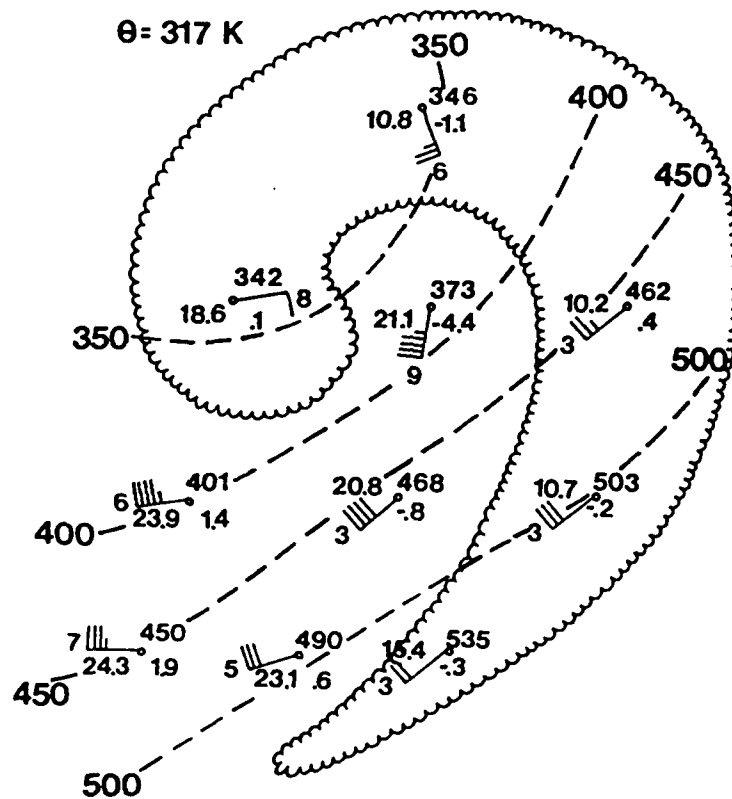


Fig. 5.15. Schematic diagram of a composite comma cloud on the 317 K isentropic surface (Carr and Millard, 1984).

Fig. 5.17. Same as 5.16. but for 500 mb.

composite  $-4.4 \mu\text{bs}^{-1}$  value derived by Carr and Millard (1984) within the dry slot.

Further evidence that rising motion is occurring in the profiler triangle exists on upper air charts of the period. Figure 5.16 is the NMC 850 mb analysis for 0000 GMT, 13 May. Warm air advection is evident in northwest Oklahoma and southwest Kansas. Note that this warm air is quite dry from the Texas Panhandle through southwest Kansas at this time. At 500 mb (Fig. 5.17), the presence of a short wave trough in the Texas Panhandle at 0000 GMT implied that cyclonic vorticity advection was occurring immediately downstream within the profiler triangle.

In short, evidence from satellite imagery and upper air charts reveals that rising motion probably was occurring within the profiler triangle - in support of the derived omega field findings. This rising air was too dry to saturate during that portion of its ascending trajectory within the triangle, however, resulting in the lack of thunderstorm activity and the prevalence of clear skies in this domain.

### 5.3 26-27 June

While the omega field results from this data set (Fig. 5.18) were less interesting than the other two, the strongest rising motions (between  $-10.0$  and  $-10.2 \mu\text{bs}^{-1}$ )

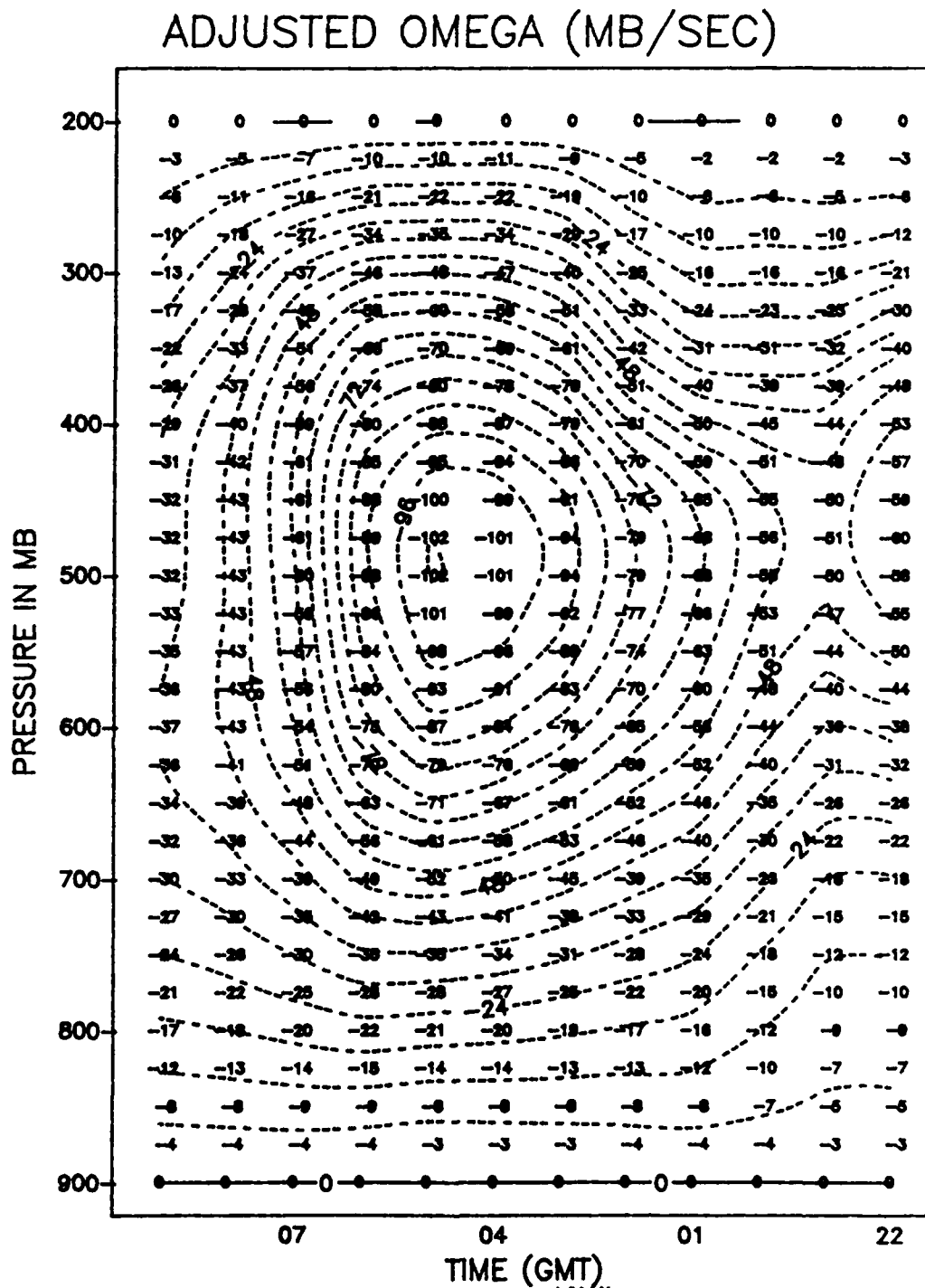


Fig. 5.18. Kinematically derived omega field for 26-27 June. Values are in units of  $10^1 \mu\text{bs}^{-1}$ .



Fig. 5.19. GOES infrared imagery at 2100 GMT, 26 June.

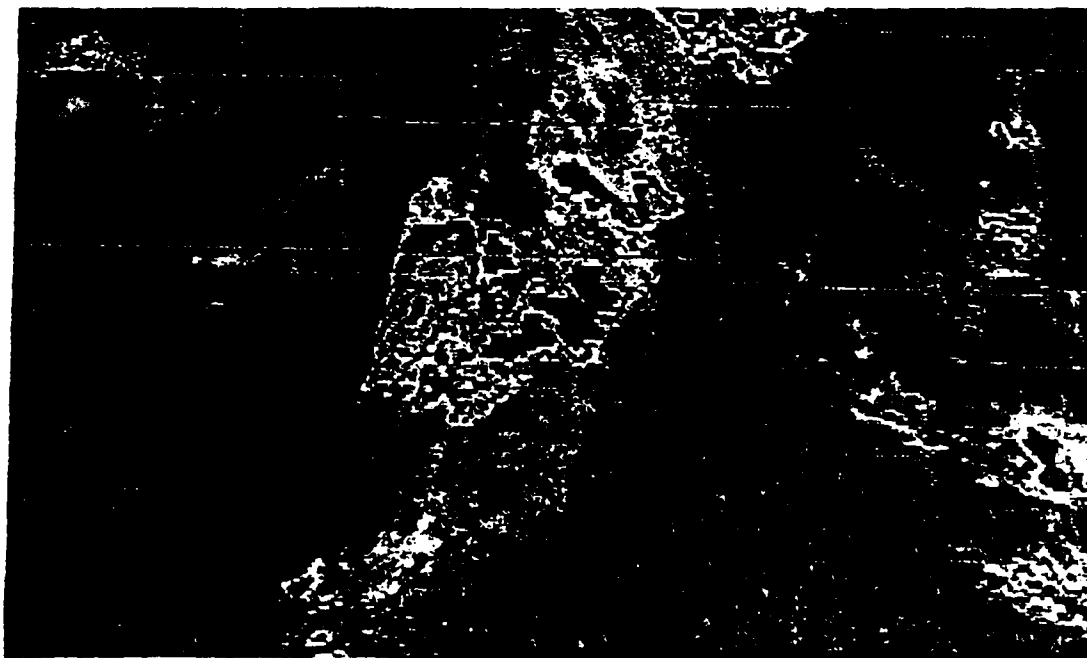


Fig. 5.20. Same as 5.19. but for 0300 GMT, 27 June.

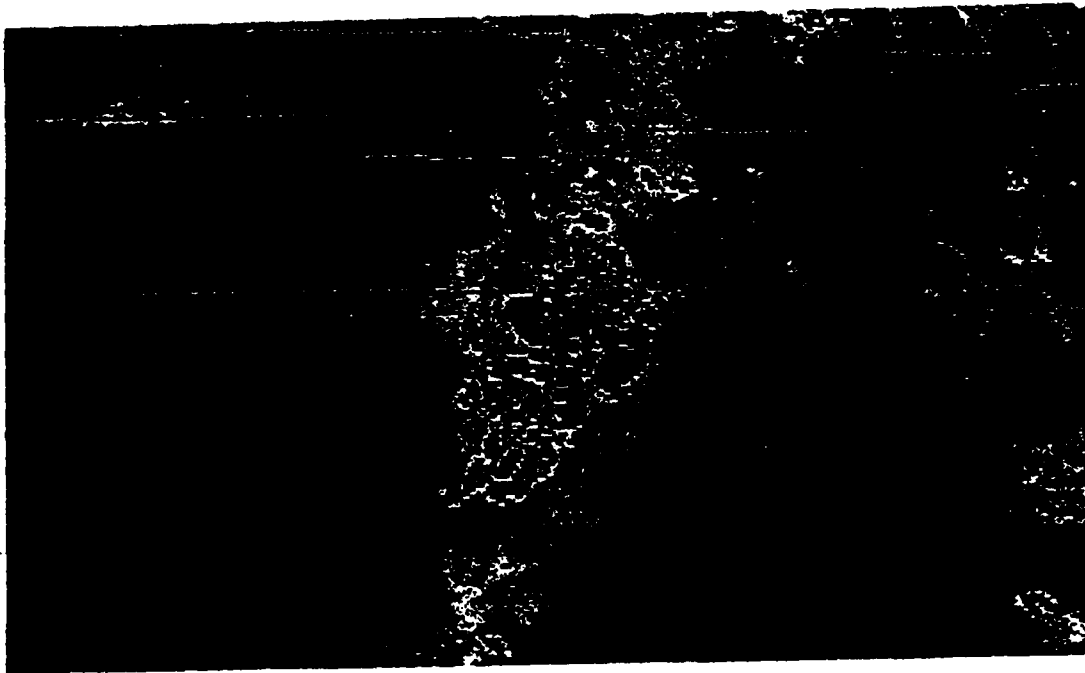


Fig. 5. 21. Same as 5.19. but for 0500 GMT.

were obtained from this case.

As discussed in Chapter II, the dominating weather feature in this data set was a slow moving cold front traveling southeastward across the profiler triangle. Rising motion throughout the troposphere was apparent in the omega field for the entire time frame with maximum values derived between 0400 and 0500 GMT near the 500 mb level.

Satellite imagery showed widespread deep convection along the frontal boundary at 2100 GMT (Fig. 5.19) although not continuous along the boundary within the triangle. By 0300 GMT (Fig. 5.20), the thunderstorm activity had gradually consolidated into a line stretching southwest to northeast through the triangle. After 0500 GMT (Fig. 5.21), thunderstorm activity within the triangle rapidly became unorganized and began collapsing. All of these observations seem to verify the gradual increase in derived rising motions through 0400 GMT and a rapid decrease after 0500 GMT. These trends are most noticable in the middle troposphere.

#### 5.4 Sensitivity Studies

Although, as mentioned in Chapter IV, a constant normalized time to space conversion factor of 640 meters was used to aid in the calculation of the domain "area" for each case study, an omega field comparison was performed for the

3-4 June data set between a field using  $\Delta n = 600$  meters and another using  $\Delta n = 1200$  meters. Figure 5.22 shows the latter derived field. Because of its larger  $\Delta n$  value, the omega field in Fig. 5.22 contains less detail and structure than in Figure 5.1. Doubling  $\Delta n$  from 600 to 1200 meters decreases the amplitude response from 0.84 to 0.37 at the  $L = 2400$  meter wavelength (see equations 11, 15 and 16 in Chapter IV).

Of the three data set omega fields, the 3-4 June field contains the most structure by far; - even with  $\Delta n = 1200$  meters. While the other data set omega fields were dominated by one or, at most, two major features, the 3-4 June omega field contained no less than five rising or sinking motion centers. With  $\Delta n = 600$  meters, the resultant rough omega field contained an even higher number of local maxima and minima.

For 3-4 June, the smoother omega field suggests that rising motion is never re-established at any level under the second MCS. However, the return of rising motion is seen at the very end of the time frame (ie. 1100 GMT, 4 June) between 600 and 750 mb. While several short-lived centers of relatively weak rising motion are indicated at low and mid levels in Fig. 5.1 around 0300 and 0400 GMT, the greater degree of smoothing inherent of the larger station separation value in Fig. 5.22 reduces their maximum values. The low level center of rising motion at 0400 GMT becomes a broad area of weak subsidence in Fig. 5.22. The 0335 GMT

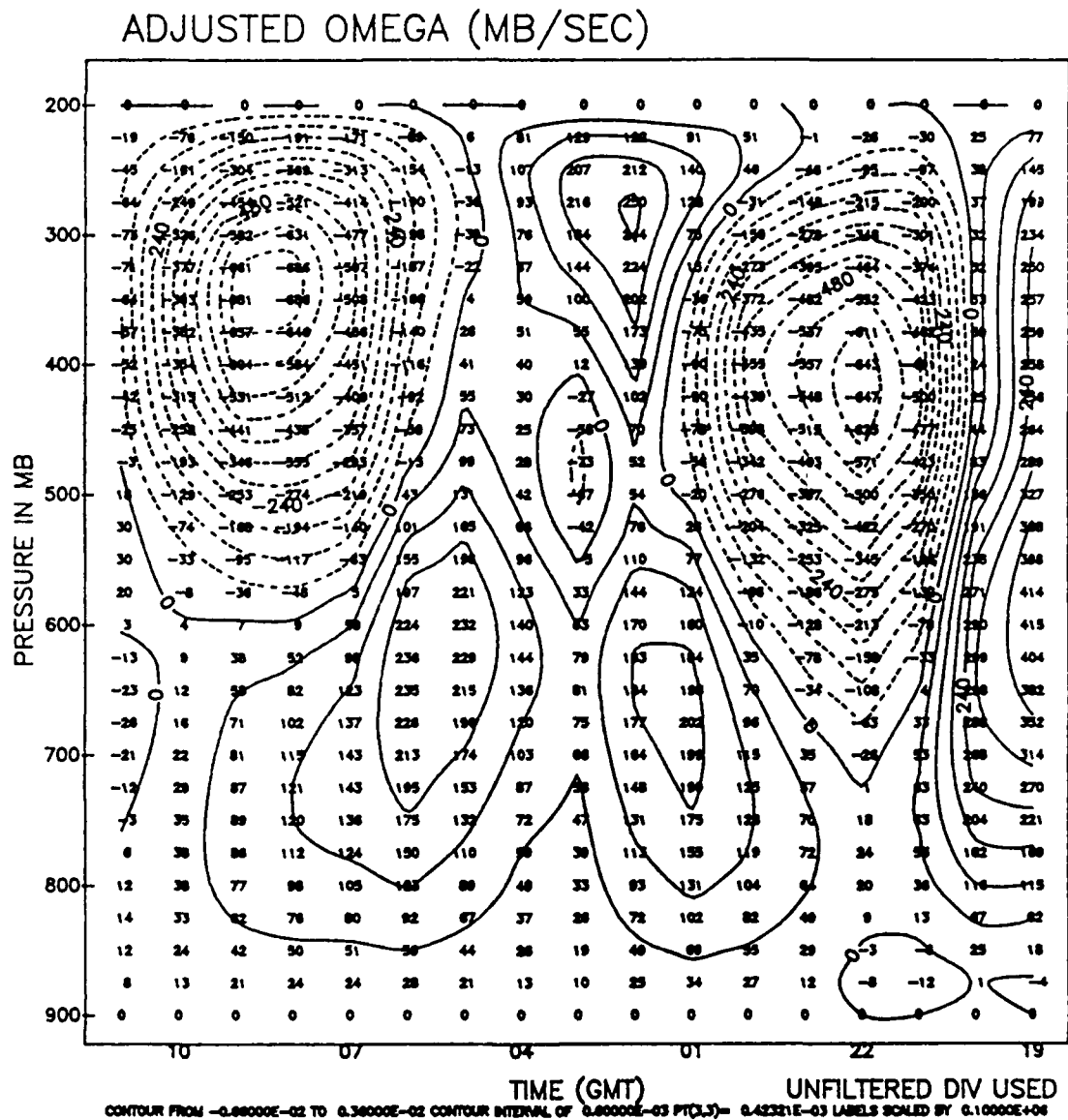


Fig. 5.22. Same as 5.1. but for  $\Delta n = 1200$  meters.

NMC radar summary (Fig. 5.8) would seem to provide evidence supporting the existence of subsidence at all levels around this time since no echoes are indicated within the triangle. In contrast, the two strong centers of rising motion at 2200 and 0800 GMT are only mildly affected by doubling the station separation value. The two centers of sinking motion at 0100 and 0600 GMT at 700 mb are also only mildly affected. The phase of the vertical velocity "wave" isn't altered at all between the two analyses.

A sensitivity study was also performed on the 26-27 June data set. Figure 5.23 shows the omega field for this period derived from an objective analysis scheme using a convergence factor of 0.6 instead of 0.2. Recall from Chapter IV that this should result in a smoother final analysis of the quality controlled wind field. A comparison of Figs. 5.18 and 5.23 reveals that the one main center of rising motion, while dampened in amplitude slightly, is virtually unaffected by the rather large variation of this key Barnes analysis parameter.

A further test was performed with the 26-27 June case. Using winds analyzed with a Barnes convergence factor of 0.6, the divergence and omega fields were derived as previously described. When the divergence field was adjusted, however, the 100 mb level was specified as the upper boundary for zero vertical velocity instead of 200 mb. The resultant omega field is shown in Fig. 5.24. Note that the omega values are now in units of  $10^1 \mu\text{bs}^{-1}$  instead of  $10^2$

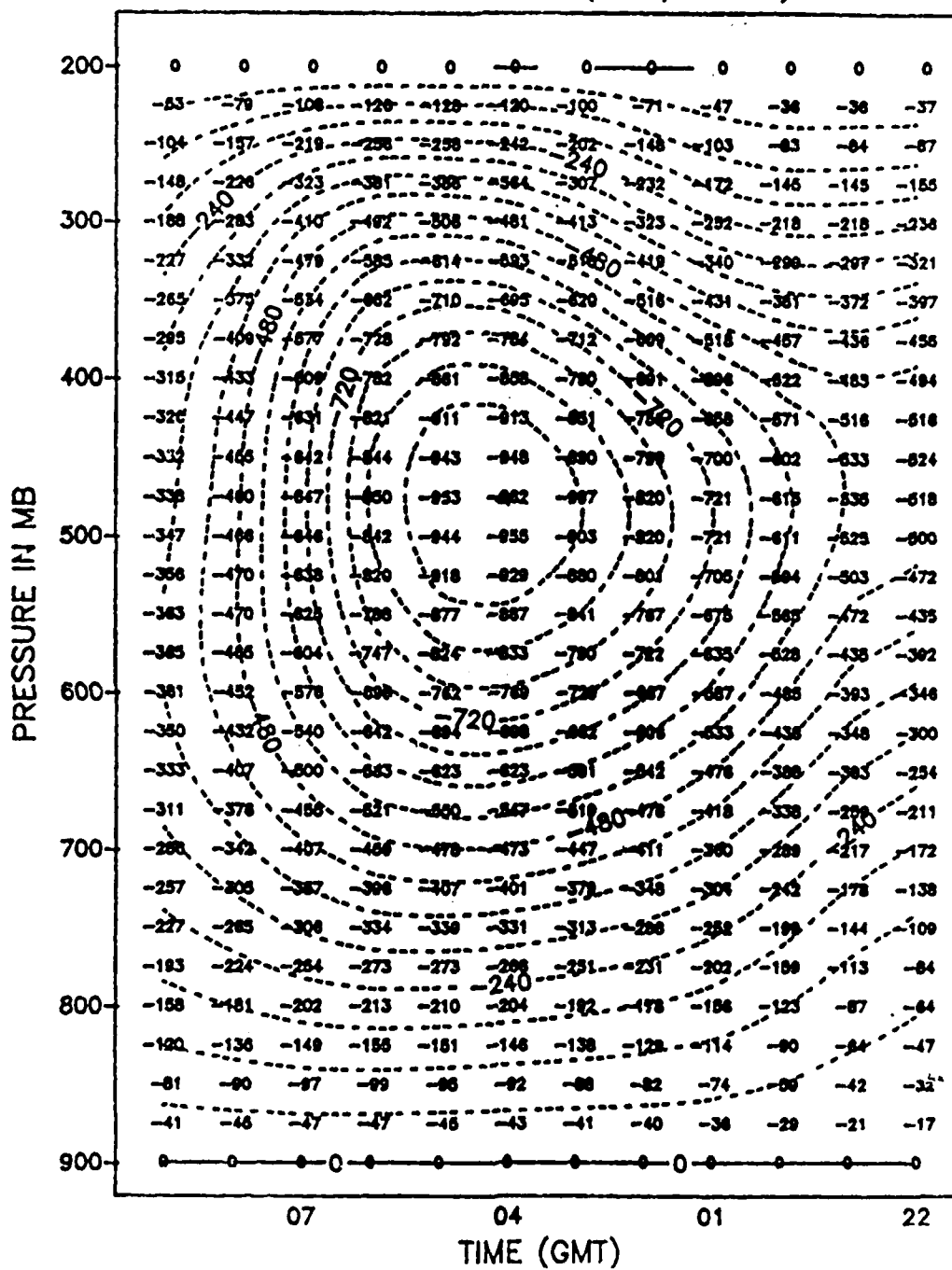


Fig. 5.23. Same as 5.18. but for  $\gamma = 0.6$ .

## ADJUSTED OMEGA (MB/SEC)

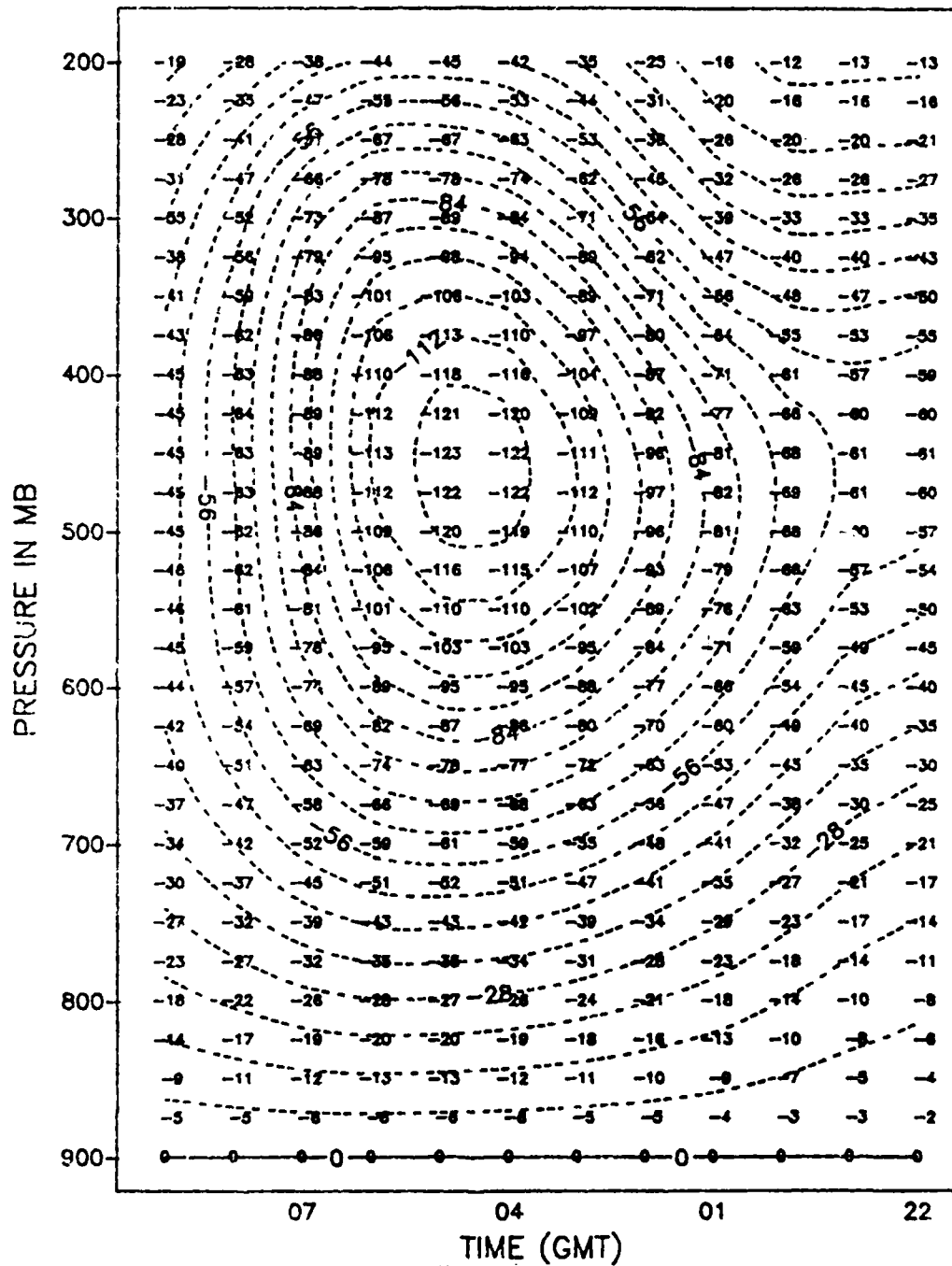


Fig. 5.24. Same as 5.23. but for  $\omega = 0$  at 100 mb after divergence adjustment.  $10^4 \mu \text{bs}^{-1}$

$\mu\text{bs}^{-1}$ . Comparing Figs. 5.23 and 5.24 reveals that raising the upper boundary has the effect of stretching the field features slightly in the vertical. The center of rising motion has been displaced upwards by about 25 mb and its maximum value has increased by about 20%.

## CHAPTER VI

### CONCLUSIONS AND FUTURE WORK

Wind profilers are capable of providing meteorologists with high vertical resolution data throughout the troposphere at temporal intervals small enough to adequately sample mesoscale wind field features. As part of the 1985 Oklahoma-Kansas PRE-STORM experiment, three 50 MHz wind profilers collected wind data during a two month period. Numerous temporal gaps in the McPherson profiler data archive severely restricted the total time of simultaneous profiler operation. As a result, only three data sets of 12 hours or longer were available.

While all three profilers operated at almost identical frequencies, different antenna configurations and operating specifications resulted in mismatched temporal and spatial sampling intervals. To simplify the kinematic calculation process, interpolation to common  $z$ - $t$  grids to achieve one-to-one data correspondence was necessary. The large gaps that existed in several data sets required filling. Because kinematically derived values can be highly sensitive to wind observation errors, it was desirable to design a

quality control procedure to eliminate the spurious wind data that were apparent in all three data sets. In short, the "raw" profiler data sets were far from perfect and required extensive processing before kinematic analysis could begin. An adaption of the Barnes objective analysis technique for use in a  $z$ - $t$  domain, however, not only combined the filling and interpolation processing steps but performed the filtering step as well.

The combined median and vertical consistency checks developed for the quality control procedure were highly successful at eliminating poor quality data without jeopardizing existing mesoscale features. Because the two-pulsewidth operation of the Norman profiler resulted in vertical overlapping of long and short pulse samples, problems occurred when the "blended" data didn't mesh well. These problems, most apparent in the two 12-hour data sets, were dealt with by subjective quality control decisions. These were deemed necessary to reduce the number of objective quality control passes through the data field. The fact that rawinsonde data were used to aid in these decisions illustrates the point that profilers will supplement the existing rawinsonde network but should not replace it.

The time versus height nature of profiler time series created an OBAN obstacle. A rationale for treating the time and space dimensions equally in the analysis procedure was sought and use of wind data covariance statistics provided a

good starting point. The decision to design a Barnes weight function which assigned equal weight to equally correlated data in time and in height generated the desired time and space equivalence or "conversion factor". Features in the omega fields derived, in part, from this technique exhibited the same spatial and temporal scales as the phenomena responsible for their formation (as observed in satellite imagery). While the numerous gaps in the profiler data archive (especially McPherson's) prevented the development of correlation tables for the three PRE-STORM profiler such as seen in Brewster and Schlatter (1988), the use of the Fleming CO correlation tables gave generally good results.

It was found that omega field values can be relatively insensitive to changes in certain Barnes analysis parameters. Doubling the average station separation,  $\Delta n$ , from 600 to 1200 meters decreases the details of features within the field (as expected) but doesn't alter the good correspondence between derived vertical motions and satellite features. Likewise, increasing the Barnes convergence parameter from 0.2 to 0.6 smooths the features in the omega field but doesn't degrade the degree of field verification.

Specifying zero vertical velocity at 100 mb versus 200 mb during divergence field adjustment has small effects on the shape, magnitude, and location of omega field features. In general, 200 mb was selected as the upper boundary for vertical motion as this represented the top of the data

domain. Although standard soundings (modified for surface conditions) were used to establish the pressure field for the two 12-hour data sets, real rawinsonde data were used for 3-4 June. Since the composite tropopause height in this case was about 190 mb, the decision for the general use of 200 mb as the upper boundary seemed to be an acceptable one.

In the 3-4 June case, two MCS's influenced conditions within the triangle resulting in changing vertical motion regimes every four to five hours. Kinematically derived omega fields based on the 0000 and 1200 GMT, 4 June rawinsonde data would have missed the inter-MCS subsidence apparent between 0100 and 0500 GMT. The peak rising motion values would have been smaller also as these occurred several hours before rawinsonde ascent times. Similar fields for the other two cases would have completely missed the peak rising motion centers.

Since 1985, the selection of 404 MHz as an operation frequency and improvements in profiler design have allowed effective wind sampling as low as 500 meters AGL (versus about 1500 meters for the 50 MHz PRE-STORM profilers). If on-site surface (or acoustic sounder) wind observations are available as well, the Barnes method developed in this study would produce a better facsimile of the actual boundary layer conditions within the analyzed wind or derived vertical velocity fields.

When designing the Barnes weight function, seasonal covariance statistics for each PRE-STORM profiler site would

have reduced the uncertainty caused by using another site's statistics. The Fleming profiler statistics used for this study were calculated from data collected during the same time of year as the PRE-STORM experiment. This fact probably reduced the off-site incompatibility.

Once long periods of continuous profiler data are available from different geographic regions,  $u$  and  $v$ -component (or natural coordinate) covariance statistics can be calculated for each season. Climatologically based time to space conversion can thus be performed using "local" data. Many comparison studies between this method and the one proposed by Doswell (1977) to deal with the two different time series dimensions could be undertaken to determine the "better" method (if one exists).

If data from profiler triangles set up on sloping terrain are used, kinematic fields on height levels (or on terrain-following coordinates) would be preferable to pressure levels if a method to adjust the former were developed. Analysis on height surfaces would eliminate the neglect of the lowest station's boundary layer when computing these fields.

The kinematic method for computing vertical velocities is only one of several methods available. If reliable temperature profiles can be obtained at profiler sites, objective analysis can be used to interpolate winds onto isentropic surfaces and a subsequent comparison study can be performed between isentropic and kinematic methods. The

Q-vector method could be performed as well once the effective static stability is calculated across the profiler domain. Accurate retrieval of the horizontal temperature gradients would also be necessary.

In Chapter IV, it was stated that a value of 600 meters for  $\Delta n$  was considered "conservative". The legitimacy of features seen in an omega field using  $\Delta n = 300$  meters (or smaller) can be tested when one has more complete, less clustered data.

The wind fields used in this study were not adjusted to correspond with adjusted divergence fields since they weren't used after determination of this kinematic property. It is recommended that a wind field adjustment be made (after Rusk, 1985) if further wind field calculations are needed.

## BIBLIOGRAPHY

- Augustine, J.A., and E.J. Zipser, 1987: The use of wind profilers in a mesoscale experiment. Bull. Amer. Meteor. Soc., 68, 4-17.
- Barnes, S.L., 1964: A technique for maximizing details in numerical weather map analysis. J. Appl. Meteor., 3, 396-409.
- Barnes, S.L., 1973: Mesoscale objective map analysis using weighted time-series observations. NOAA Tech. Memo. ERL NSSL-62, Norman, Oklahoma, 60 pp.
- Brewster, K.A., and T.W. Schlatter, 1986: Automated quality control of wind profiler data. Preprints 11th Conf. Weather Forecasting and Analysis, Kansas City, MO, Amer. Meteor. Soc., 171-176.
- , 1987: PROFS operational profiler quality control. unpublished manuscript.
- , and T.W. Schlatter, 1988: Recent progress in automated quality control of wind profiler data. Preprints Eighth Conf. Num. Wea. Pred. ,Baltimore, MD, Amer. Meteor. Soc., 331-338.
- Brock, F.V., 1986: A nonlinear filter to remove impulse noise from meteorological data. J. Atmos. Ocean. Tech., 3, 51-58.
- Browning, K.A., and R. Wexler, 1968: The determination of kinematic properties of a wind field using Doppler radar. J. Appl. Meteor., 7, 105-113.
- Carr, F.H., and J.P. Millard, 1985: A composite study of comma clouds and their association with severe weather over the Great Plains. Mon. Wea. Rev., 113, 370-387.
- Cressman, G.P., 1959: An operational objective analysis system. Mon. Wea. Rev., 87, 367-374.

- Cunning, J.B., 1986: The Oklahoma-Kansas Preliminary Regional Experiment for STORM-Central. Bull. Amer. Meteor. Soc., 67, 1478-1486.
- Doswell, C.A., III, 1977: Obtaining meteorologically significant surface divergence fields through the filtering property of objective analysis. Mon. Wea. Rev., 105, 885-892.
- Gage, K.S., and B.B. Balsey, 1978: Doppler radar probing of the clear atmosphere. Bull. Am. Meteor. Soc., 59, 1074-1093.
- Gandin, L.S., 1988: Complex quality control of meteorological observations. Mon. Wea. Rev., 116, 1137-1156.
- Hermes, L.G., 1988: Retrieval of horizontal gradients of virtual temperature using winds from the Oklahoma-Kansas PRE-STORM profilers. M.S. Thesis, School of Meteorology, University of Oklahoma, Norman, Oklahoma, 133 pp.
- Hogg, D.C., M.T. Decker, F.O. Guiraud, K.B. Earnshaw, D.A. Merritt, K.P. Moran, W.B. Sweezy, R.G. Strauch, E.R. Westwater, and C.G. Little, 1983: An automatic profiler of the temperature, wind, and humidity in the troposphere. J. Climate Appl. Meteor., 22, 807-831.
- Koch, S.E., M. DesJardins, and P.J. Kocin, 1983: An interactive Barnes objective map analysis scheme for use with satellite and conventional data. J. Climate and Appl. Meteor., 22, 1487-1503.
- Kuo, Y.H., and R.A. Anthes, 1985: Calculation of geopotential and temperature fields from an array of nearly continuous wind observations. J. Atmos. and Oceanic Tech., 2, 22-34.
- Kuo, Y.H., D.O. Gill, and L. Cheng, 1987a: Retrieving temperature and geopotential fields from a network of wind profiler observations. Mon. Wea. Rev., 115, 3146-3165.
- Kuo, Y.H., E.G. Donall, and M.A. Shapiro, 1987b: Feasibility of short-range numerical weather prediction using observations from a network of profilers. Mon. Wea. Rev., 115, 2402-2427.
- Maddox, R.A., 1983: Large scale meteorological conditions associated with midlatitude, mesoscale convective complexes. Mon. Wea. Rev., 111, 1475-1493.

- Meitin, J.G., and J.B. Cunning, 1985: The Oklahoma-Kansas preliminary regional experiment for STORM-central, Volume I. Daily operations summary, NOAA Tech. Memo. ERL ESG-20, 313 pp.
- O'Brien, J., 1970: Alternative solutions to the classical vertical velocity problem. J. Appl. Meteor., 9, 197-203.
- Rusk, D.J., 1985: Examination of a static initialization procedure for a regional primitive equation model. M.S. Thesis, School of Meteorology, University of Oklahoma, Norman, Oklahoma, 101 pp.
- Schaefer, J.T., and C.A. Doswell III, 1979: On the interpolation of a vector field. Mon. Wea. Rev., 107, 458-476.
- Shapiro, M.A., T. Hample, and D.W. van de Kamp, 1984: Radar wind profiler observations of fronts and jet streams. Mon. Wea. Rev., 112, 1263-1266.
- Smith, T.L., and T.W. Schlatter, 1988: A study of kinematic fields in the pre-convective environment derived using the Colorado wind profiler network. Preprints, 15th Conf. on Severe Local Storms, Baltimore, Maryland, AMS, Boston, Massachusetts, 347-350.
- Strauch, R.G., D.A. Merritt, K.P. Moran, K.B. Earnshaw, and D.W. van de Kamp, 1984: The Colorado wind-profiling network. J. Atmos. Oceanic Tech., 1, 37-49.
- Van de Kamp, D.W., 1988: Profiler Training Manual #1 - Principles of Wind Profiler Operation. NOAA/ERL. 49 pp.
- Zamora, R.J., and M.A. Shapiro, 1984: Diagnostic divergence and vorticity calculations using a network of mesoscale wind profilers. Preprints 10th Conf. on Weather Forecasting and Analysis, Clearwater Beach, Florida, AMS, Boston, Massachusetts, 386-391.
- Zamora, R.J., M.A. Shapiro, and C.A. Doswell III, 1987: The diagnosis of upper tropospheric divergence and ageostrophic wind using profiler wind observations. Mon. Wea. Rev., 115, 871-884.

## APPENDIX

### THE LINE INTEGRAL METHOD

The line integral method is a computationally simple way of estimating the divergence and vorticity within a polygon of wind observations and is discussed by Schaefer and Doswell (1979). The triangle of PRE-STORM wind profilers provides us with the minimum of three non-colinear wind observations required for this method.

The profiler triangle area was computed using:

$$A = [s(s-a)(s-b)(s-c)]^{1/2}$$

where a, b, and c were the lengths of the triangle legs in kilometers and:

$$s = (a+b+c)/2$$

The leg lengths were calculated as the great circle distance between the two end points given the longitude and latitude of each. The results were as follows:

<u>LEG</u>	<u>LENGTH (km)</u>
Liberal-McPherson	325.3
McPherson-Norman	372.8
Norman-Liberal	373.9

Using this method, the triangle area was  $5.47 \times 10^4 \text{ km}^2$ , or to keep the units compatible with wind observation units,  $5.47 \times 10^{10} \text{ m}^2$ .

Using the assumption of linear wind variation along a triangle leg, the average value of the two wind observations at the end points of a leg were assigned to the midpoint of that leg. The normal ( $\vec{n}$ ) and parallel ( $\vec{s}$ ) average wind components ( $\vec{V} \cdot d\vec{n}$  and  $\vec{V} \cdot d\vec{s}$ ) on a leg were computed with sign orientations as shown in Figure A1.

The last step is the calculation of divergence and vorticity within the triangle. Adding all three normal components and dividing this sum by the triangle area gives us divergence while addition of the three parallel components and subsequent division by the triangle area yields the vorticity - both in units of  $\text{s}^{-1}$ :

$$\text{DIV} = (\vec{V} \cdot d\vec{n}_a + \vec{V} \cdot d\vec{n}_b + \vec{V} \cdot d\vec{n}_c) / A$$

$$\text{VORT} = (\vec{V} \cdot d\vec{s}_a + \vec{V} \cdot d\vec{s}_b + \vec{V} \cdot d\vec{s}_c) / A$$

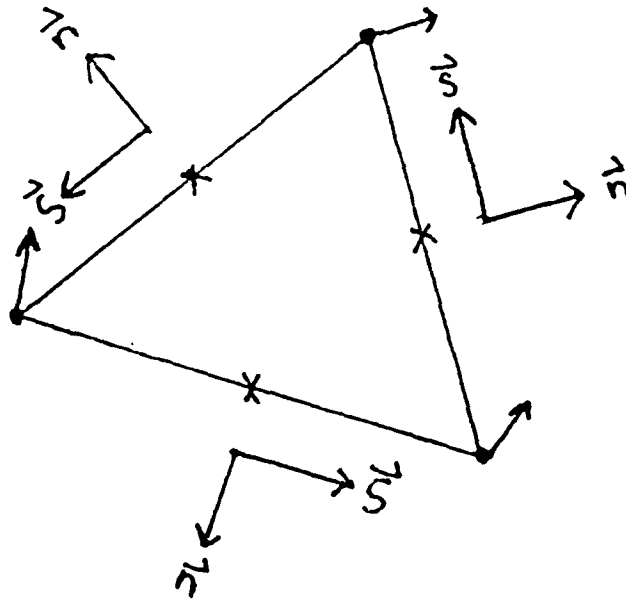


Fig. A1. Orientation of unit vectors for line integral calculations around a triangle.